The Effects of Rotation on Heat Transfer in Turbine Blade Cooling

by

Andrew Jones,Jr.

Submitted to the Department of Mechanical Engineering
in partial fulfillment of the requirements for the degree of

at the

MASSACHUSETTS INSTITUTE OF TECHNOLOGY

September 1994

© Massachusetts Institute of Technology 1994. All rights reserved.

Author . . . .
Department of Mechanical Engineering
August 22, 1994

Certified by . . . .
Jack L. Kerrebrock
Richard Cockburn Maclaurin Professor of Aeronautics and
Astronautics
Thesis Supervisor

Accepted by . . . .
Ain A. Sonin
Chairman, Departmental Committee on Graduate Students

The Effects of Rotation on Heat Transfer in Turbine Blade Cooling

by

Andrew Jones,Jr.

Submitted to the Department of Mechanical Engineering
on August 22, 1994, in partial fulfillment of the
requirements for the degree of
Master of Science

Abstract

This thesis discusses the trends of heat transfer in rotating turbine cooling passages as a function of Rotation Number, Density Parameter, Reynolds Number, Buoyancy Parameter, and Geometry. Previous experimentalists have documented consistent trends about heat transfer in rotating cooling passages relative to stationary data. The heat transfer on the trailing face improves with increasing Rotation number, Density parameter, and Buoyancy parameter. On the leading face, heat transfer decreases near the inlet and increases again further upstream with these same parameters. The objective of this work is to provide more localized data about these phenomena, to expand the range of parameters investigated, and to perform a more detail study on the effect of geometry and surface distortion.

The data confirms some of the previous results for flow in rotating passages. In addition, some new conclusions are presented. Heat transfer increases as rotation number increases. At moderate density parameters around 0.2, the heat transfer reaches a minimum increasing at both higher and lower values. The effect of Reynolds number on the heat transfer is close to that predicted by the Colburn equation. Flow channel geometry has strong effects on the heat transfer. For square passages and rectangular passages with an aspect ratio of 3.3, the Nusselt ratio varies along the flow direction principally in the entrance region. Compared to a flow channel with a smaller aspect ratio, the rectangular flow channel forces the boundary layers to merge almost immediately reducing heat transfer in the inlet region. Turbulators continually enhance heat transfer as the flow travels radially outward. The uneven walled test section shows higher Nusselt ratios than both the smooth square and smooth rectangle. This thesis presents a detailed discussion about the effects these parameters have on heat transfer in rotating turbine blades.

Thesis Supervisor: Jack L. Kerrebrock
Title: Richard Cockburn Maclaurin Professor of Aeronautics and Astronautics

Acknowledgments

To the youth who march onward and upward toward the light, this volume is respectfully dedicated.[*The History of Alpha Phi Alpha: A Development in College Life*]

First , I would like to thank Professor Jack L. Kerrebrock for the opportunity and his patience. The knowledge I have gained working with Prof. Kerrebrock is immeasureable and has helped to greatly enhance my personal development.

Secondly, I would like to thank Pamela Barry, George Govatzidakis, and Dr. Gerald Guenette for all the assistance and advice they provided to complete this project. They made long days in the Gas Turbine Lab tolerable.

Next, I would like to thank General Electric: Industrial and Power System for the sponsorship.

Finally, I would like to thank Viktor Dubrowski for all the machining jobs he completed for the experiment, William Ames and James Letendre for all there assistance in maintaining the experiment, and all the staff and students in the Gas Turbine Lab for there advice and encouragement.

Contents

C NOMENCLATURE   118

D DATA   120

List of Figures

List of Tables

Chapter 1

INTRODUCTION

The following thesis is motivated by work being conducted at General Electric: Industrial and Power Systems. General Electric is in the process of designing a new engine for which the Gas Turbine Lab's heat transfer experiment is to provide data. While providing data, the information expands the range of knowledge available in the turbine cooling field. The project involves a study of the effects of rotation on heat transfer in turbine blade cooling passages. This thesis completes the second part of the research program first reported in *Rotational Effects on Turbine Blade Cooling* by Pamela Barry[3]. Barry compares Gas Turbine Lab(GTL) data with that presented by other experimentalists.

1.1 Motivation for Research

Until the 1970's, turbine inlet temperatures were limited by the blade material (nickel and cobalt based alloys) to temperatures of about 1100°F. The introduction of turbine cooling enabled an increase in combustor exit temperature.

It is necessary to study turbine cooling to expand the limited knowledge about the design of efficient turbine cooling passages. Bleeding cooling air from the compressor causes engine losses. Therefore, less cooling is better. Turbine cooling is entering an era where experience and the brute force methods are no longer feasible. Data is necessary to design cooling passages efficiently in one or two trials.
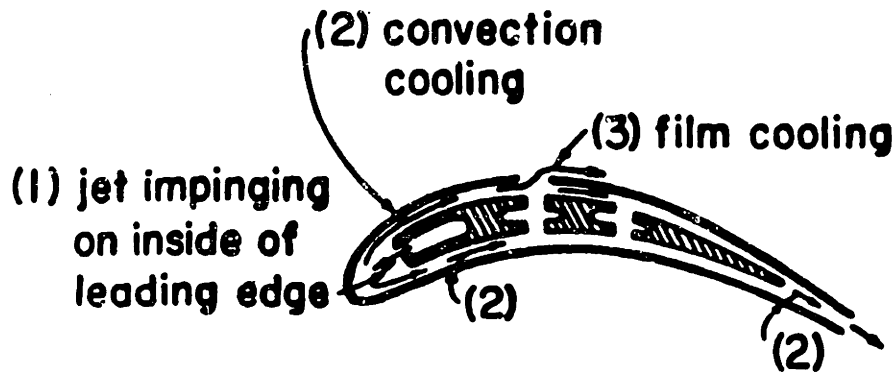
Figure 1-1: Different Forms of Turbine Blade Cooling

1.2 Turbine Blade Cooling

There are several types of blade cooling: convection, film, and impingement. Turbine blade cooling is used in almost every modern engine. Generally, different methods of cooling are used in combination. The focus of this study is convection cooling, which involves the flow of a cool fluid through passages in the blade, see figure 1-1. [10]

1.3 Previous Work

A great deal of empirical work has been done in the area of turbine cooling. Experimental and numerical work has been done on smooth rectangular, circular, square, and triangular sections. The different shapes refer to the cross section of the passage, while smooth refers to the surface condition. Work has also been done on turbulated square passages. Turbulators are short bumps on the surface of the passage which break up the boundary layer flow to enhance heat transfer. Very little work has been done on rectangular turbulated passages. The results generally agree on a qualitative level as discussed below. The heat transfer coefficient on the trailing side increases with rotation . Along the passage, the heat transfer coefficient decreases from a high value at the inlet reaching a minimum and increasing again at the outlet. There are

qualitative explanations for this but no ability to accurately predict the heat transfer theoretically, therefore, data is very important.

Prakash and Zerkle [6], performed a numerical simulation on a smooth square section with a constant wall temperature. They confirmed that centrifugal buoyancy increases the radial velocity of the cooler fluid near the trailing face while decreasing the radial velocity of the warmer fluid near the leading face. They also documented an increase in heat transfer on the trailing surface due to rotation. Near the leading surface, the heat transfer decreased near the inlet and increased further downstream due to rotation. The simulation predicted a difference in heat transfer in a rotating duct due to both Coriolis and Centrifugal forces. Prakash and Zerkle focused on three areas: centrifugal buoyancy effects, inlet sensitivity, and exit condition in a single and double passage. A single passage involves computation of the flow in one direction, inward or outward. A double passage is two single passages connect at one end by a 180° bend. The flow in the second passage is opposite the direction of the flow in the first passage. They concluded that Coriolis forces induce cross streams which transfer cooler fluid from the center to the trailing surface. Using a $\kappa - \epsilon$ model including buoyancy, the heat transfer is predicted to improve with rotation number and density parameter. When compared with experimental data, the Nusselt number is under-predicted over the trailing surface and inlet of the leading surface and over-predicted midway and near the exit of the leading surface. They concluded that the inlet conditions have to be specified and the $\kappa - \epsilon$ model has to be modified for rotation and buoyancy. The inclusion of buoyancy is deemed essential for correct predictions.

W.D. Morris and R.Salemi [15] performed experiments on circular tubes with constant wall temperature. The Reynolds number varied from 15,000 to 30,000. The speed ranged from 0 and 2700 revolutions per minute(RPM). Five different power settings were used to maintain constant temperature. When stationary the leading and trailing faces showed identical heat transfer. When rotating, they found that the Nusselt number rose with Reynolds number, the trailing face being higher than the leading face. Nusselt number also increased with buoyancy. As Prakash and Zerkle

13

found, Coriolis induced cross streams created circumferential variations in the local heat transfer, improving heat transfer on the trailing edge.

Johnson and Wagner[16] performed experiments on smooth square serpentine passages with both radially outward and inward flow. The baseline case was at a Reynolds number, Re, of 25,000, a Density parameter, $\frac{\Delta\rho}{\rho}$, of 0.13, a Rotation number,Rot, of 0.24, and a geometrical ratio, $\frac{R}{D_h}$, of 49. These parameters were in the central region of the operating range of current large aircraft gas turbine engines. They concluded that density differences and rotation cause large changes in heat transfer for radially outward flow and relatively small changes for radially inward flow. On the low pressure side, the heat transfer varied with the Buoyancy parameter, which is a correlation of the Density parameter, Rotation number, and geometrical parameter, regardless of the flow direction. On the high pressure side, the heat transfer was a function of Buoyancy parameter for radially outward flow and almost unaffected for radially inward flow. Increasing the Density ratio increased the heat transfer although the increase was less for radially inward flow than for radially outward flow.

Johnson and Wagner[17] performed a second set of experiments on square serpentine passages with turbulators. They used the same baseline case as in the previous experiment. They found that rotation improves heat transfer on the trailing surfaces of the 1st passage by 60% at a Rot=.35 compared to stationary. Rotation decreased the heat transfer on the leading side by 50% compared to stationary. As in the previous experiment, the heat transfer increased again further downstream. They suggest that the decrease in heat transfer on the low pressure side with trips is dominated by Coriolis generated cross streams. The heat transfer on the high pressure side is affected by a combination of the Coriolis and centripetal buoyancy forces. For flow through a rotating tripped passage, Johnson and Wagner drew the following additional conclusions; trips improved heat transfer on both the low and high pressure faces and at high rotation and buoyancy, there were no significant changes between trips and smooth walls.

Other interesting results come from J.C. Han and Zhang [9] who performed their experiments for three different cases: Case A: constant wall temperature, Case B:

constant heat flux, and Case C: hot leading and trailing and cold sidewalls. It must be noted that an actual turbine blade has neither a constant wall temperature nor a constant heat flux. The range of parameters Han studied is Re=2,500-25,000, Rot=0-.352. He stated that there are inconsistencies due to measurement systems, models, and test conditions in previous data. Han proposed that heat transfer increased due to the de-stabilization of the thinner boundary layer which causes near-wall turbulence on the trailing side, while on the leading side, the boundary layer grew as a result of hot fluid accumulating near the leading face from the cross stream flow. In agreement with others, Han attributed the improved heat transfer to both the increased strength of the cross stream flow and the centripetal buoyancy. The heat transfer is higher on the trailing face due to the coolant impinging on the surface as a result of the cross stream flow. The profile distortion produces stronger buoyancy-induced wall turbulence near the de-stabilized trailing boundary layer. On the leading surface, the heat transfer decreases initially near the inlet and the thicker stabilized boundary layer increases the heat transfer near the end of the channel. Han concluded that the Nusselt Number ratio may be as high as 2.5-3.0 on the trailing side in a constant temperature experiment. It decreased to about 0.4 or more then increased further downstream on the leading side in a constant temperature experiment. On the trailing face, the heat transfer is 10-20% higher in a constant flux experiment than in a constant wall temperature experiment. On the leading face, the heat transfer is 40-80% higher in a constant flux experiment than in a constant wall temperature experiment.

A conclusion most important to the G.T.L. experiment which Han found is that the heat transfer in a constant flux experiment is higher than that in a constant wall temperature experiment. In reality, cooling passages in Gas Turbine Engines are somewhere in between. Han's correlation is used by Pamela Barry in *Rotational Effects on Turbine Blade Cooling* to correct the Nusselt numbers obtained in the G.T.L. constant flux experiment for comparison to Johnson & Wagner's constant temperature data. In fact, Barry compares G.T.L. data with the data of Han[9] and Guidez[8] as well.

Temperature
Measurement

Resolution in previous
Experiments

Resolution of G.T.L.
Heat Transfer
Experiment up to
1mm x 1mm
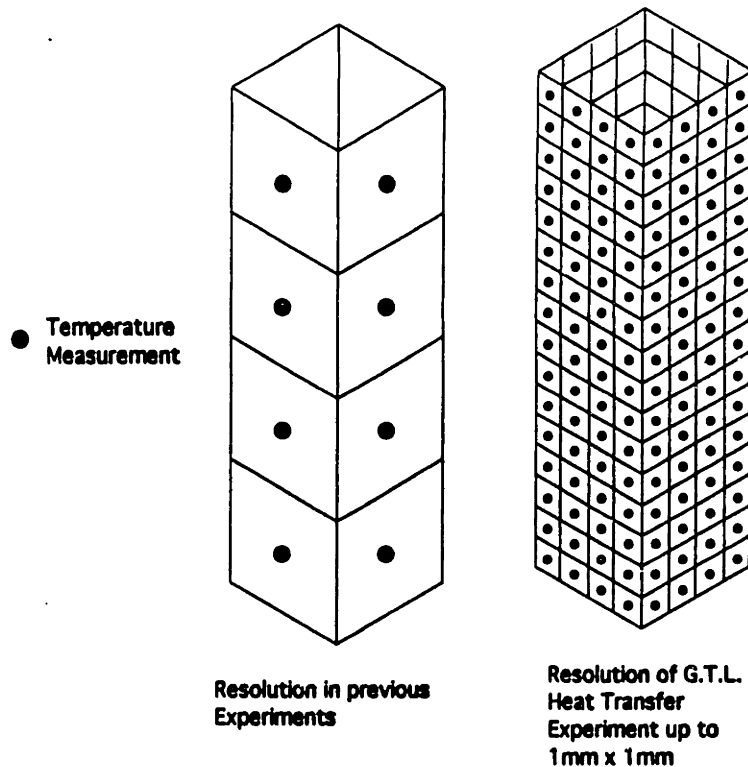
Figure 1-2: Example of Resolution Capabilities

1.4 The M.I.T. Gas Turbine Lab Internal Heat Transfer Research Program

The existing data on heat transfer in rotating passages has low spatial resolution and is for a limited range of parameters. The focus of the present experiment is to expand the range of data available as well as provide better spatial resolution. Figure 1-2 shows a general example of the resolution the G.T.L. heat transfer experiment is capable of obtaining. All experiments mentioned above collected surface temperature measurements using thermocouples, limiting the spatial resolution. In most cases, the data consist of sixteen measurements, four radially and four circumferentially, over an entire passage. Most data available is in the range of 0-25,000 Reynolds number and 0-.35 rotation number.

As mentioned earlier, the project is motivated by the need for more information about the effects of rotation on heat transfer in cooling passages. A preliminary study was performed to determine the range of parameters feasible on the existing rotating

16

L/D_h	13-25
R/D_h	90-170
Reynolds Number	$4.0 \times 10^5 - 8.0 \times 10^5$
Rotation Number	0.1-0.4
Grashof Number	$4.0 \times 10^{11} - 2.0 \times 10^{12}$
T_w/T_c	1.2-1.4

Table 1.1: Parameters of Interest to General Electric

heat transfer apparatus in the Gas Turbine Lab. Appendix A discusses some of the limitations on the G.T.L. heat transfer experiment. The parameters in Table 1.1 were judged of interest for the General Electric Application.

Buoyancy parameter is used instead of Grashof number or Rayleigh number. The Buoyancy parameter is the standard used in the area of turbine blade cooling. Density parameter is used instead of T_w/T_c. The present L/D_h is set at 12-14 and the present R/D_h is approximately 61-67. The mean radius of the G.T.L rig is limited by the size of the vacuum chamber.

The Gas Turbine Lab's heat transfer experiment is capable of eliminating many of the problems mentioned above by making surface temperature measurements using an infrared detector. The detector allows measurements with a spatial resolution of about 1mm. Test have been conducted at Reynolds number ranges from 0-160,000 but the flow system is capable of reaching Reynolds numbers on the order of 1.0×10^6 with the facilities Blackmer compressor. The wall temperature is raised by resistance heating, allowing a wider range of density parameters. The rotating system is capable of operating up to 2400 RPM which yields rotation numbers in the range of 0-.90 depending on the flow velocity.

Chapter 2

FLOW IN A ROTATING HEATED DUCT

Heat transfer in a rotating heated channel is very complex making the characteristics of the flow unpredictable with present day theory. Numerical solutions have been produced as mentioned earlier in the introduction. Unfortunately, numerical solutions are inaccurate due to the complexity of the forces acting in a turbine cooling passage. In addition, there are those unknown surface conditions which effect the boundary layers and flow distribution not to mention, inlet and outlet conditions. Therefore, experiments are necessary to gain a better understanding of such a system. Through the laws of mass, momentum, and energy conservation, the influential parameters and their significance are determined.

2.1   Conservation Laws

By taking a control volume around the flow inside the channel, the laws of mass, momentum and energy conservation are applied.

Mass Conservation

$$\frac{\partial \rho}{\partial t} + \nabla \bullet (\rho \bar{u}) = 0 \tag{2.1}$$

Momentum Conservation

$$\rho \frac{D\bar{u}}{Dt} = -\nabla P + \mu[\frac{\nabla(\nabla \bullet \bar{u})}{3} + \nabla^2 \bar{u}] + \rho \bar{B}$$ (2.2)

Energy Conservation

$$\rho \frac{DH}{Dt} = k\nabla^2 T + \frac{Dp}{Dt} + \mu\Phi + W + \rho(\bar{B} \bullet \bar{u})$$ (2.3)

It is necessary to briefly discuss these equations to explain what each term represents. In mass conservation, the first term represents the change in mass with time while the second term monitors changes in massflow with position. In the momentum conservation equation, which states Newton's second law, the left side is mass times acceleration. Thus, the right hand side equals the sum of all the forces. The first term is the force resulting from the pressure gradient. The second and third terms on the right represent forces due to the normal and shear stresses, respectively. The final term is the body force which includes axes, buoyancy, and gravitational effects. The terms in the energy conservation equation are very similar to those in the momentum equation. The term on the left is the convection or enthalpy transport. The terms on the right are the sum of energy dissipating terms. The first term on the right is the conduction in the fluid. The second term is the pressure distribution term. The third term is the effect of viscous dissipation where $\Phi = (\frac{\partial u_i}{\partial x_j} + \frac{\partial u_j}{\partial x_i})\frac{\partial u_i}{\partial x_j}$ summed from i,j=1-3. The fourth term is an energy source term. The final term is all other body forces which includes the effects of rotation, buoyancy, and gravitational effects.

There are a number of assumptions that are used to simplify these equations. The first and most important assumption is that the turbine cooling passage is operating at steady state. Therefore, all references to time in the equation are eliminated. Variations in viscosity, density, and thermal conductivity, are assumed negligible over the span of the test section. In order to gain a better understanding of the equations, the equations are non-dimensionalized to determine which parameters have a dominant effect on the heat transfer coefficient in turbine blade cooling.

The vector $\bar{B}$ is the body force in the rotating reference frame. The body force

has three components, an axial component, $\bar{B}_a$, a buoyancy component, $\bar{B}_b$, and a gravitational component, $\bar{B}_g$. The gravitational component is very small compared to the other two terms. The force $\bar{B}_a$ due to axes motion is the force acting on a fluid in an accelerating reference frame. The experimental system, xyz, must be studied relative to an inertial reference frame, XYZ. The following equation transforms the non-inertial reference frame,xyz, into the inertial reference frame, XYZ[7].

$$\bar{V}_{XYZ} = \bar{V}_{xyz} + \frac{d\bar{R}}{dt} + \bar{\Omega} \times \bar{r} \qquad (2.4)$$

Therefore, the acceleration relative to an inertial reference frame is $\frac{d\bar{V}_{XYZ}}{dt}$.

$$\frac{d\bar{V}_{XYZ}}{dt} = \frac{d\bar{V}_{xyz}}{dt} + \frac{d^2\bar{R}}{dt^2} + \frac{d\bar{\Omega}}{dt} \times \bar{r} + 2\bar{\Omega} \times \bar{V}_{xyz} + \bar{\Omega} \times \bar{\Omega} \times \bar{r} = \frac{\sum F}{\rho} \qquad (2.5)$$

The experiment studies steady state turbine cooling, so time dependence is removed. In addition, there is no translational acceleration, so $\frac{d^2\bar{R}}{dt^2}$ is zero. Since $\frac{d\bar{V}_{xyz}}{dt}$ represents the rate of change of xyz momentum, the other terms are moved to the right hand side of equation 2.5 and the axes force is revealed.

$$\frac{\bar{B}_a}{\rho} = -2\bar{\Omega} \times \bar{u} - \bar{\Omega} \times (\bar{\Omega} \times \bar{r}) \qquad (2.6)$$

The second important body force, the buoyancy force, occurs whenever a body is placed in a fluid of higher or lower density. The term ∇P is actually $\nabla P_o - \rho g h + P$ [4] where $\nabla P_o - \rho g h$ is the pressure due to hydrostatic equilibrium and P is the pressure resulting from the motion of the fluid present in equation 2.2. It is the hydrostatic term which leads to the buoyancy force, B_b. Taking the gradient of the hydrostatic component, $\nabla(P_o - \rho g h) = -\rho_\infty g$, along with the body force ρg the term $g(\rho - \rho_\infty)$ appears. Using $p = \rho R T$ for a perfect gas and $\beta = \frac{-(\partial \rho / \partial T)_p}{\rho} = \frac{1}{T_\infty}$, the above equation is re-arranged into the following [12].

$$g(\rho - \rho_\infty) \approx g\rho\beta(T - T_\infty) \qquad (2.7)$$

20

$$\acute{\rho} = \frac{\rho}{\rho_m} \qquad \acute{u} = \frac{u}{v_m} \qquad \acute{\Omega} = \frac{\Omega}{\Omega_m}$$
$$\acute{r} = \frac{r}{R_m} \qquad \acute{\nabla} = d_h \nabla \qquad \acute{p} = \frac{p}{\rho_m v_m^2}$$
$$\acute{\Phi} = \frac{\Phi d_h^2}{v_m^2} \qquad \acute{H} = \frac{H}{C_p \Delta T} \qquad \acute{T} = \frac{T}{\Delta T}$$

<div align="center">Table 2.1: Non-dimensional terms</div>

In a rotating reference frame, the 'g' is no longer gravity but the motion of the particle $\frac{D\bar{V}}{Dt}$ relative to an inertial reference frame. Therefore, the buoyancy force becomes a multiple of the axes force.

$$\frac{\bar{B}_b}{\rho} = \left[-2\bar{\Omega} \times \bar{u} - \bar{\Omega} \times (\bar{\Omega} \times \bar{r})\right] * \beta\Theta \tag{2.8}$$

In the above equation, $\Theta = (T - T_\infty)$.

These body forces apply directly to the energy equation with one exception. The first term $2\bar{\Omega} \times \bar{u}$ vanishes because the dot product of the previous term and the velocity vector $\bar{u}$ is zero. There are no heat sources in the fluid so W = 0. Using the non-dimensional parameters listed below, the three equations are transformed into the following.

Mass Conservation:

$$\acute{\nabla} \bullet \acute{\rho}\acute{u} = 0 \tag{2.9}$$

Momentum Conservation:

$$\acute{\rho}(\acute{u} \bullet \acute{\nabla})\acute{u} = -\acute{\nabla}\acute{p} + \frac{\mu}{\rho_m v_m d_h}\left[\frac{\acute{\nabla}(\acute{\nabla}\bullet\acute{u})}{3} + \acute{\nabla}^2\acute{u}\right]$$
$$+ \acute{\rho}(1 - \beta\acute{\theta})\left[\left(\frac{\Omega_m d_h}{v_m}\right)(-2\acute{\Omega} \times \acute{u}) + \left(\frac{\Omega_m d_h}{v_m}\right)^2 \frac{R_m}{d_h}(-\acute{\Omega} \times (\acute{\Omega} \times \acute{r}))\right] \tag{2.10}$$

Energy Conservation:

$$\acute{\rho}(\acute{u} \bullet \acute{\nabla})\acute{H} = \frac{k}{c_p\mu}\frac{\mu}{\rho_m v_m d_h}\acute{\nabla}^2\acute{T} + \frac{v_m^2}{c_p\Delta T}(\acute{u} \bullet \acute{\nabla})\acute{p} + \frac{\mu}{\rho_m v_m d_h}\frac{v_m^2}{c_p\Delta T}\acute{\Phi}+$$
$$\acute{\rho}(1 - \beta\acute{\theta})\frac{v_m^2}{c_p\Delta T}\left(\frac{\Omega_m d_h}{v_m}\right)^2\frac{R_m}{d_h}(-\acute{\Omega} \times (\acute{\Omega} \times \acute{r})) \tag{2.11}$$

2.2 Dominant Parameters

At this point, the individual terms of the equations can be analyzed. It also becomes obvious what parameters have to be controlled in the experiment. The first non-dimensional term is the Reynolds number.

$$Re_d = \frac{V\rho d_h}{\mu} \qquad (2.12)$$

The Reynolds number is a ratio of inertial forces to viscous forces. It is expected to have an influence in turbine blade cooling because it influences the growth of shear layers. The Reynolds number appears in both the energy and the momentum conservation balance.

The next familiar term is the inverse Rossby number which is denoted as the Rotation number in the Gas Turbine Lab Heat Transfer experiment.

$$Rot = \frac{\Omega d_h}{V} \qquad (2.13)$$

The Rotation number is the ratio of rotation to radial velocity. It is also an indicator of Coriolis forces on the heat transfer in turbine blade cooling. If you look at equations 2.10 and 2.11, the Rotation number multiples the Coriolis term, $2\Omega \times \bar{u}$, in the momentum conservation equation. The Rotation number has a first order influence on the Coriolis term and a second order influence on the centripetal term.

The next non-dimensional term is the Prandtl number.

$$Pr = \frac{C_p \mu}{k_f} \qquad (2.14)$$

As seen by its terms, it is a ratio of momentum transfer to heat conduction in the fluid stream. The Prandtl number is fortunately constant for most perfect gases between $\frac{2}{3}$ and $\frac{5}{7}$. Since, air can be modeled as a perfect gas there are no Prandtl number dependencies on the heat transfer in turbine blade cooling. Therefore, the cooling fluid used in the experiment should reflect the same perfect gas properties.

The next non-dimensional parameter of interest is the Eckert number which is a function of the Mach number times the inverse of the Density parameter, $\frac{\Delta T}{T}$, where ΔT is the wall temperature minus the bulk temperature, $T_w - T_b$.

$$Eck = \frac{V^2}{C_p \Delta T} = (\gamma - 1)M^2 \frac{T}{\Delta T} \tag{2.15}$$

The Eckert Number, which is represented by the Density parameter in the G.T.L. heat transfer experiment, is a measure of the ratio of kinetic energy to thermal energy. It does not account for viscous dissipation, which plays an important part in the conversion of kinetic energy to thermal energy[14]. The Brinkman number, Br=2EckPr, which is the product of the Eckert and Prandtl number is appropriate for characterizing viscous dissipation. If equation 2.11 is multiplied by the Prandtl number, the Brinkman number scales the pressure and viscous dissipation terms. It is thus another important parameter that is measured in the experiment to determine the effects of rotation on heat transfer in turbine blade cooling. Any variance with Density parameter can be attributed to changes in the mode of energy dissipation.

The final non-dimensional parameter is a matter of preference because there are several terms which are used for the same purpose. The term, whether it is the Buoyancy parameter, the Grashof number, or the Rayleigh number, is used to determine the effect of buoyancy on heat transfer in a rotating heated channel. They all involve different combinations of the terms mentioned above. The Buoyancy parameter most closely resembles the term multiplying the buoyancy force in equation 2.11.

$$Bu = \frac{(\gamma - 1)M^2}{Eck} Rot^2 \frac{R_m}{d_h} = \frac{\Delta T}{T} \left(\frac{\Omega d_h}{V_m}\right)^2 \frac{R_m}{d_h} \tag{2.16}$$

The G.T.L. heat transfer experiment uses the Buoyancy parameter along with the Density parameter, $\frac{\Delta T}{T}$, to consolidate effects on heat transfer in a rotating heated passage due to buoyancy.

The second term used to determine buoyancy effects is the Grashof Number. The Grashof number is a function of the Reynolds number, the Rotation number, and the

Eckert number.

$$Gr = \frac{R_m}{d_h}\frac{(\gamma - 1)M^2}{Eck}Re_d^2 Rot^2 = \frac{\Omega^2 R_m \beta \Delta T d_h^3}{\nu^2} \qquad (2.17)$$

The addition of Reynolds number along with the Density parameter and the Rotation number makes representing the effect of buoyancy in an experiment more difficult.

The third parameter used for the same purpose is the Rayleigh number, which is a function of the Grashof number and the Prandtl number.

$$Ra = \frac{R_m}{d_h}\frac{(\gamma - 1)M^2}{Eck}Re_d^2 Rot^2 Pr = \frac{\Omega^2 R_m \beta \Delta T d_h^3}{\alpha\nu} \qquad (2.18)$$

Like the Grashof, number the Rayleigh number includes a lot more terms than necessary. It is simply another way of monitoring the buoyancy.

Upon placing the non-dimensional parameters in equations 2.10 and 2.11, the relative importance of each terms is determined by the magnitude of these non-dimensional parameters.

Momentum Conservation:

$$\acute{\rho}(\acute{u} \bullet \acute{\nabla})\acute{u} = -\acute{\nabla}\acute{p} + \frac{1}{Re_{D_h}}[\frac{\acute{\nabla}(\acute{\nabla}\bullet\acute{u})}{3} + \acute{\nabla}^2\acute{u}]$$

$$+ \acute{\rho}(1 - \acute{\beta}\acute{\theta})[(Rot)(-2\acute{\Omega} \times \acute{u}) + (Rot)^2\frac{R_m}{d_h}(-\acute{\Omega} \times (\acute{\Omega} \times \acute{r}))] \qquad (2.19)$$

Energy Conservation:

$$\acute{\rho}(\acute{u} \bullet \acute{\nabla})\acute{H} = \frac{1}{Pr}\frac{1}{Re_{D_h}}\acute{\nabla}^2\acute{T} + Eck(\acute{u} \bullet \acute{\nabla})\acute{p} + \frac{1}{Re_{D_h}}Eck\acute{\Phi}+$$

$$\acute{\rho}(1 - \acute{\beta}\acute{\theta})Eck(Rot)^2\frac{R_m}{d_h}(-\acute{\Omega} \times (\acute{\Omega} \times \acute{r})) \qquad (2.20)$$

2.3 The Heat Transfer Coefficient and Nusselt Number

The heat transfer coefficient is determined by performing a heat balance on the test section. The forms of heat which have to be considered within the test section are

convection, conduction, radiation, and heat generation or accumulation. If a control volume is drawn around the test section, the following equation yields the heat transfer coefficient.

$$hA_s(T_w - T_\infty) - K_n\nabla T \bullet A_n + \epsilon\sigma A_s(T^4 - T_o^4) = Q_{gen}A_s \qquad (2.21)$$

The Nusselt number is the ratio of the energy convected by the fluid to energy conducted by the fluid[13]. It is the standard non-dimensional representation of heat transfer in the turbine blade cooling field. In the G.T.L. Heat Transfer Experiment the Nusselt number is normalized as follows for comparison with fully developed flow in a channel.

$$\frac{Nu}{Nu_\infty} = \frac{\bar{h}D_h}{k_f}\frac{1}{0.023Re_d^{4/5}Pr^{1/3}} \qquad (2.22)$$

The denominator being given by the Colburn equation [13] which is applicable for Reynolds numbers in the range of 20,000 - 300,000 which covers all the data produced by the G.T.L. heat transfer experiment. Like the Rayleigh number, the Nusselt number is also a function of the Grashof and the Prandtl number. The results are presented in the form of equation 2.22 versus radial distance or circumferential distance. The data compares the variation with one non-dimensional parameter when the other non-dimensional parameters are kept constant.

Chapter 3

EXPERIMENTAL OVERVIEW

Before discussing the results, this chapter gives a brief overview of the experimental procedure and how the final data is obtained. Chapter 8 discusses the experimental apparatus used to obtain the data presented in Chapter 4. Chapter 2 discusses the important non-dimensional parameters relevant to rotational effects on heat transfer in turbine blade cooling. These non-dimensional parameters are computed using the manually recorded data shown on the table in figure 3-1 along with the infrared detector measurements.

3.1   The Non-Dimensional Parameters

The Reynold number, $\frac{\dot{m}D_h}{\mu A}$, is computed using manually recorded data from various measuring devices described in Chapter 8. The Reynold number is based on hydraulic diameter in this particular experiment. The hydraulic diameter, $D_h = \frac{4A}{P}$ where A is area and P is perimeter, varies for each test section but is approximately 7.5mm. The local bulk temperature is obtained from a linear fit of the measured inlet and outlet temperatures. It is used to compute the dynamic viscosity, μ, using a curve fit to experimental data taken from *Thermophysical Properties of Refrigerants*[2].

$$\mu = 1.0 \times 10^{-6} \frac{\sqrt{Tb_{avg}}}{0.75309 + \frac{188.969}{Tb_{avg}} - \frac{803.786}{Tb_{avg}^2}} \tag{3.1}$$

Data Sheet-Heat Transfer Experiment

	TEST____				TEST___				TEST___			
	Front	Right	Left	Back	Front	Right	Left	Back	Front	Right	Left	Back
Mflow(%)												
Tflow8(F)												
Pflow(psig)												
Tinlet1(F)												
Tinlet2(F)												
Toutlet3(F)												
Toutlet4(F)												
Pstatic(psi)												
P2(psi)												
P3(psi)												
P4(psi)												
P5(psi)												
Icur.(Amps)												
Speed(rps)												
Vacuum(psi)												
Voltage												
	Red	Buoy.	Dens.	Rot.	Red	Buoy.	Dens.	Rot.	Red	Buoy.	Dens.	Rot.

Test Section Geometry & Angle: Comments: Date:_____

Name:_____

Figure 3-1: Manually Recorded Parameters

The massflow is computed using equation 3.2. Perc is the measurement taken from the flow meter. Temperature, T, and pressure, Pres, are the inlet flow temperature and pressure measured immediately after the flow meter. The one constant, 6.85, depends on the float used in the F. & P. Co. flow tube, see Chapter 8. 120.93 is the molecular weight of freon-12. All other numbers are constants which yield $\dot{m}$ in kg/s. The Reynolds number used in the Colburn equation, which normalizes the Nusselt number, changes with radial pass because the local bulk temperature varies.

$$\dot{m} = perc * \frac{6.85 * 1.183 * 0.06243}{2.204^? * 60.0} * \sqrt{\frac{Pres * 298.16 * 120.93}{1.013 \times 10^5 * T * 28.97}} \qquad (3.2)$$

The Prandtl number,$\frac{C_p \mu}{k_f}$, also varies along the test section effecting the local Nusselt number computed using the Colburn equation. It only varies between 0.73 and 0.75 for most of the data. Both the specific heat, C_p, and the thermal conductivity, k_f, are computed using curve fits to experimental data[2]. Both terms are functions of temperature and yield C_p and k_f in J/kg-K and W/m-K. These parameters change as the flow travels radially outward. In equation 3.4, the bulk temperature is in degrees Rankine. Equations 3.3 uses temperature in degrees Kelvin. As shown by the analysis, the Colburn equation varies along the test section with Reynolds and Prandtl number.

$$C_p = 1000 * (0.116661 + 2.37994 \times 10^{-3} * Tb_{avg} -$$

$$2.94788 \times 10^{-6} * Tb_{avg}^2 + 1.37282 \times 10^{-9} * Tb_{avg}^3) \qquad (3.3)$$

$$k_{freon} = \frac{1.78873 * \sqrt{Tb_{avg}}}{(727.58 + \frac{1.2495 \times 10^6}{Tb_{avg}} + \frac{3.26554 \times 10^8}{Tb_{avg}^2})} \qquad (3.4)$$

The Rotation number, $\frac{\Omega D_h}{u}$, also requires information from a measuring device. Rotation is computed using information received from the optical encoder, see Chapter 7 and 8. The speed is computed from the pulses received from the optical encoder mounted to the end of the shaft. The speed is monitored by the computer along with an addition pulse counter. Using continuity, $u = \frac{\dot{m}}{\rho A}$, the mean radial velocity is calculated. Density is obtained from a look-up table for freon-12 taken from

Thermodynamic Properties of Refrigerants[1] given pressure and temperature.

The Density parameter, $\frac{\Delta \rho}{\rho}$, is calculated by averaging the wall and bulk temperatures over the test section. The temperatures of each element measured on the test section are averaged to one wall temperature. The bulk temperature is averaged between the inlet and outlet temperatures. Given the Density parameter and Rotation number, the Buoyancy parameter is calculated using equation 2.16. Based on the non-dimensional parameters the relative importance of the terms in equation 2.19 and 2.20 are determined.

3.2 Converting Infrared Energy into Surface Temperatures

In addition to the non-dimensional parameters the surface temperature and the Nusselt ratio have to be computed. The surface temperatures are obtained from the raw data measured by the infrared detector. The calibration procedure is discussed later in this chapter and also in Chapter 7: Experimental Procedure.

The computer collects energy from the infrared detector in the form of voltages. These voltages represent the temperature distribution of four surfaces of the test module. In order to analyze the heat transfer properties of a given test section under specific conditions, the voltages are converted into surface temperatures. There are a number of considerations which make the conversion process less than simple. The surface emissivity of the model is not necessarily uniform. The optical system does not see each surface directly which introduces optical distortion and view factor variations. For example, at the top and bottom of the model part of the view of the detector is obscured. The back of the test module is viewed through two mirrors, the leading and trailing through one, and the front directly. The calibration removes the effects of emissivity, optical distortion, and energy losses. The calibration provides an energy versus temperature mapping over a range of temperatures for each element. Having a calibration curve for each element, the raw data from the infrared detector is quickly

converted into temperatures.

The calibration procedure creates five or six voltage versus temperature pairs for each element. The voltage versus temperature mapping is created by running the calibration procedure described in Chapter 3: Experimental Procedure. The calibration scan is identical to the test scan in order to creating an independent curve for each element.

The temperature versus element mapping is determined by fitting a second order equation to three radial temperature measurements made along the test section. The assumption is made based on the heat equation.

$$\nabla \bullet (k \nabla T) + q = \rho c_p \frac{\partial T}{\partial t} \tag{3.5}$$

The calibration procedure is designed to simplify equation 3.5 so it is easy to solve. The heat generation is the electric heating per unit volume. The test is run at steady state, eliminating variations in time. The test module is thin so that temperature drops through the thickness are negligible. There is no flow during the calibration and the module has uniform thickness. Without fluid flow, conduction around the uniform perimeter tends to zero in steady state. Now, equation 3.5 is simplified.

$$\frac{\partial^2 T}{\partial r^2} = -\frac{q}{k} \tag{3.6}$$

Upon integrating twice, the temperature of the test module under the given conditions is a second order polynomial. Therefore the assumption of fitting a second order equation to the three surface temperature measurements is justified.

All the voltages are converted to temperatures by indexing through the data. Given a temperature mapping of the test module, the heat transfer properties at various conditions are determined. Appendix B provides a detailed computation of the temperature using the calibration files.
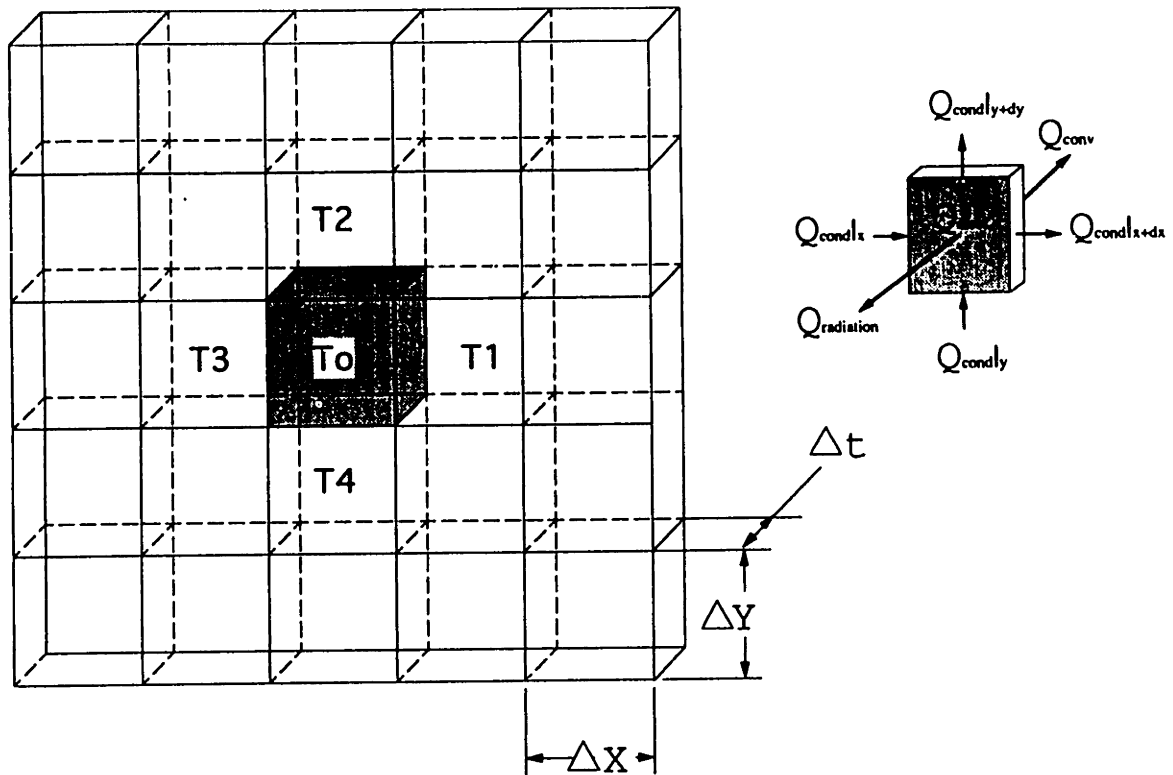
Figure 3-2: Difference Scheme Explanation

3.3 Computing the Nusselt Number Ratio

There are now data files containing a temperature mapping of the four surfaces of the test section. Given a temperature mapping, the heat transfer coefficient is calculated using a difference scheme in the heat balance. For most of the tests, radial passes are taken in 0.25in increments. A data sample is taken along the perimeter of the module every 0.02 inches. The size of each element is $\Delta X x \Delta Y x \Delta t$. ΔX is 0.02in, the sampling rate. ΔY is 0.25in, the radial increment. Δt is 0.01-0.02in, the model thickness. Figure 3-2 shows the model for the difference scheme.

$$h_{elem} = \frac{Q_{elec} - Q_{cond} - Q_{rad}}{A_{elem}(T_w - T_b)} \qquad (3.7)$$

$$h\Delta X \Delta Y (T_w - T_{bulk}) = \frac{I^2 R_f}{2(L+W)t}\Delta X \Delta Y \Delta t + K_f \nabla T \bullet A_n - \epsilon\sigma\Delta X \Delta Y[T_o^4 - T_a^4] \quad (3.8)$$

Four forms of energy transfer occur within the element. There is heat generation in the form of electrical heating from the power supply. There is circumferential and radial condition. Conduction through the test model film is negligible as can be seen by the small Biot number. Energy radiating from the model is measured by the detector. Finally, fluid cools the test section through convection. Using equation 3.8, a heat transfer coefficient is calculated for each element on the test module. There is now both a temperature and a heat transfer mapping of the test module. An example calculation of the heat transfer coefficient is performed in Appendix B.

The conduction term is calculated by taking the derivative of polynomial curve fits to the temperature data. The radial length of the elements are over ten times larger than the circumferential length. The size of the elements cause large variations in the derivative when computed using a finite difference method. Therefore, another method is used to compute the conduction. The temperature profiles are fitted with curves in both the circumferential and radial direction for each element. The derivative is then computed analytically from the polynomial coefficients. In the radial direction, a fourth order polynomial is used in all cases. In the circumferential direction, the front and back faces of the rectangular sections are fitted with second order polynomials. The leading and trailing faces of the rectangular modules are fitted with a linear polynomial because of the small temperature variation across the short face. The short faces of the square module are fitted with linear polynomials for the same reason. Further explanation of the conduction correction factor is given in Chapter 6 on Error Analysis.

In the field of turbine blade cooling, it is standard practice to present data in the form of Nusselt number, $\frac{hD_h}{k}$. Upon computing the heat transfer coefficient, h, the program indexes through the heat transfer coefficient data file and converts the heat transfer coefficients into Nusselt numbers. The Nusselt number is calculated using

equation 2.22. k_f in equation 2.22 is the thermal conductivity of freon-12 calculated using equation 3.4. It is normalized by the Nusselt number in a stationary fully developed flow, $0.023 * Re^{0.8}Pr^{0.333}$, as correlated by the Colburn equation. The Colburn equation is a function of Reynolds number, Re, and Prandtl number, Pr. These parameters are computed locally as the flow travels outward. Once in this form, the data is analyzed and compared with the data of other experimentalists as shown in Chapter 4: Results and Discussion.

Chapter 4

RESULTS AND DISCUSSION

The data presented in the following thesis is a compilation of data collected for four test modules, a smooth square, a smooth rectangular, a turbulated rectangular, and a uneven walled, smooth rectangular module. The uneven walled rectangle is a rectangular test section of the same aspect ratio on which one faces is approximately twice the thickness of the other faces. There are three major parameters which have an effect on the heat transfer in turbine blade cooling; density parameter, Rotation number , and Reynolds number. Variations with each parameter are discussed for each module. The data is presented in the form of temperature in degrees Kelvin versus x/D_h and Nusselt number ratio versus x/D_h. x/D_h is the radial distance along the module divided by the hydraulic diameter. The Nusselt number ratio is the Nusselt number computed from temperature measurements, $\frac{hD_h}{K_f}$ divided by the Nusselt number for fully developed flow in a channel, $0.023 * Re^{0.8} * Pr^{0.33}$. The temperature plots contain two curves for each face of each test. The lower curve which varies linearly represents the bulk temperature profile that is determined from the inlet and outlet temperatures. The more radically varying profile represents the wall temperature measured by the infrared detector. The data is spatially averaged in the circumference direction to create one curve for each face. All the test conditions are presented in appendix D.

Each curve has a certain level of experimental error. The experimental error is negligible except at low Density parameters as shown in the plots that follow. The

error at low Density parameters is between 15-40%. Low Density parameters refers to values below 0.10. In viewing low density data, observations are based on the temperature profiles. The temperature profiles depict enough information to make initial observations that are re-affirmed at higher Density parameters.

In addition, each curve contains a certain level of systematic error. This error is a result of improperly monitoring the cold junction temperature. For the data being presented, the cold junction is always assumed to have a temperature equal to that of the room. Unfortunately, the assumption may not be valid. The temperature of the cold junction may vary significantly as discussed in Chapter 6 on Error Analysis. Any correction introduced as a result of the invalid assumption works to increase the bulk temperature recorded in the plots. The wall temperature measurements suffer less from this error because the calibration is always conducted at low speeds with no flow in which case the cold junction is very close to room temperature. The systematic error does not effect the shape of these curves on the magnitude. Therefore, the trends show are valid.

4.1   Smooth Rectangular Test Module

The smooth rectangular test module simulates a blade cooling passage with an aspect ratio of 3.3. The results of the smooth rectangular geometry are presented first because the most data is available for this particular geometry.

4.1.1   Smooth Rectangle: Effects of Rotation number

In figure 4-1, heat transfer increases with increasing Rotation number on the trailing face. At high rotation, the wall temperature appears to cool below the bulk temperature. The trailing face cools to $280^o K (26^o F)$ which merits further investigation and will be pursued in futur periments. On the leading face, the temperature profiles remain within $20^o K$ of each other over the span of the module despite changing rotation. The heat transfer varies radically on the leading surface showing more heat transfer at lower rotations below x/D_h of 7 and more uniform heat transfer above 7.

Line	Test	Reynolds Number	Density Parameter	Rotation Number	Buoyancy Parameter
Solid	a03	26,000	0.061	0.16	0.094
Dashed	a05	25,000	0.063	0.32	0.397
Dash-Dot	a07	26,000	0.063	0.46	0.810
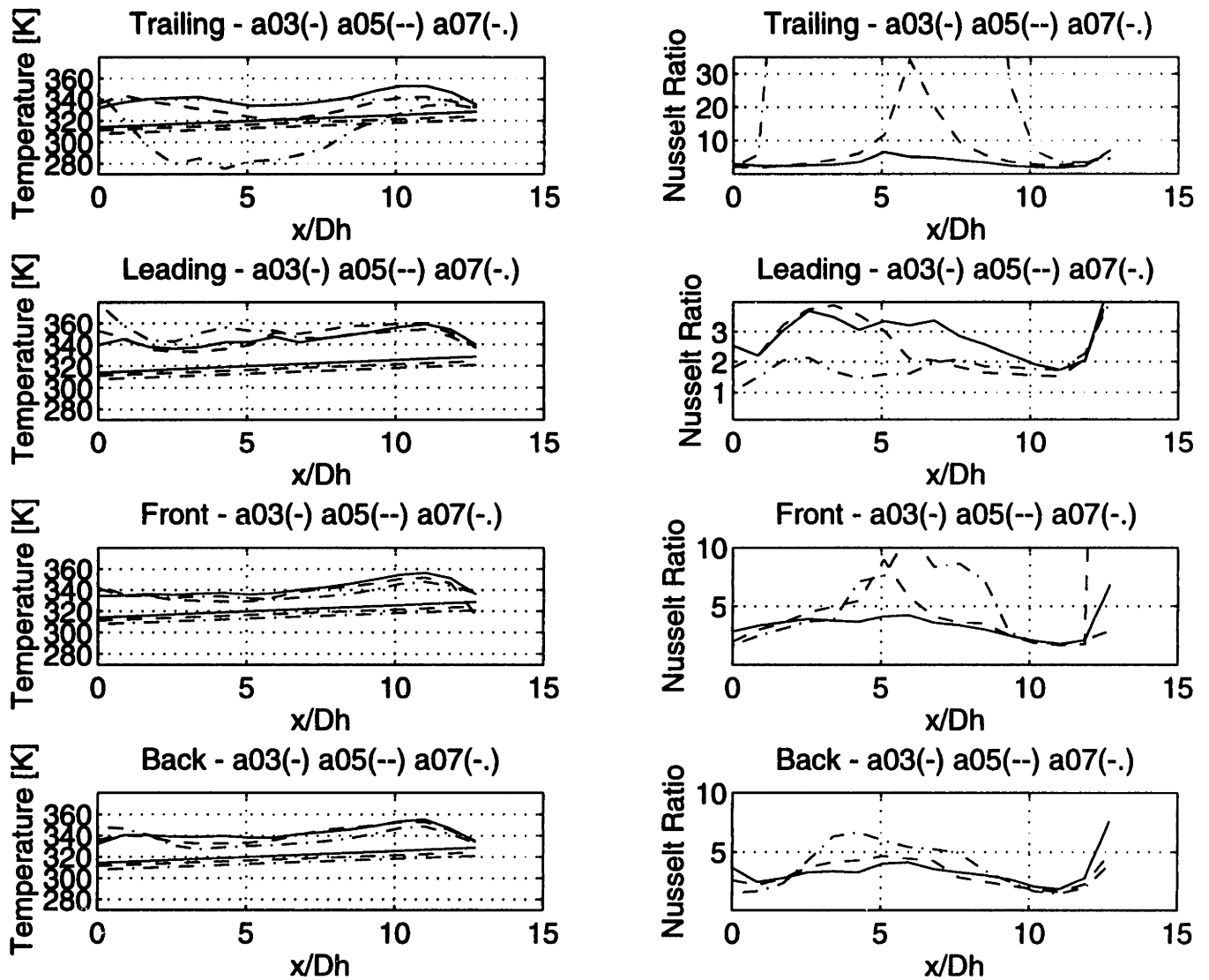
Figure 4-1: Smooth Rectangle- Variation with Rotation number

On the front and back, the temperature only varies $10^o K$ between Rotation numbers of 0.15 and 0.46. On the front and back, the heat transfer is improving with increasing rotation as the flow travels outward.

At a slightly higher Density parameter around 0.2, trends begin to develop as shown in figure 4-2. The error at the moderate Density parameters varies between 6-13% of the measured temperature. The Coriolis forces act quickly on the trailing face, effecting heat transfer almost immediately upon entering the passage. On the trailing face, the Nusselt ratio increases from 1.1 to 1.4 to 1.8 at an x/D_h of 8.5 as Rotation number increases from 0.15 to 0.40. By increasing the Rotation number to 0.29, the trailing side becomes 20-40$^o K$ cooler. As rotation is increased even more, the tra''ng face is up to 85$^o K$ cooler at some points. On the leading face, rotation has a small effect as shown by the small variation in the curves. The heat transfer does not vary consistently on the leading face although the Nusselt ratio is consistently lower than or equal to that of the trailing face. The leading surface experiences inlet effects below x/D_h of 5 where the Coriolis forces do not influence the flow. In the inlet region, at low rotation the leading surface experiences a larger Nusselt ratio. At low Rotation numbers, the Nusselt ratio on the trailing face matches closely with that on the leading face. The temperature profiles of the leading and trailing faces vary by less than 10$^o K$. The Colburn equation, $0.023 * Re^{0.8} * Pr^{0.33}$ [13] can provide a fairly accurate model at low rotation.

At even higher Density parameters around 0.3, rotation continues to enhance heat transfer. Heat transfer improves on all surfaces as shown in figure 4-3. The majority of the effect is still on the trailing face. Even at a low rotation of 0.13 in figure 4-3, the temperature difference between the leading and trailing surface is about 40$^o K$. The difference is as large as 100$^o K$ at high rotation. On the trailing face, the Nusselt ratio increases from 1.2 to 1.7 at x/D_h of 8.5 as Rotation number increases from 0.13 to 0.25. The Nusselt ratio reaches a minimum of 2.0 on the trailing face at the higher rotation. As the wall temperature approaches the bulk temperature, the Nusselt ratio increases sharply above an x/D_h of 11. Even with the small variations, the curves increase in the same order on all faces above an x/D_h of 5. The leading

Line	Test	Reynolds Number	Density Parameter	Rotation Number	Buoyancy Parameter
Solid	a10	25,000	0.205	0.15	0.299
Dashed	a11	25,000	0.198	0.29	0.979
Dash-Dot	a12	26,000	0.205	0.40	2.039

Figure 4-2: Smooth Rectangle- Variation with Rotation number

38

Line	Test	Reynolds Number	Density Parameter	Rotation Number	Buoyancy Parameter
Solid	a13	25,000	0.302	0.13	0.306
Dashed	a16	25,000	0.289	0.25	1.064
Dash-Dot	a18	25,000	0.297	0.39	2.696
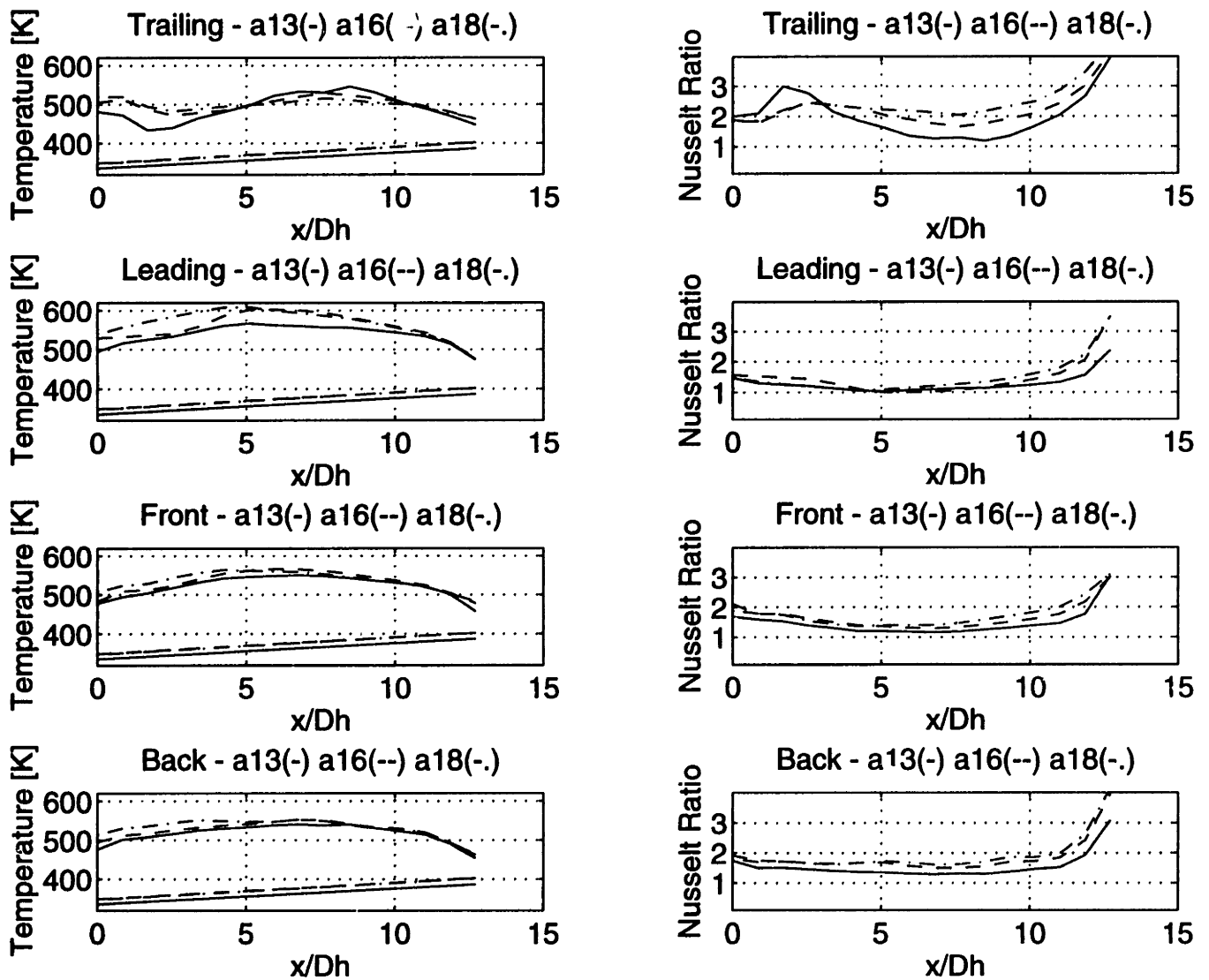
Figure 4-3: Smooth Rectangle- Variation with Rotation number

face experiences the same flow phenomena described above in its inlet region below x/D_h of 5. The leading, front, and back show very little variation with rotation as shown on both the temperature and Nusselt ratio plots.

At a higher Reynolds number of approximately 70,000, rotation has less of an effect on the heat transfer as shown in figure 4-4. Neither the temperature nor Nusselt ratio profiles show much variation with rotation. The low rotation cases below 0.10 have very similar temperature and Nusselt ratio profiles. As rotation is increased to 0.20, the heat transfer reaches a minimum on all the faces. The trend has changed from that noticed in the low Reynolds number cases. At a Rotation number of 0.26, the Nusselt ratio begins to grow again as Coriolis forces become stronger and the heat transfer improves. On the trailing face, the Nusselt ratio is between 1.7 and 2.0 over most of the section for Rotation numbers below 0.20. On the leading face, the Nusselt ratio is consistently lower at about 1.6 to 1.7 except at low rotation. According to the Nusselt plots, the leading face experiences a large heat transfer at a low Rotation number of 0.06. According to the temperature plots, the effect of rotation is very minimal below a Rotation number of 0.10 where the temperature of the leading and trailing faces vary by less than 12^oK. At a Rotation number of 0.20, the difference is 20^oK or less. Rotational effects appear at a Rotation number of 0.26 at this higher Reynolds number.

At the highest Reynolds number conditions, figure 4-5 shows the same fluctuations as the previous case. Due to speed limitations, very high Rotation numbers are not available at high Reynolds numbers. The high flow velocity decreases the Rotation number. Once again, the Nusselt ratio is higher at the lowest rotation below an x/D_h of 4. On the leading surface, the Nusselt ratio is almost identical over the entire section between Rotation numbers of 0.05 and 0.13. The Nusselt ratio is approximately 1.4-1.8 between x/D_h of 3 and 10 on all faces. The Nusselt ratio is lower on the leading face and highest on the trailing. At low rotation, the Nusselt ratio on the leading and trailing surface is about 1.7. The temperature profiles confirm the small effect of rotation at low Density parameters and high Reynolds numbers because the temperatures for all cases vary approximately 10^oK between the leading and trailing

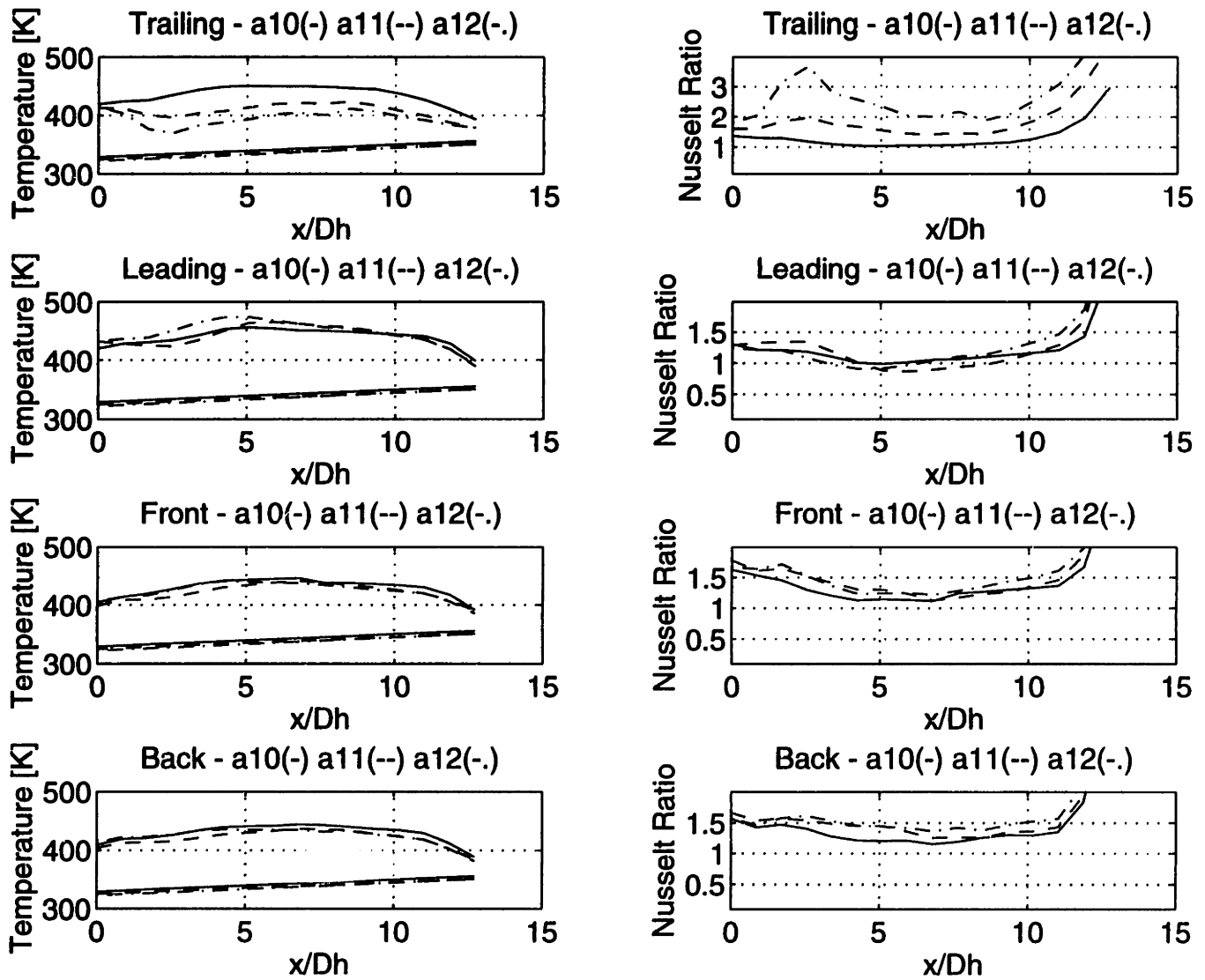| Line	Test	Reynolds Number	Density Parameter	Rotation Number	Buoyancy Parameter
Solid	a25	70,000	0.102	0.06	0.020
Dashed	a26	69,000	0.096	0.10	0.059
Dash-Dot	a36	71,000	0.114	0.20	0.291
Dotted	a34	69,000	0.104	0.26	0.442
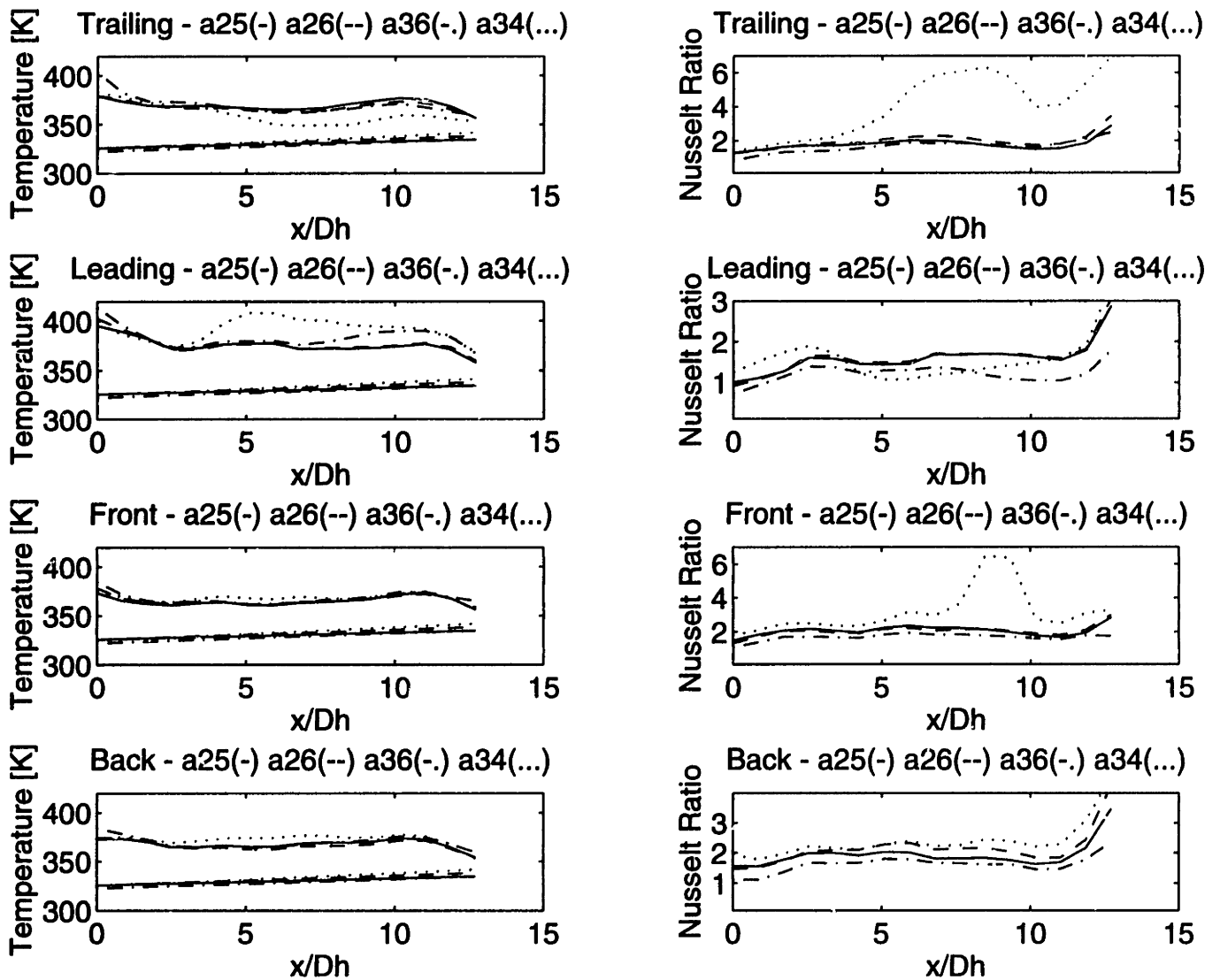
Figure 4-4: Smooth Rectangle- Variation with Rotation number

41

Line	Test	Reynolds Number	Density Parameter	Rotation Number	Buoyancy Parameter
Solid	a19	141,000	0.103	0.03	0.004
Dashed	a21	144,000	0.106	0.05	0.016
Dash-Dot	a41	144,000	0.107	0.10	0.066
Dotted	a40	141,000	0.104	0.13	0.106
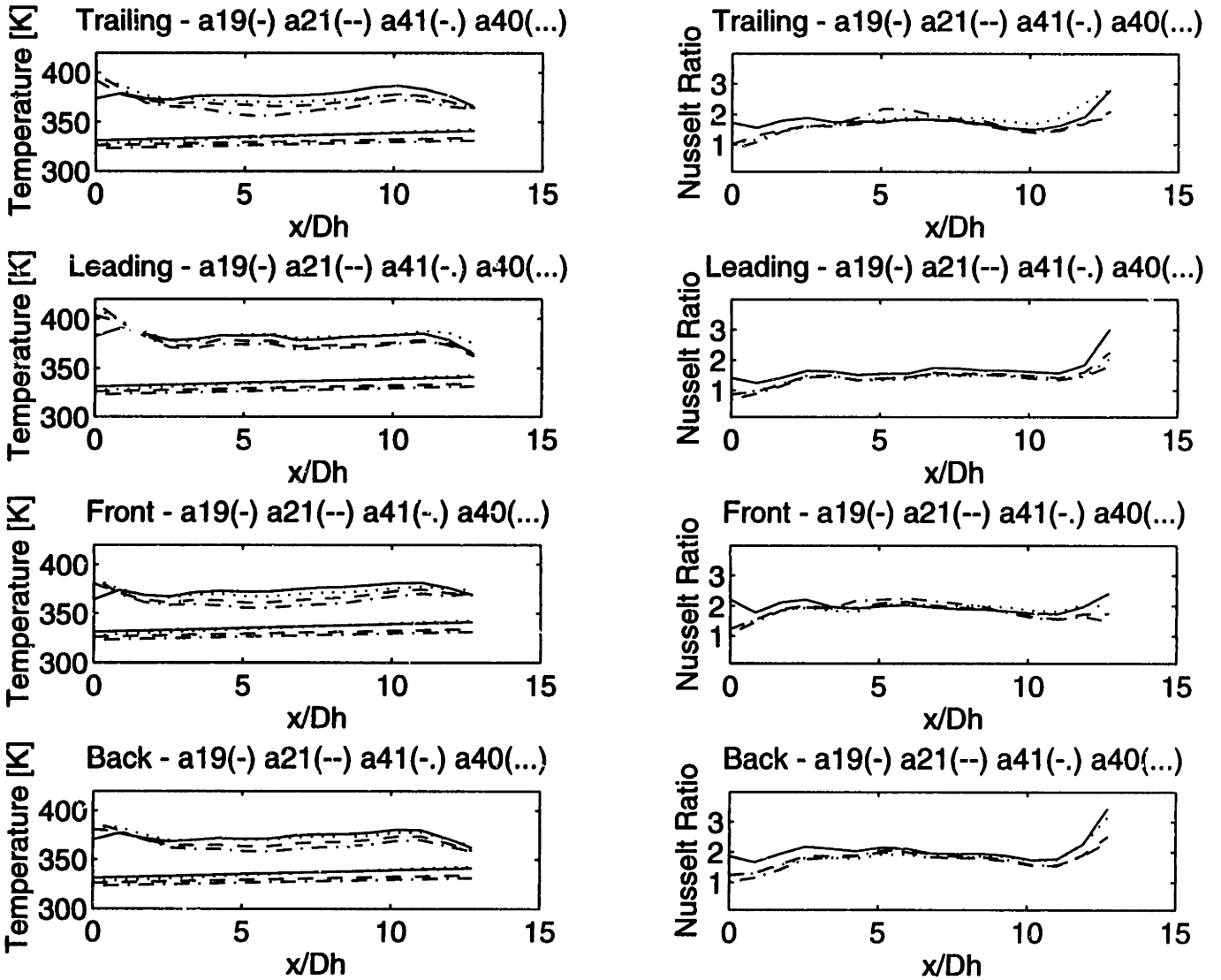
Figure 4-5: Smooth Rectangle- Variation with Rotation number

face at all rotations. At the particular high Reynolds numbers cases in figure 4-5, the Coriolis effects have not had time to develop due to high flow velocities resulting in a different trend. The heat transfer decreases slightly as Rotation number changes from 0.03 to 0.10. As Coriolis effects begin to grow at a Rotation number of 0.13, the heat transfer improves. Test at higher Rotation numbers are necessary to confirm these observations.

4.1.2   Smooth Rectangle: Effects of Density parameter

Figure 4-6 shows that increasing Density parameter decreases heat transfer to a minimum at some moderate value. As in previous cases, the heat transfer rises sharply at low Density parameter. But as the Density parameter increases from a moderate level to a high level, heat transfer begins to increase again at a slower rate. Figure 4-6 shows the Nusselt ratio increasing between 0.06 and 0.3 on each face as the Density parameter increases from 0.205 to 0.278. Figure 4-7 also shows a slight improvement in Nusselt ratio as the Density parameter changes from 0.205 to 0.297 at a higher Rotation number of 0.40. The two figures confirm the existence of a minimum level of heat transfer at some moderate Density parameter. Such information provides a lower bound for heat transfer calculations. In previous experiments involving constant wall temperature instead of constant flux, the data presented by Johnson and Wagner shows that heat transfer increases with increasing Density parameter between values of 0.07 and 0.22[16] in a constant wall temperature experiment.

4.1.3   Smooth Rectangle: Effects of Reynolds Number

The Nusselt number ratio removes most Reynolds dependency. When rotation and buoyancy effects are at a minimum, the Nusselt ratio should approach unity. There is low rotation data at different Reynolds numbers but no data at moderate Density parameters in which heat transfer is minimized. In comparing conditions at the same Density parameter and the same rotation, the effect of Reynolds number comes out. According to figure 4-8, the temperature and Nusselt ratio profiles have

43

Line	Test	Reynolds Number	Density Parameter	Rotation Number	Buoyancy Parameter
Solid	a04	25,000	0.046	0.16	0.074
Dashed	a03	26,000	0.061	0.16	0.094
Dash-Dot	a10	25,000	0.205	0.15	0.299
Dotted	a09	21,000	0.278	0.16	0.459
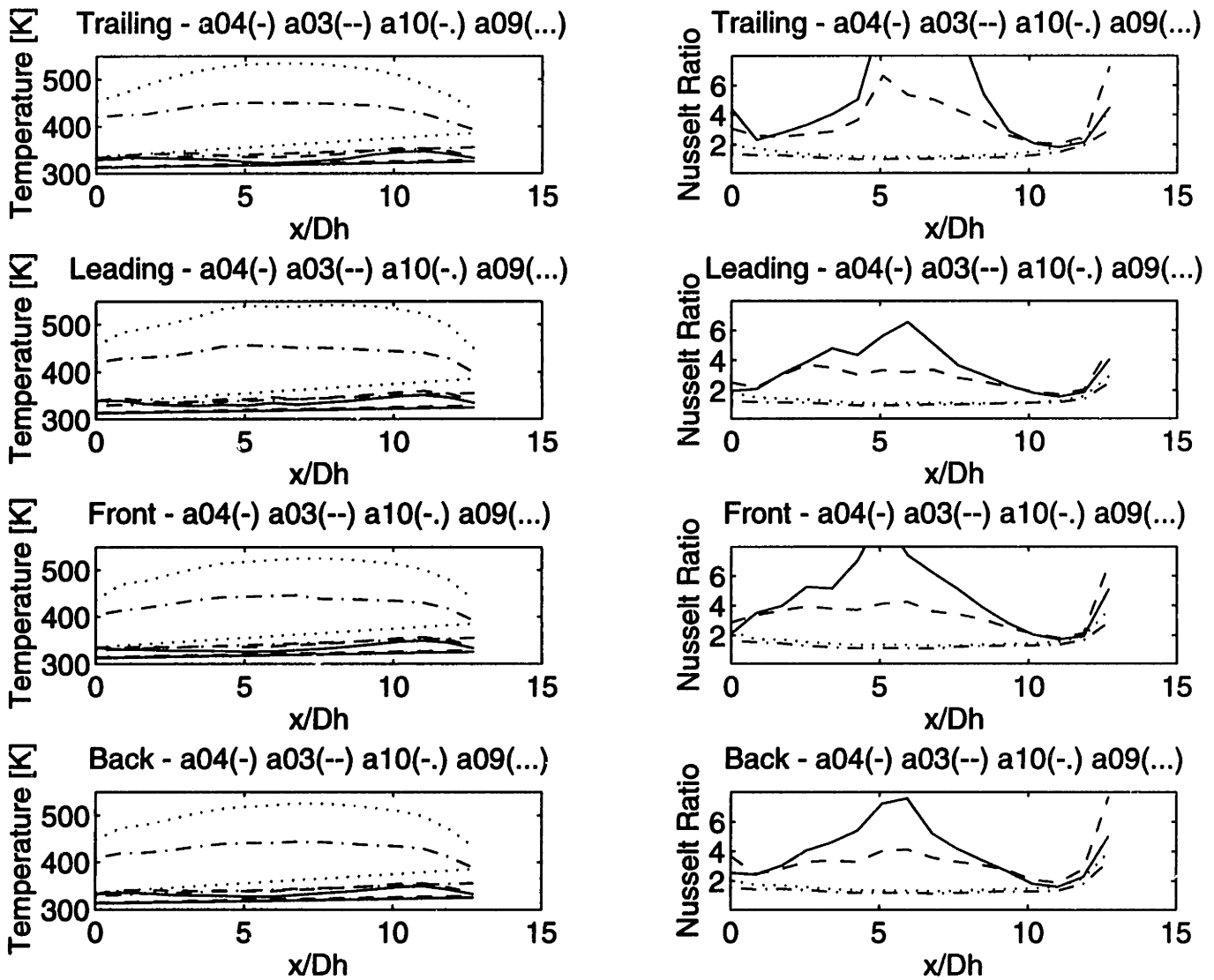
Figure 4-6: Smooth Rectangle- Variation with Density parameter

Line	Test	Reynolds Number	Density Parameter	Rotation Number	Buoyancy Parameter
Solid	a12	26,000	0.205	0.40	2.039
Dashed	a18	25,000	0.297	0.39	2.696
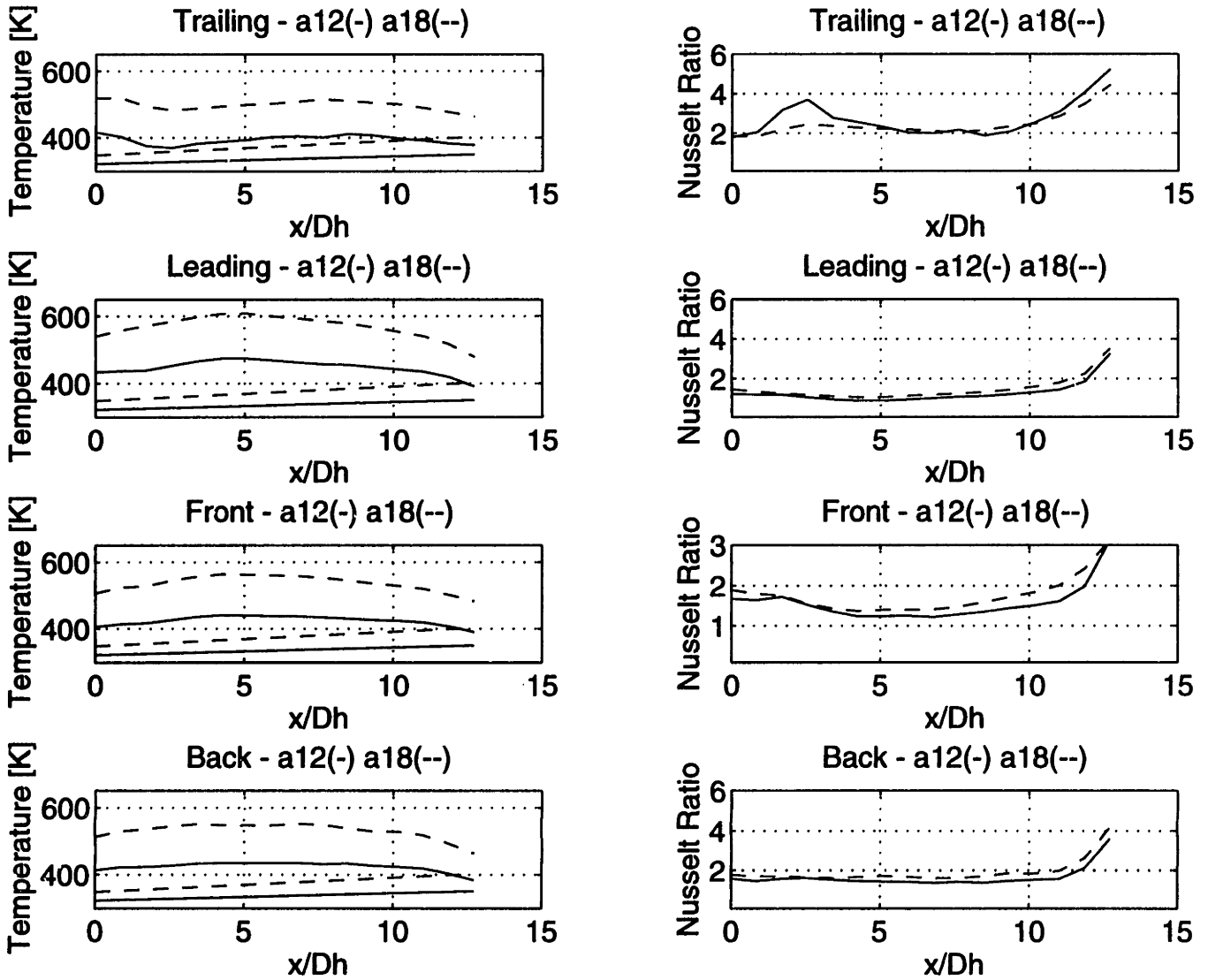
Figure 4-7: Smooth Rectangle- Variation with Density parameter

Line	Test	Reynolds Number	Density Parameter	Rotation Number	Buoyancy Parameter
Solid	a24	73,000	0.095	0.05	0.016
Dashed	a21	144,000	0.106	0.05	0.016
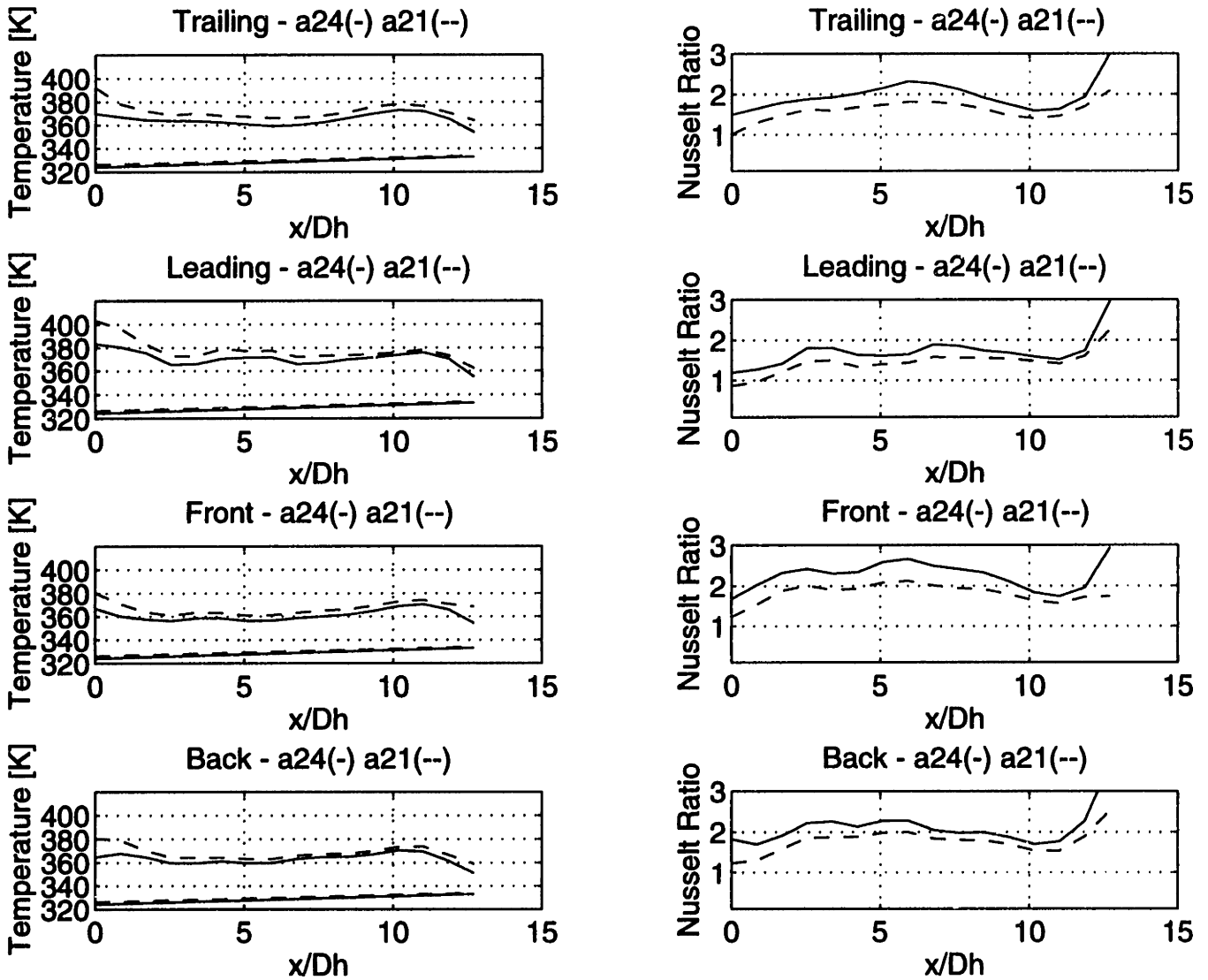
Figure 4-8: Smooth Rectangle- Variation with Reynolds Number

the same shape but the Nusselt ratio at the low Reynolds number is consistently higher. Because the profiles have similar shapes but the temperature of a21 is higher than a24 by some constant temperature around 5^oK, the Density parameter appears to drive the heat transfer in this figure. At these levels, heat transfer decreases with increasing Density parameter. Additional test at moderate Density parameters can help confirm the effect of Reynolds number on the Nusselt ratio for smooth rectangular sections.

4.2   Square Test Module

The square test module simulates a blade cooling passage with an aspect ratio of 1. The data for the square test section can be most directly compared to data other experimentalists have collected.

4.2.1   Smooth Square: Effects of Rotation number

The smooth rectangular data shows increasing Rotation number improves heat transfer at low Reynolds. Figures 4-9 and figure 4-10 show that a similar trend exist for the square geometry. According to previously discussed data, rotational effects are present at a value of 0.21. The most noticeable difference is that the heat transfer is larger at the inlet compared to the smooth rectangle. As flow enters the rectangular cross-section, the boundary layers merge quickly because of its aspect ratio. With a square cross section, the boundary layers have more room taking longer to develop. In the entry region, the boundary layers are thinner and heat transfer improves. As the module reaches a maximum temperature on the leading face, the Nusselt ratio reaches a minimum at 1.08 and 2.02 for an x/D_h of 7.6 in figure 4-9. Increasing the Rotation number to 0.55 increases the Nusselt ratio to 1.68 and 2.72 on the trailing face. These values are very close to a similar case for the smooth rectangle. The developing boundary layers drive the inlet temperatures down creating a larger Nusselt ratio at the inlet. At a slightly higher Density parameters, figure 4-10 shows the same trend. Test m55 is a low Rotation number where rotation has negligible

47

Line	Test	Reynolds Number	Density Parameter	Rotation Number	Buoyancy Parameter
Solid	m47	32,000	0.239	0.21	0.671
Dashed	m43	29,000	0.229	0.55	4.300

Figure 4-9: Smooth Square- Variation with Rotation number at Moderate density

Line	Test	Reynolds Number	Density Parameter	Rotation Number	Buoyancy Parameter
Solid	m55	33,000	0.266	0.11	0.197
Dashed	m44	29,000	0.274	0.35	2.102
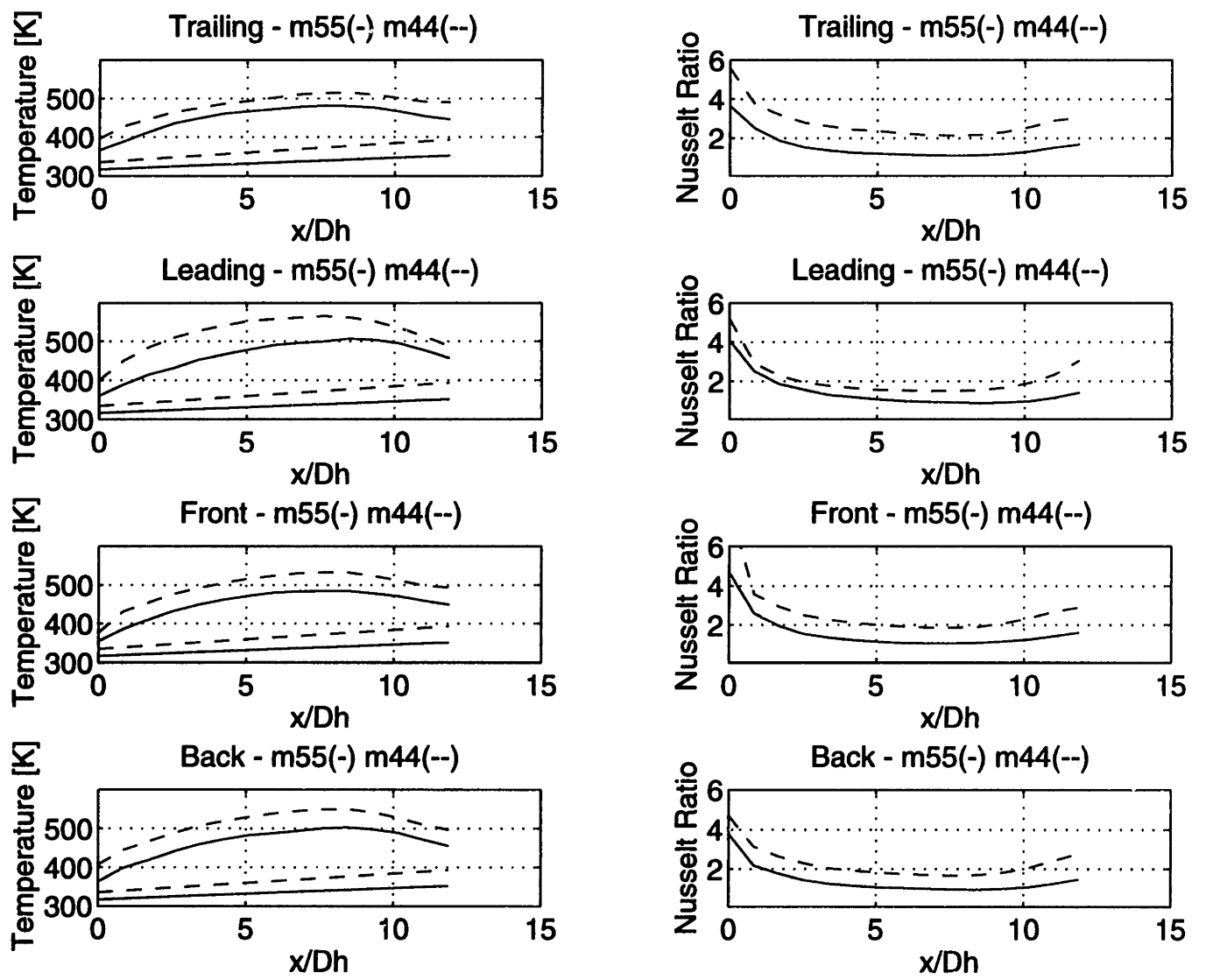
Figure 4-10: Smooth Square- Variation with Rotation number at Moderate density

effects on the Nusselt ratio as it approaches a minimum of 0.95 on the leading face and 1.1 on the trailing face at an x/D_h of 7.6. As rotation increases to 0.35, the Nusselt ratio grows to 1.5 on the leading and 2.2 on the trailing. The effect of rotation continues to enhance heat transfer.

Figure 4-11 shows that the trend continues for the square module at a Reynolds number of 60,000 and a high Density parameter. The error at these run conditions is significantly reduced. The smooth rectangular module shows less of an effect on heat transfer at 70,000 relative to the effect shown in figure 4-11. At higher Reynolds numbers the entry length grows[13] helping the square geometry enhance heat transfer. The Nusselt ratio on the leading and trailing surfaces are almost identical at low Rotation number while the difference grows as rotation increases. At low rotation, the trailing side is only slightly cooler than the leading, approximately $10\text{-}20^o K$. The small effect of rotation at low rotation is duplicated in the Nusselt ratio plot as the Nusselt ratio only increases from 1.0 on the leading to 1.1 on the trailing. At a Rotation number of 0.15, the effect begins to grow as the trailing Nusselt ratio increases to 1.3 compared to unity on the leading face. The effects are even stronger at a Rotation number of 0.26 where the Nusselt ratio on the leading face has grown to 1.3 and that on the trailing face to 2.0. The square geometry enhances rotation better than the smooth rectangle at higher Reynolds numbers.

The effect of rotation is more difficult to determine at high Reynolds numbers. The temperature shows an average temperature difference of $30\text{-}40^o K$ for both test cases in figure 4-12. The effect of rotation is less significant at high Reynolds numbers as captured in the Nusselt ratio plots. Test m53 and m54 are at low Rotation number where, according to previous test, rotational effects are small. Despite the lower Density parameter in m53 rotation enhances heat transfer. According to previously discussed data, heat transfer increases with increasing Density parameter at such levels. So, the rotation is driving the heat transfer despite the slightly different Density parameters. In the low rotation cases, the Nusselt ratio reaches a minimum of 0.9 on the leading face and a minimum of 1.1 on the trailing faces. The difference grows to 1.0 and 1.3 at a Rotation number of 0.10. Although the effect is small,

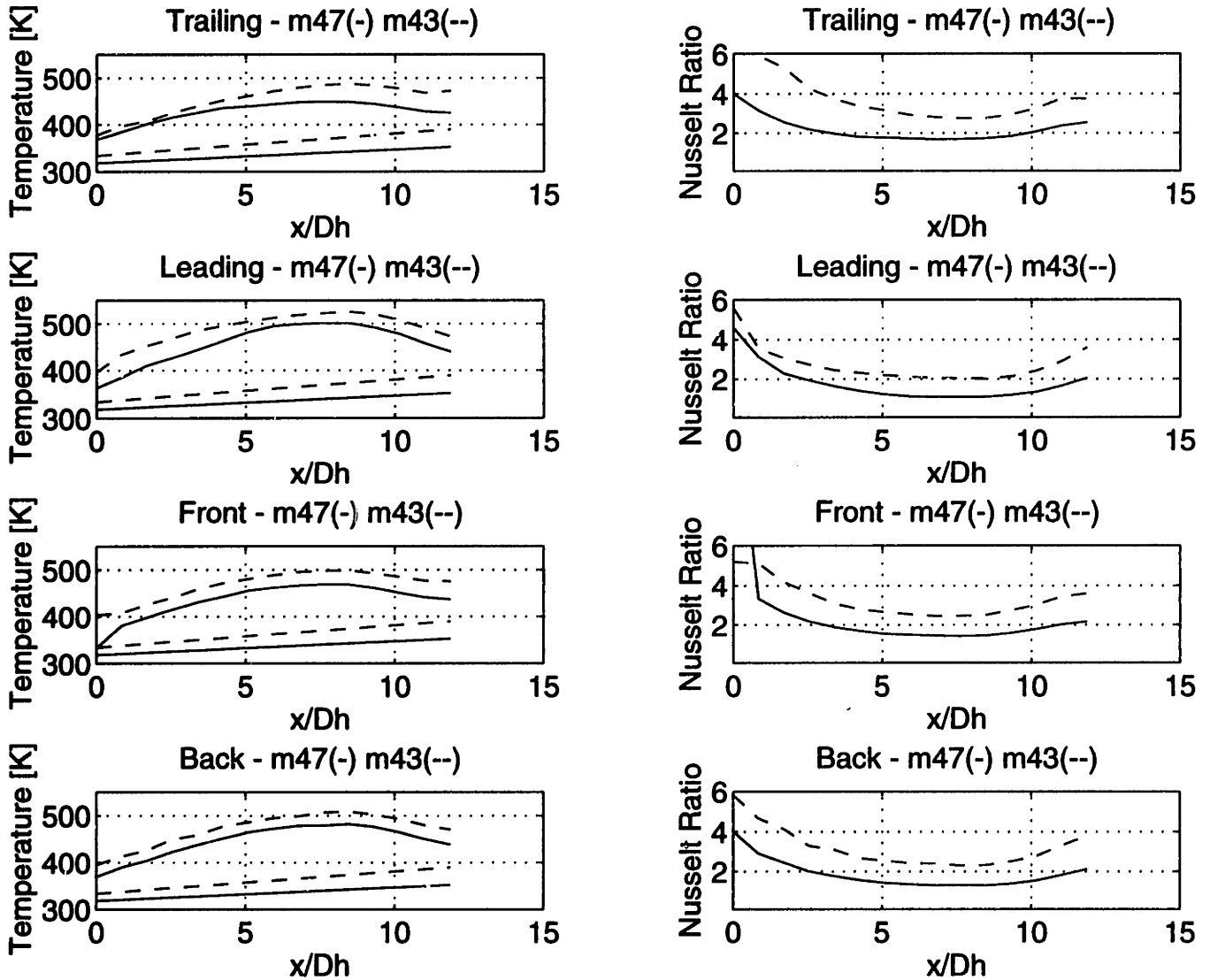| Line	Test	Reynolds Number	Density Parameter	Rotation Number	Buoyancy Parameter
Solid	m49	61,000	0.323	0.10	0.192
Dashed	m51	61,000	0.302	0.15	0.424
Dash-Dot	m50	56,000	0.290	0.26	1.232

Figure 4-11: Smooth Square- Variation with Rotation number at High density

Line	Test	Reynolds Number	Density Parameter	Rotation Number	Buoyancy Parameter
Solid	m54	120,000	0.302	0.06	0.066
Dashed	m53	124,000	0.278	0.10	0.173
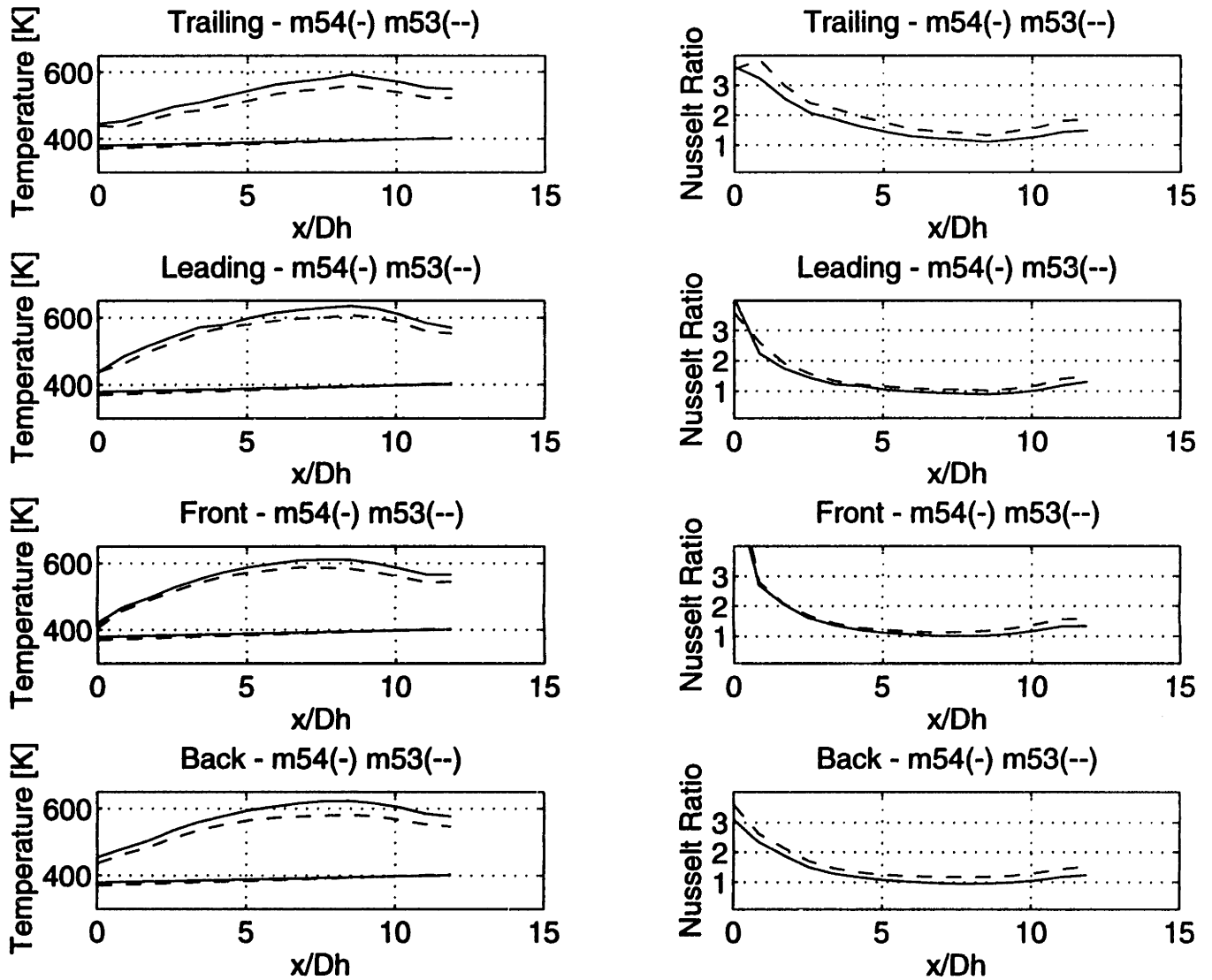
Figure 4-12: Smooth Square- Variation with Rotation number at High density

Coriolis forces continue to act at higher Reynolds numbers.

4.2.2 Smooth Square: Effects of Density parameter

Comparison of m55 and m46 shows that Density parameter has very little effect on the heat transfer above 0.266. The slight improvement in heat transfer shown in figure 4-13 is consistent with smooth rectangular data. At a low rotation where rotational effects are small, increasing the Density parameter slightly improves heat transfer above some moderate value. The Nusselt ratio on the leading and trailing faces varies from a minimum of 0.9 to 1.1 at an x/D_h of 6.8 in test m46. It varies from 1.0 to 1.2 at the same location in test m55. The improvement is very small. Smooth rectangular data shows a minimum in heat transfer at some moderate Density parameter around 0.2. No comparable low density data is available to determine a significant trend on the smooth square at this time.

4.2.3 Smooth Square: Effects of Reynolds Number

Figure 4-14 shows that Reynolds number has very little effect on the leading face but a larger effect on the trailing face near the inlet. At a Rotation number of 0.10, the effects of rotation are just beginning to develop. On the leading face, the Nusselt ratio barely changes over the entire section varying by less than 0.1 at both Reynolds numbers. On the trailing face, the higher Reynolds flow experiences more heat transfer. Since the boundary layer takes longer to develop at higher Reynolds numbers, the trend is logical. The difference in Nusselt ratio decreases as the higher Reynolds flow becomes fully developed. The heat transfer on the other three faces is almost identical at both Reynolds numbers varying by less than 0.2 over the span of the test module. As at low Reynolds numbers, the inlet effect continues on the square test section. Unlike the smooth rectangle, the present case is at a high Density parameter in which Nusselt ratio varies slightly with increasing Density parameter.

Figure 4-15 shows a similar trend in the Reynolds number on the trailing face. The higher Reynolds number case experiences more heat transfer until the flow becomes

Line	Test	Reynolds Number	Density Parameter	Rotation Number	Buoyancy Parameter
Solid	m55	33,000	0.266	0.11	0.197
Dashed	m46	29,000	0.349	0.12	0.325
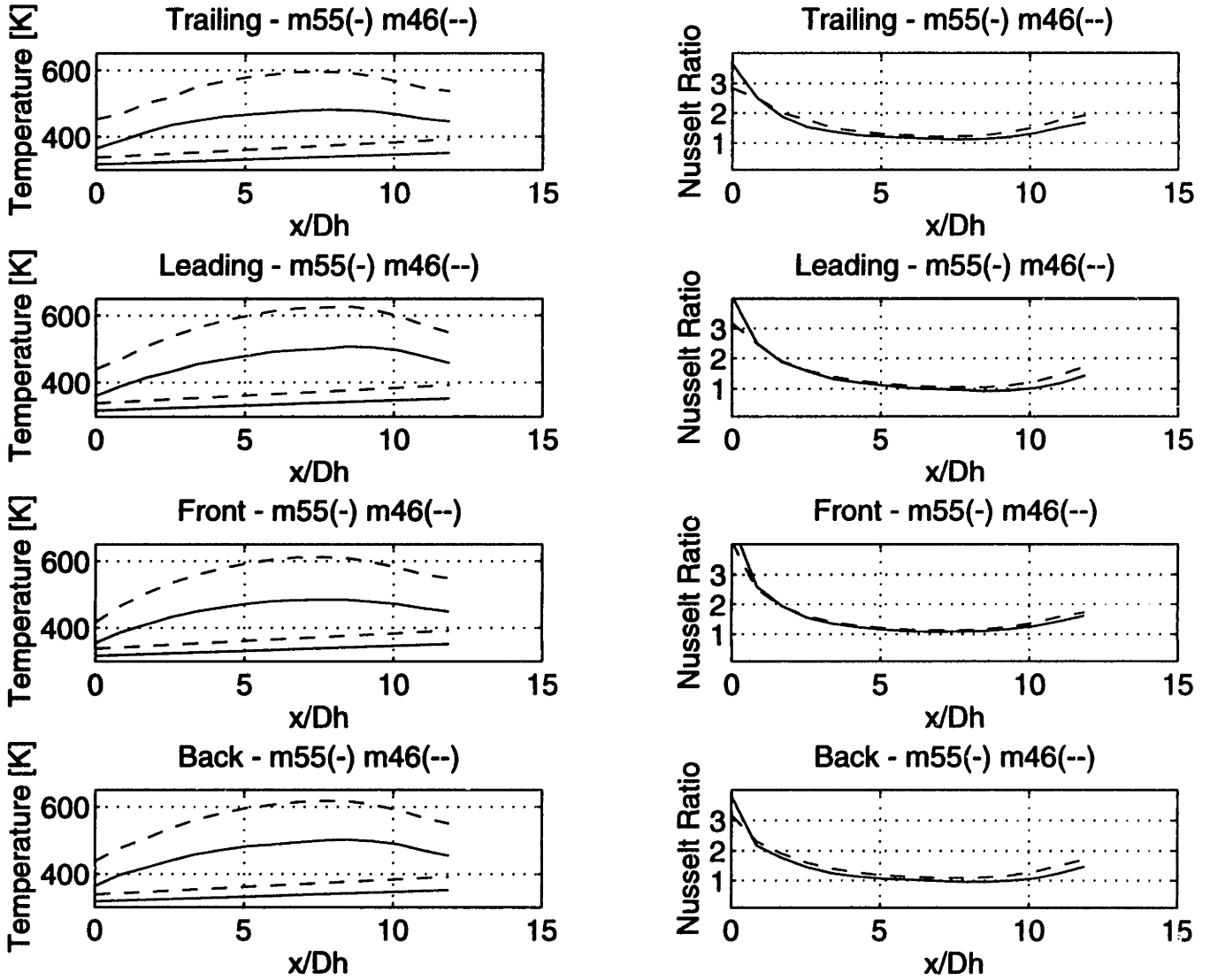
Figure 4-13: Smooth Square- Variation with Density parameter

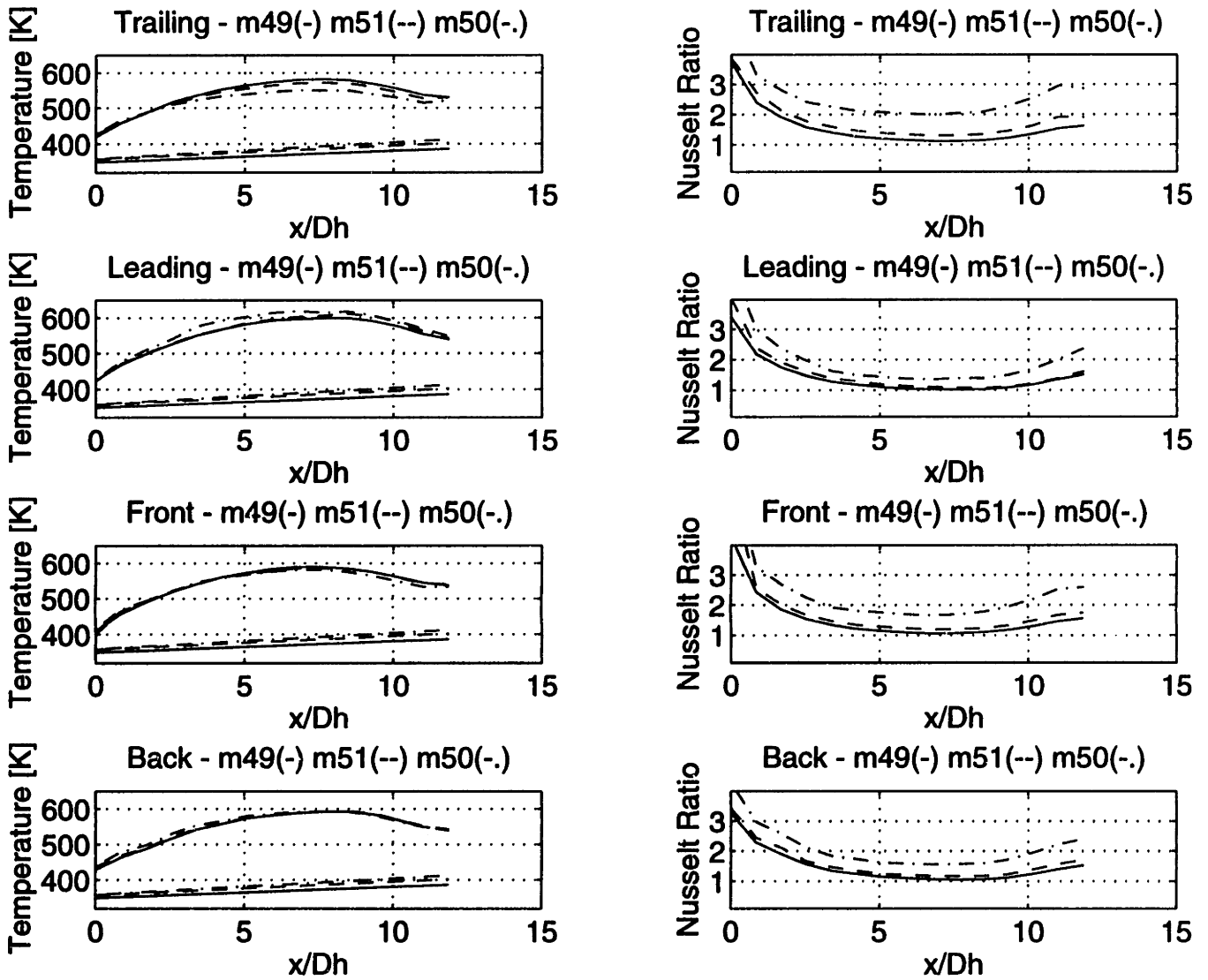| Line	Test	Reynolds Number	Density Parameter	Rotation Number	Buoyancy Parameter
Solid	m55	33,000	0.266	0.11	0.197
Dashed	m53	124,000	0.278	0.10	0.173
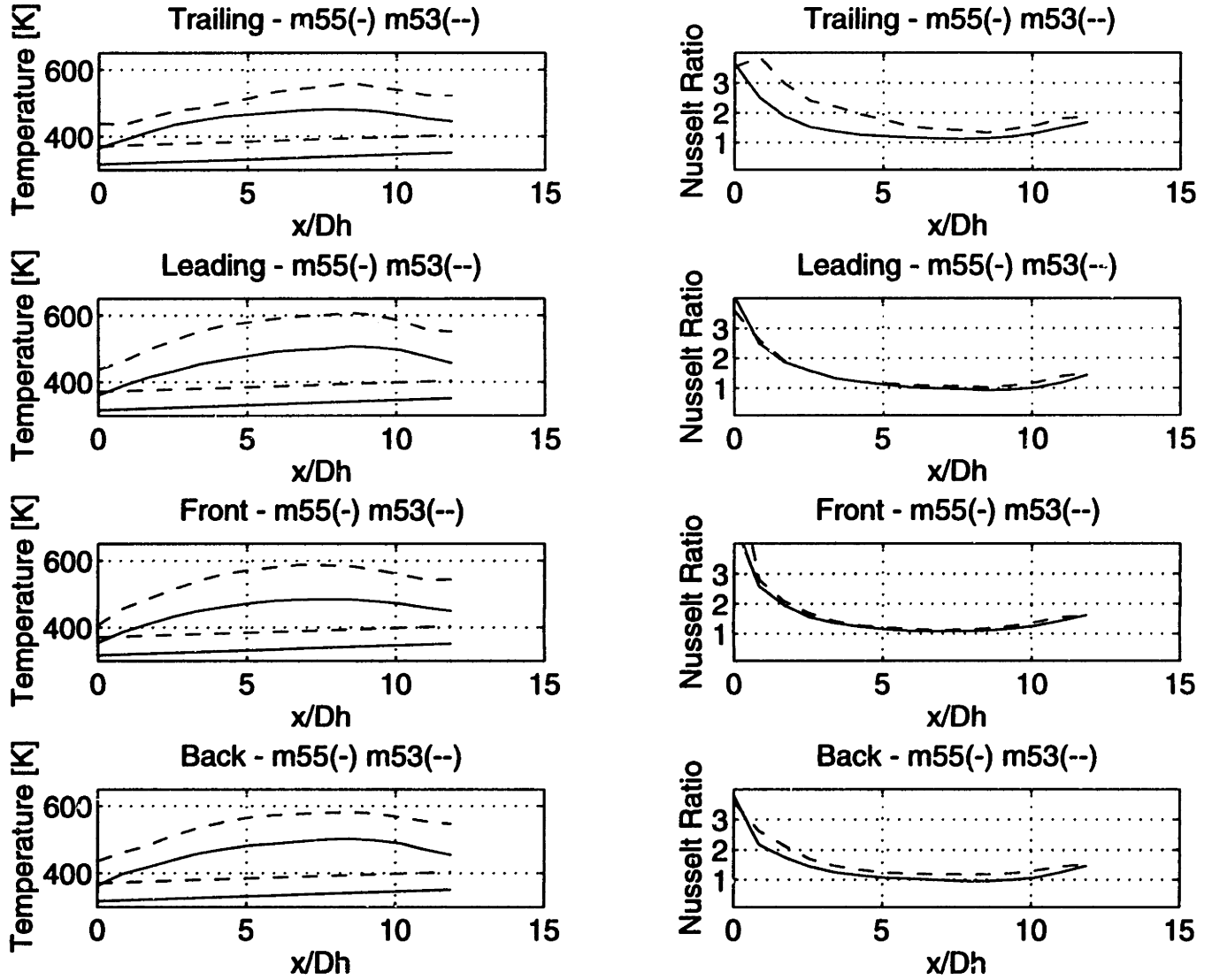
Figure 4-14: Smooth Square- Variation with Reynolds Number

Line	Test	Reynolds Number	Density Parameter	Rotation Number	Buoyancy Parameter
Solid	m64	86,000	0.301	0.07	0.081
Dashed	m54	120,000	0.302	0.06	0.066
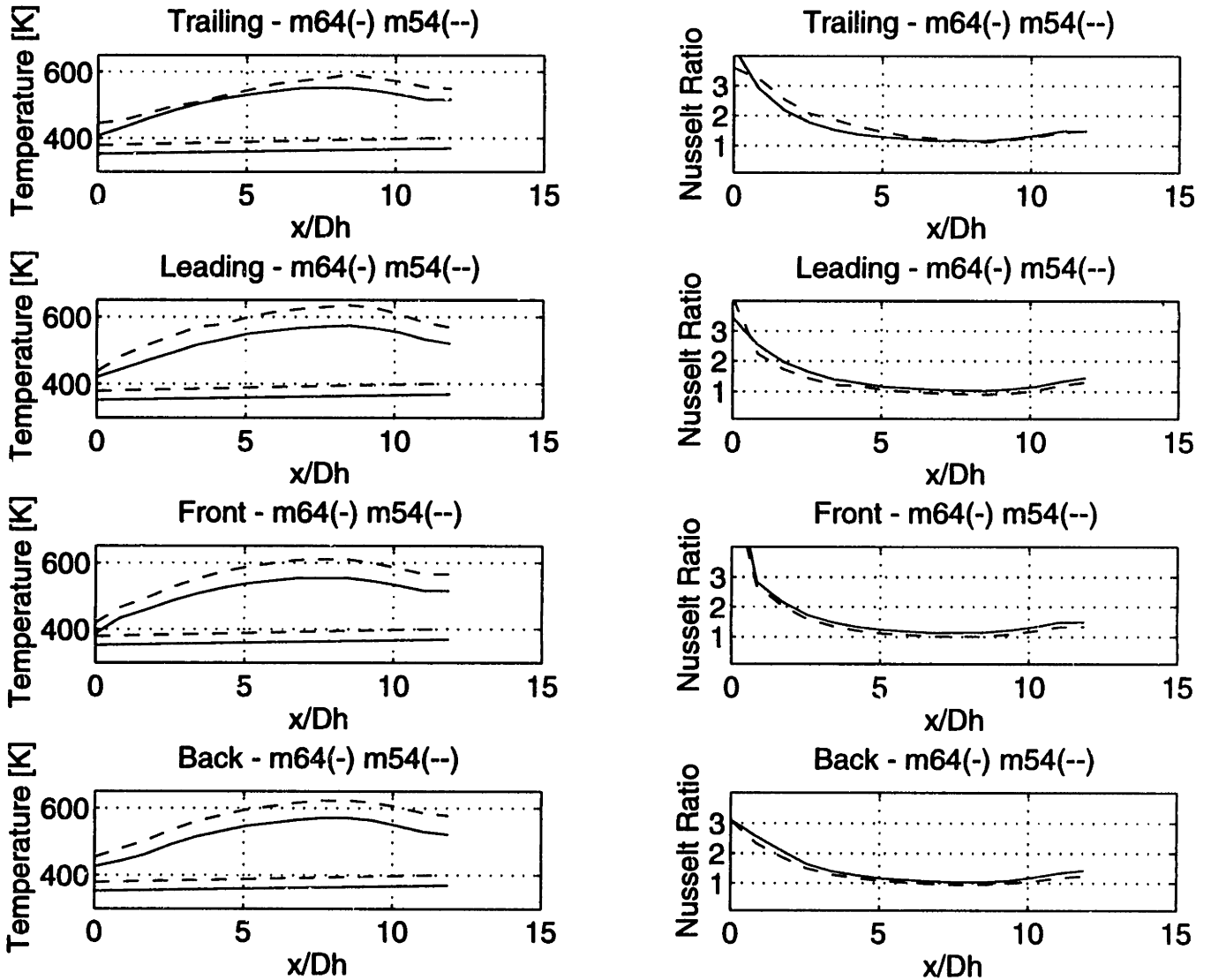
Figure 4-15: Smooth Square- Variation with Reynolds Number

fully developed around an x/D_h of 8. Above an x/D_h of 8, the small increase in Rotation number drives the heat transfer of m64 above m54 on the trailing face. The heat transfer does not vary significantly on the other three faces. In fact, the Nusselt ratio curves vary by less than 0.2 over the span of the test module. According to the smooth rectangle, increasing Reynolds had negligible effect on the heat transfer. The effect is negligible on three surfaces. As the Reynolds number has minimal effect on the heat transfer, the same difference in the curve is most like the result of the large Rotation number of m64.

4.3   Turbulated Rectangle

The turbulated rectangular module is identical to the smooth rectangular module except for the fact that it has turbulators to disturb the flow. The turbulators are added in an attempt to improve heat transfer by forcing the boundary layers to re-start after each turbulator. The boundary layers never develop and remain thin. Therefore, heat transfer is increased.

4.3.1   Turbulated Rectangle: Effects of Rotation number

Figure 4-16 displays the variation of heat transfer with Rotation number. The trailing, front, and back surfaces are effected by small differences between the wall and bulk temperature. The phenomena of the wall temperature decreasing below the bulk temperature appears. Since the temperature profiles decrease consistently, the Coriolis forces are present and developing. On the leading face, the Nusselt ratio increases as the flow travels radially outward. In fact, the Nusselt ratio varies from 2.07 to 2.71 to 3.40 to 4.08 as Rotation number varies from 0.18 to 0.36 to 0.52 to 0.70 at an x/D_h of 11.0. Before Coriolis forces develop, the variation is much smaller at a x/D_h of 1.6 where the variation is from 2.06 to 1.46 to 1.45 to 1.51. The low rotation experiences more heat transfer around the inlet. At higher rotations, the heat transfer does not change much with rotation at the inlet. The turbulators continually enhance heat transfer as the flow travels radially outward.

Line	Test	Reynolds Number	Density Parameter	Rotation Number	Buoyancy Parameter
Solid	m72	25,000	0.076	0.18	0.140
Dashed	m80	25,000	0.089	0.36	0.679
Dash-Dot	m78	24,000	0.088	0.51	1.373
Dotted	m79	24,000	0.083	0.70	2.421
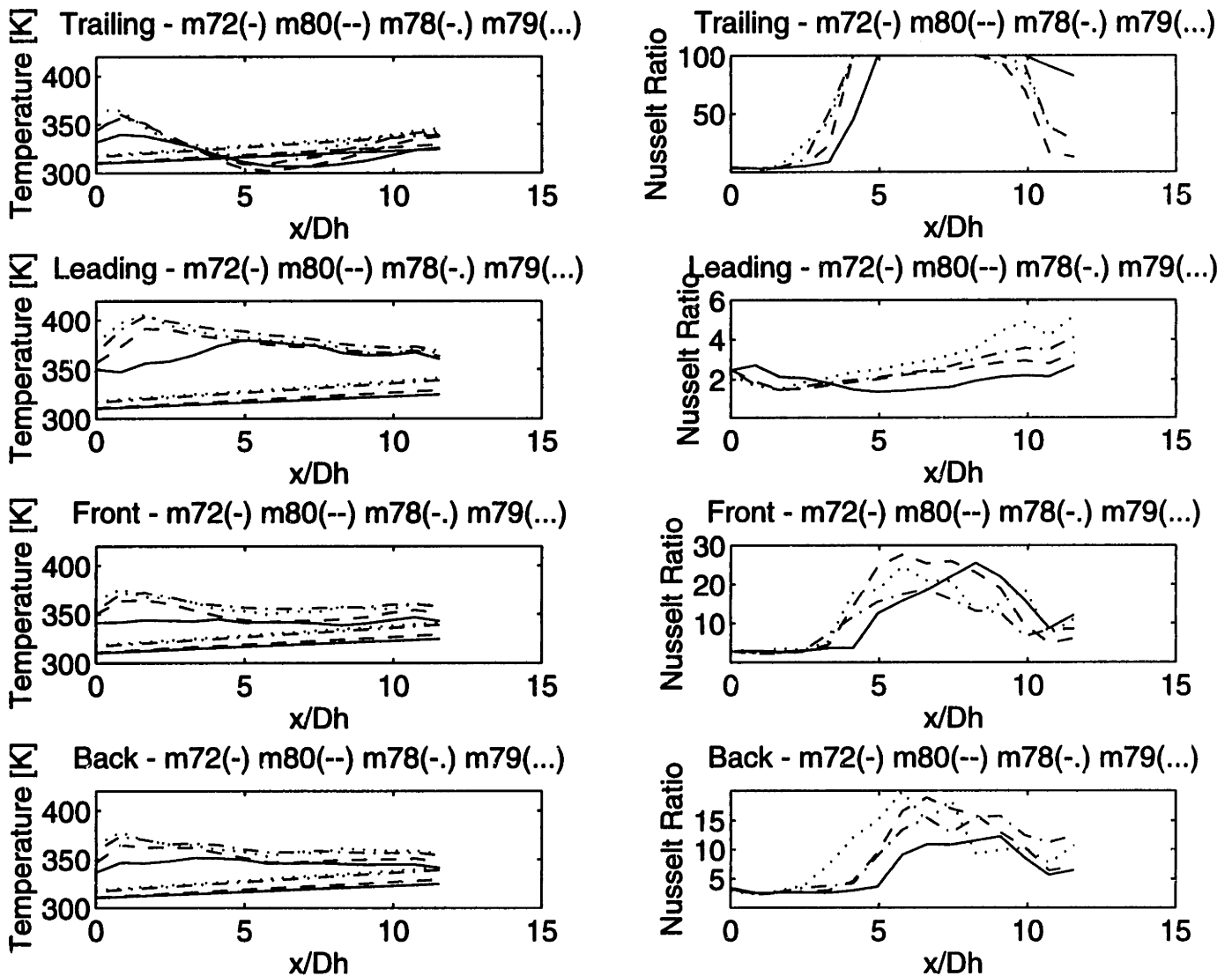
Figure 4-16: Turbulated Rectangle-Variation with Rotation number

Line	Test	Reynolds Number	Density Parameter	Rotation Number	Buoyancy Parameter
Solid	m82	25,000	0.191	0.18	0.353
Dashed	m83	24,000	0.186	0.34	1.277
Dash-Dot	m84	25,000	0.181	0.50	2.722
Dotted	m87	24,000	0.196	0.73	6.188
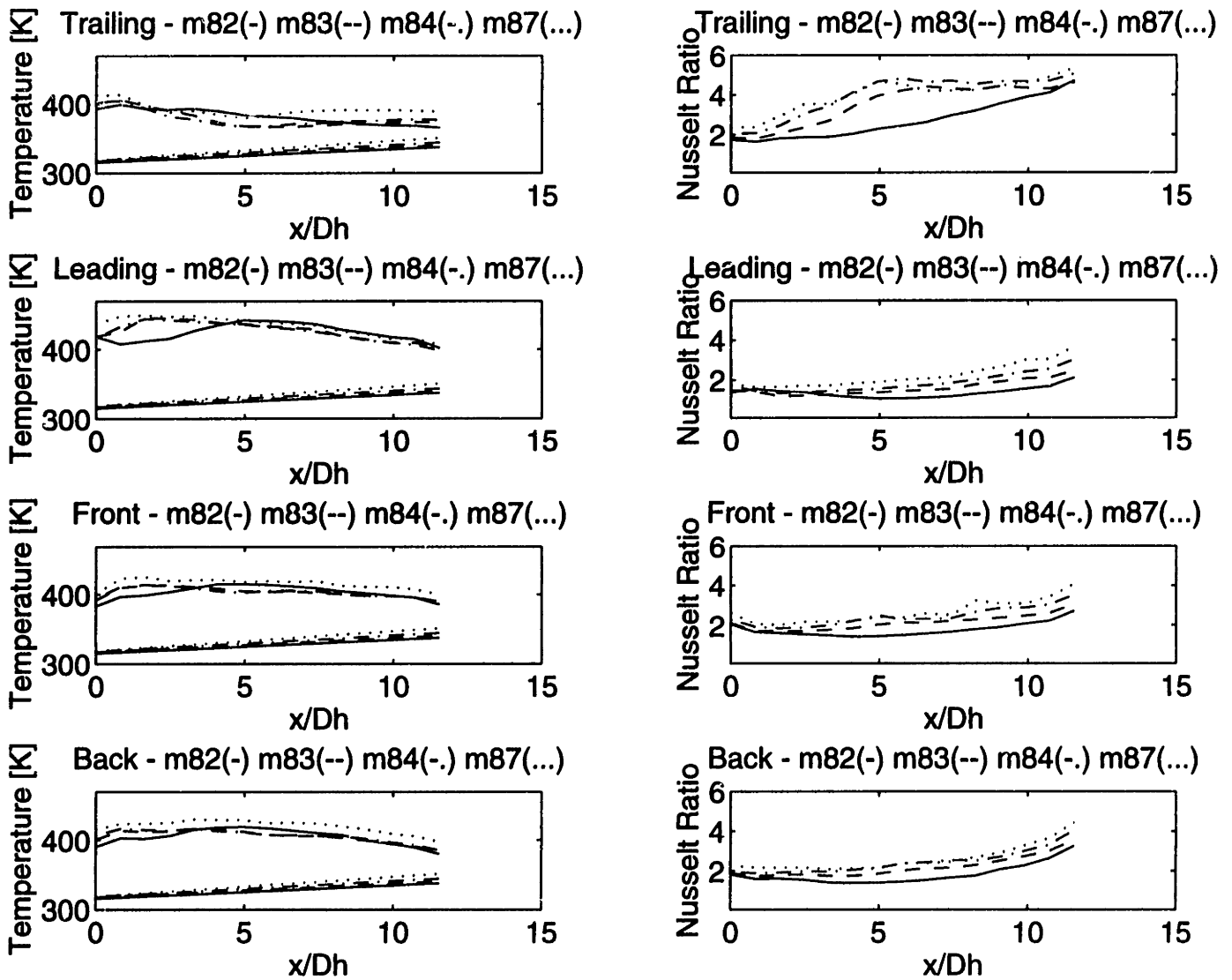
Figure 4-17: Turbulated Rectangle-Variation with Rotation number

At moderate Density parameters, the same trend exists as shown in figure 4-17. On the leading face, the Nusselt ratio varies from 1.66 to 2.08 to 2.50 to 3.00 as the rotation varies from 0.18 to 0.34 to 0.50 to 0.73 at an x/D_h of 11.0. Near the inlet, the Nusselt ratio varies from 1.54 to 1.39 to 1.45 to 1.64 at an x/D_h of 1.65. The trends are very similar on the front and back faces. On the trailing face, the Nusselt ratio peaks at 4.2 to 4.6 by an x/D_h of 5 at Rotation numbers of 0.34 and higher. Above x/D_h of 5, the turbulators have increased the heat transfer to a maximum which continues to the outlet. The turbulators constantly increase the heat transfer as the flow travels radial outward. In the previous geometries, the heat transfer reaches a minimum at and x/D_h between 7 and 8.

At even higher Density parameters, the phenomena continues. The Nusselt ratio is enhanced with rotation as seen in figures 4-18. The low Rotation number case experiences more heat transfer below a x/D_h of 5. A similar trend appears in the smooth rectangular data. There is even a slight increase in Nusselt number ratio on both the leading and trailing faces. The trailing face displays some enhancement from the turbulators as the Nusselt ratio increases radially outward until the wall temperature reaches the bulk temperature. The higher rotation continues to improve heat transfer. More data at higher rotations can help quantify any variations at high Density parameters.

4.3.2   Turbulated Rectangle: Effects of Density parameter

As shown in figure 4-19, the Nusselt ratio reaches a minimum at some moderate Density parameter. Heat transfer decreases with increasing Density parameter up to a point. Above some moderate Density parameter, the Nusselt ratio begins to grow again. The leading face makes an accurate representation over a range of Density parameters. The other faces are subject to inaccuracies as a result of the small difference between the wall and bulk temperature. In going from a Density parameter of 0.089 to 0.271, the Nusselt ratio shows a minimum at a Density parameter of 0.186. On the leading face, the Nusselt ratio goes from 2.71 to 2.40 to 2.08 to 2.77 as the Density parameter varies from 0.89 to 0.11 to 0.186 to 0.271 at an x/D_h of 10.7. At

60

Line	Test	Reynolds Number	Density Parameter	Rotation Number	Buoyancy Parameter
Solid	m33	25,000	0.312	0.13	0.317
Dashed	m34	24,000	0.290	0.23	0.893
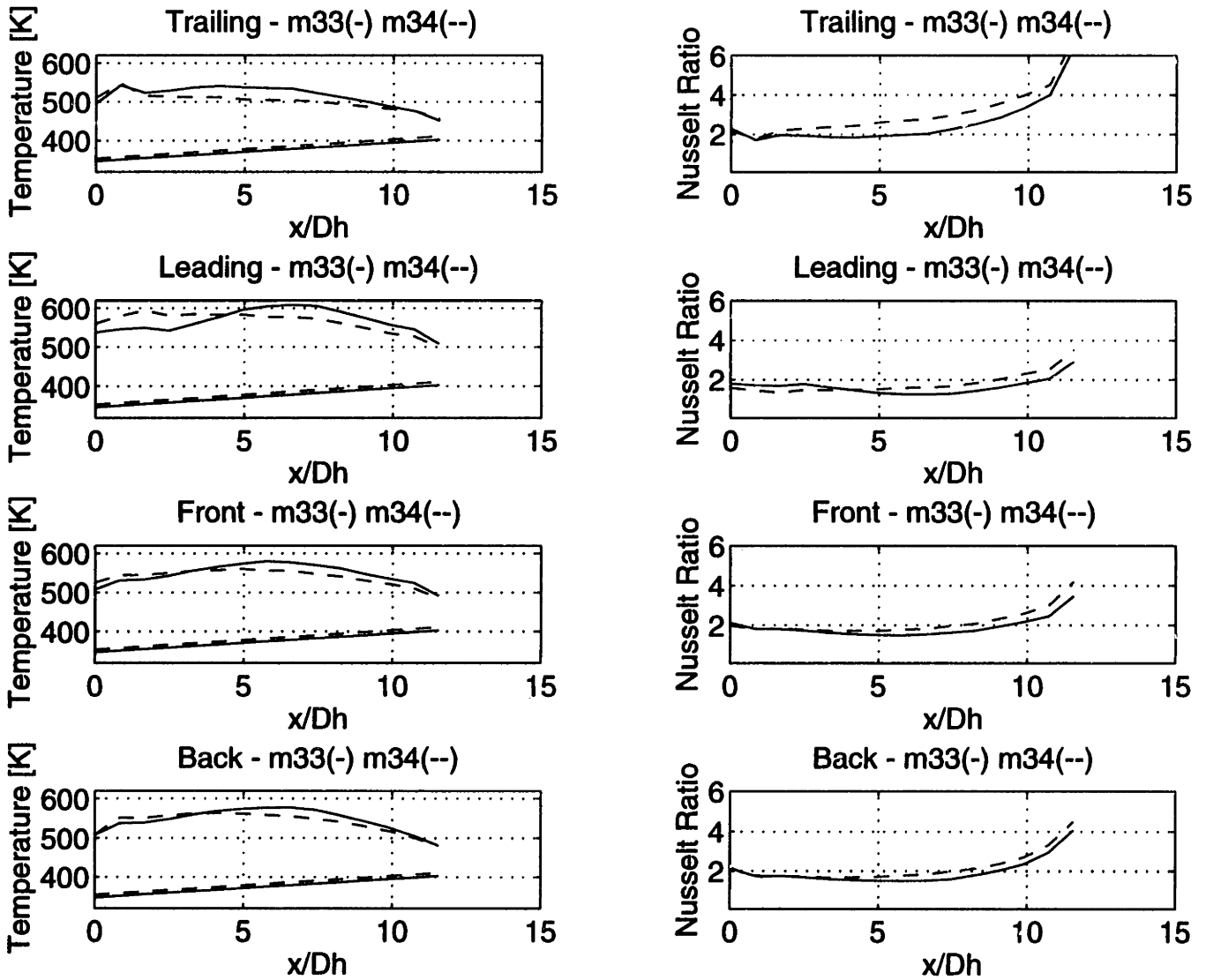
Figure 4-18: Turbulated Rectangle-Variation with Rotation number at high density

Line	Test	Reynolds Number	Density Parameter	Rotation Number	Buoyancy Parameter
Solid	m80	25,000	0.089	0.36	0.679
Dashed	m77	24,000	0.110	0.36	0.832
Dash-Dot	m83	24,000	0.186	0.34	1.277
Dotted	m35	25,000	0.271	0.32	1.673
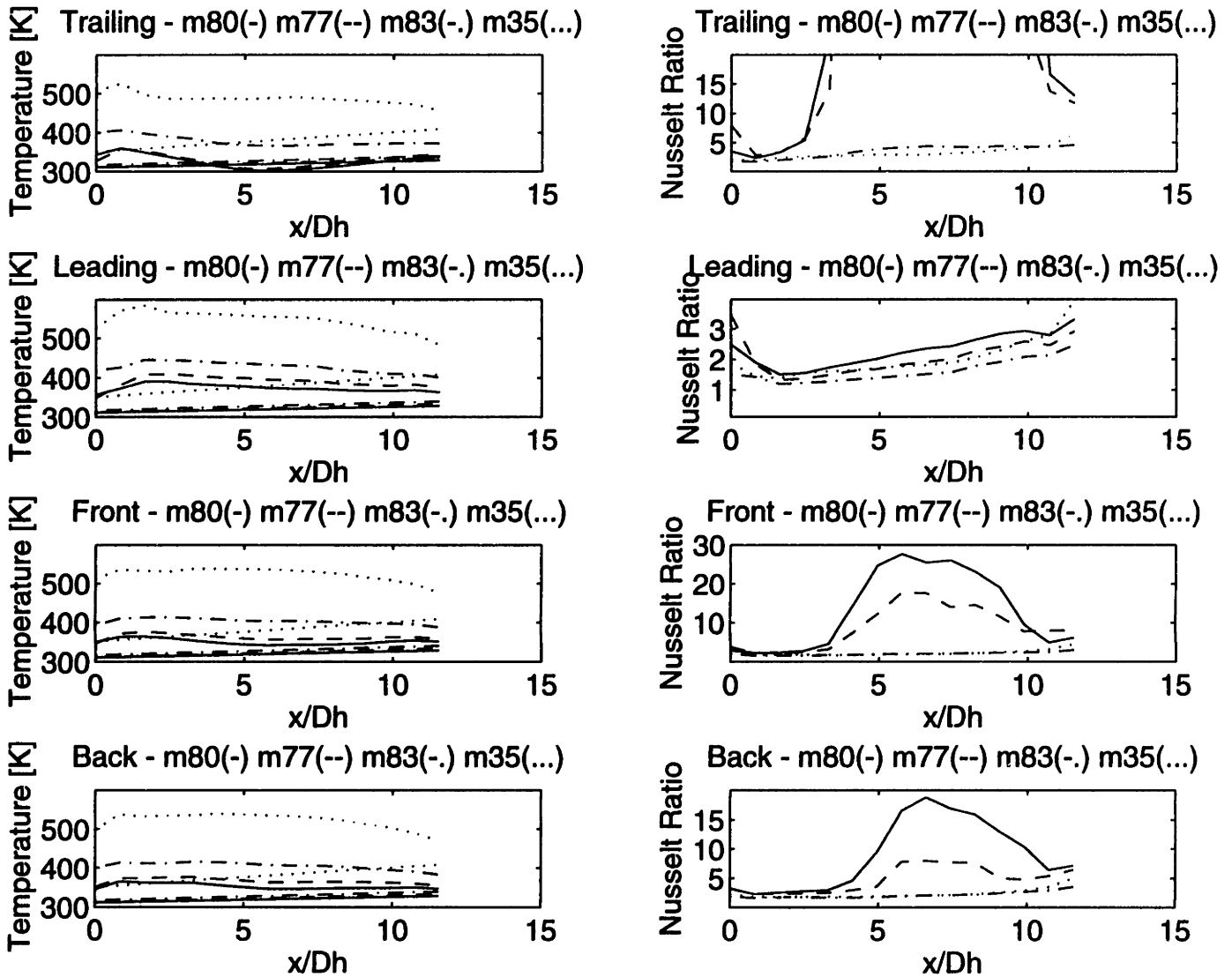
Figure 4-19: Turbulated Rectangle-Variation with Density parameter

the inlet of the leading face, the Nusselt ratio varies from 1.46 to 1.30 to 1.18 to 1.37 at an x/D_h of 1.65. The effect of the turbulators appears at all densities. A similar trend is deduced for both the smooth square and the smooth rectangle. A more accurate scheme for translating the low Density parameter temperature profiles into Nusselt ratio can improve the validity of the observed trend.

4.4 Uneven Wall, Smooth Rectangular

The uneven rectangular section has the same aspect ratio as the smooth and turbulated rectangles. The leading side of the uneven rectangular section is about twice the thickness of the other faces. The leading face has a larger joule heating as a result. The trailing face becomes much cooler. The conduction from the leading to the trailing faces is a lot more significant.

4.4.1 Uneven Rectangle: Effects of Rotation number

At low Density parameter, rotation enhances heat transfer on the uneven module as shown in figure 4-20 . The wall temperature on the trailing face appears to drop below the bulk temperature once again. A detail measurement of the bulk temperature can help determine if the discrepancy is in the bulk temperature model. The model assumes a constant local bulk temperature at each radially pass. The local bulk temperature actually varies circumferential at each radius. The bulk temperature on the trailing face is higher than the model predicts while that on the leading is lower than the model predicts. On the leading surface, the heat transfer is shown to improve with rotation above an x/D_h of 5. At an x/D_h of 4.7, the Nusselt ratio is almost identical at 1.74 and 1.75 on the leading face. At this point, Coriolis forces begin to effect the flow as the Nusselt ratio drops to 1.61 at low rotation and grows to 2.15 at high rotation. At low rotation, the leading face receives more heat transfer in the inlet region for reasons described earlier. On all faces, the heat transfer improves at low rotations in the inlet region below x/D_h of 5.

At more moderate Density parameters, the effect of rotation is more noticeable as

Line	Test	Reynolds Number	Density Parameter	Rotation Number	Buoyancy Parameter
Solid	a52	24,000	0.107	0.13	0.115
Dashed	a53	25,000	0.103	0.24	0.393

Figure 4-20: Uneven Smooth Rectangle-Variation with Rotation number

Line	Test	Reynolds Number	Density Parameter	Rotation Number	Buoyancy Parameter
Solid	a57	24,000	0.231	0.13	0.266
Dashed	a55	23,000	0.225	0.38	2.412
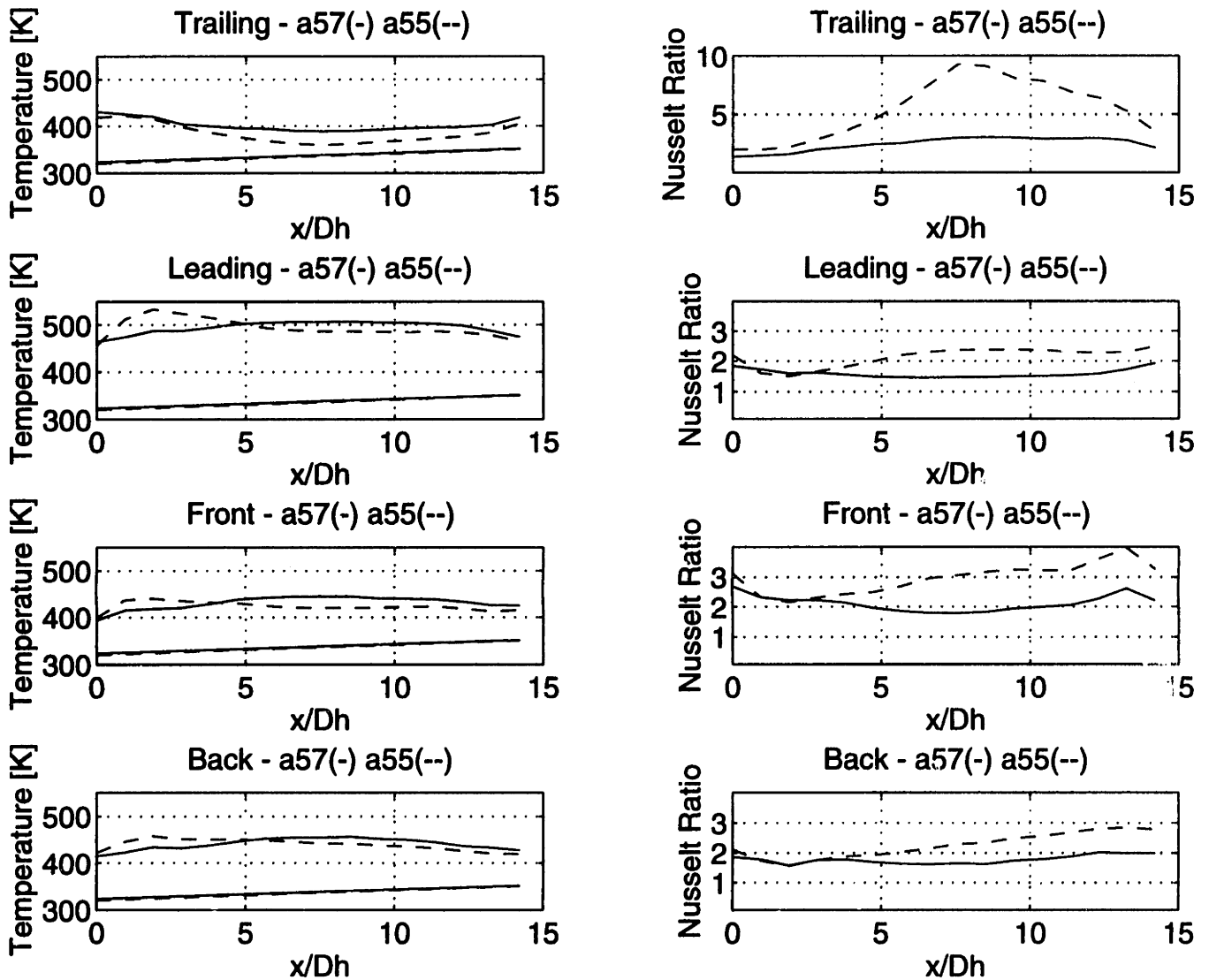
Figure 4-21: Uneven Smooth Rectangle-Variation with Rotation number

shown in figure 4-21. The inlet region effected by re-circulation disappears at higher rotation when the Coriolis forces develop earlier in the module. On the leading face, the Nusselt ratio goes from 1.5 at 0.13 rotation to 2.3 at 0.38 rotation at an x/D_h of 11.4. Because of the uneven walls, the Nusselt ratio on the trailing face is higher than that on the leading face even at low rotation. The trailing face cools much quicker than the leading. On the trailing face, the wall temperature quickly cools to the bulk temperature as noticed by the peak in the Nusselt ratio at high rotation.

At high Density parameters around 0.3, rotation continues to enhance heat transfer as shown in figure 4-22. The inlet phenomena does not exist on the trailing surface. On the other faces, the inlet region below x/D_h of 4 shows enhanced heat transfer at low rotation. The Coriolis forces begin to act above an x/D_h of 4 where the Nusselt ratio is 1.7 on the leading face. The Nusselt number remains steady around 1.7 at low rotation and grows above 2.0 at higher rotation. On the trailing face, the inlet effect does not exist and the Nusselt ratio quickly approaches 2.4 at low rotation and 3.3 at high rotation by an x/D_h of 10. Even with the large gradient, the Coriolis forces work to enhance heat transfer.

At higher Reynolds number, it is hard to determine the effect of rotation because the values are all low below 0.14. Figure 4-23 displays the data for a Reynolds number of 60,000. The data look very much like that of the smooth rectangle in which it is hard to notice any trend because information for each face implies something different.

At the very high Reynolds numbers, the effects of rotation become negligible as shown in figure 4-24. The Nusselt ratio is 1.1-1.4 over the entire section at three different Rotation numbers. On the leading face, the three Nusselt ratio curves do not vary by more than 0.06. The Rotation numbers are so small that Coriolis forces really have not had a chance to develop. The other faces show temperature profiles which appear almost identical despite changes in rotation. Further test at higher rotations are necessary validate the negligible effect of rotation at high Reynolds numbers.

Line	Test	Reynolds Number	Density Parameter	Rotation Number	Buoyancy Parameter
Solid	a58	21,000	0.331	0.13	0.368
Dashed	a59	21,000	0.311	0.22	1.007
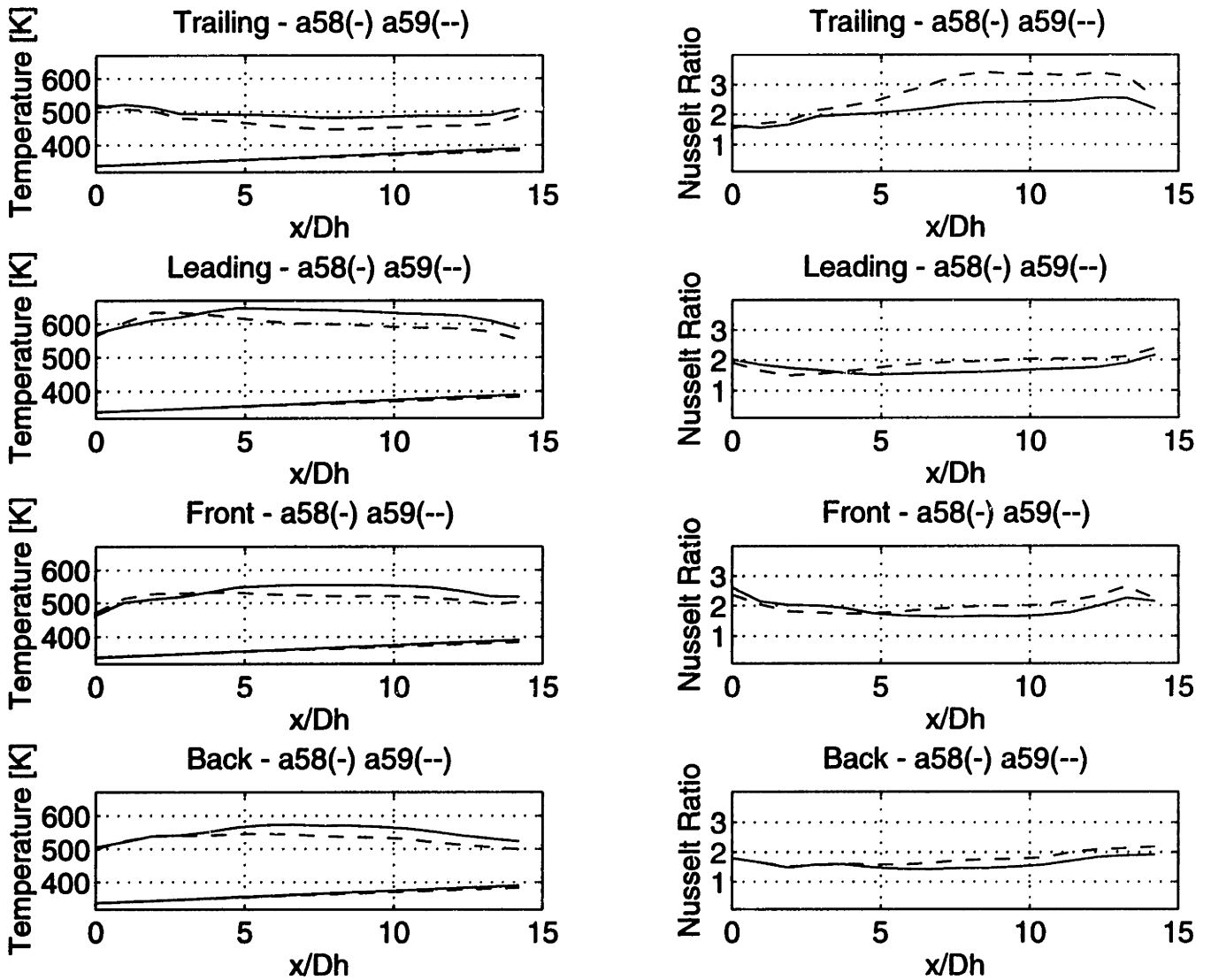
Figure 4-22: Uneven Smooth Rectangle-Variation with Rotation number

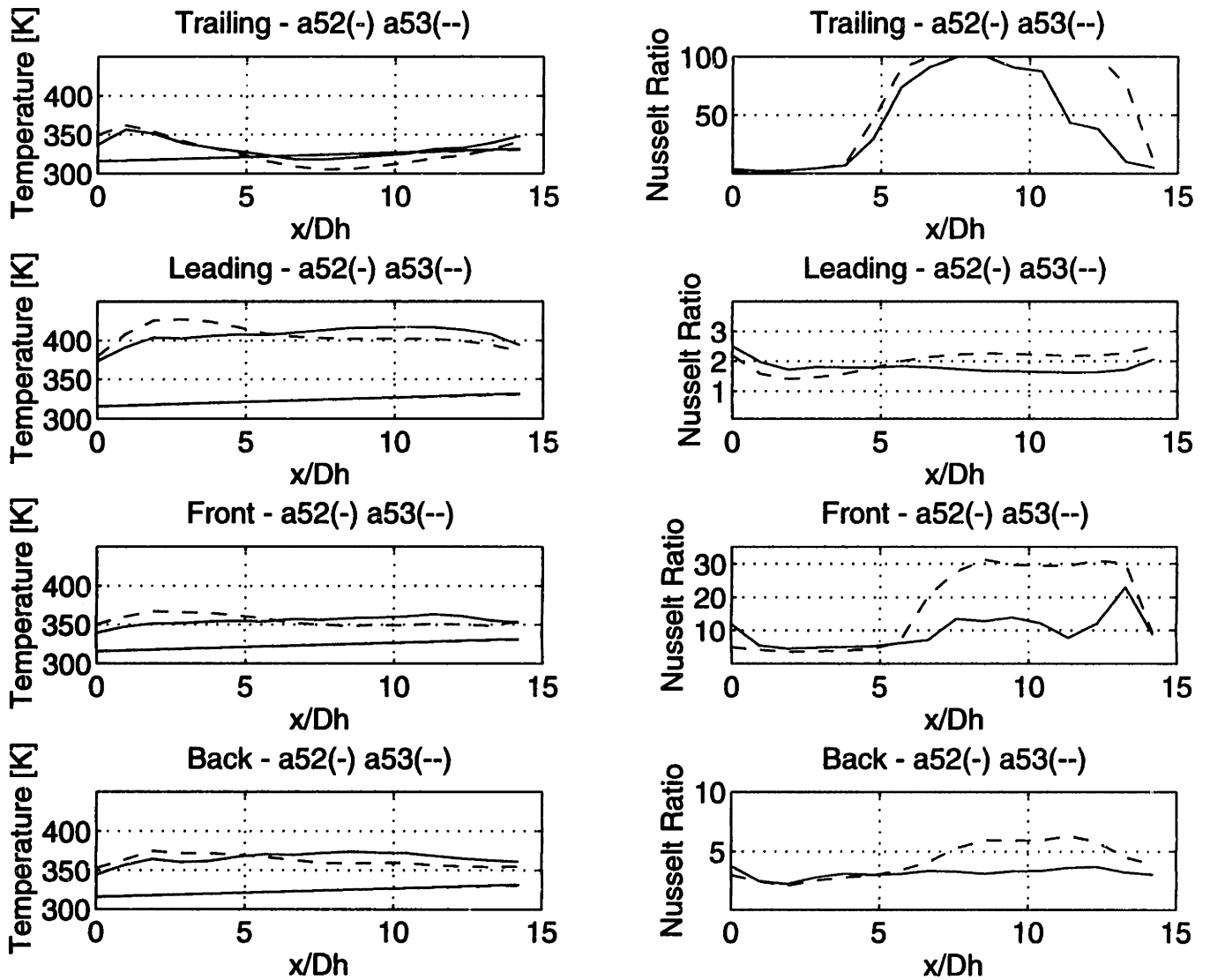| Line	Test	Reynolds Number	Density Parameter	Rotation Number	Buoyancy Parameter
Solid	a61	61,000	0.100	0.05	0.018
Dashed	a62	60,000	0.083	0.09	0.050
Dash-Dot	a63	60,000	0.089	0.14	0.126

Figure 4-23: Uneven Smooth Rectangle-Variation with Rotation number

Line	Test	Reynolds Number	Density Parameter	Rotation Number	Buoyancy Parameter
Solid	a64	114,000	0.124	0.03	0.006
Dashed	a65	113,000	0.122	0.05	0.019
Dash-Dot	a66	113,000	0.127	0.07	0.048
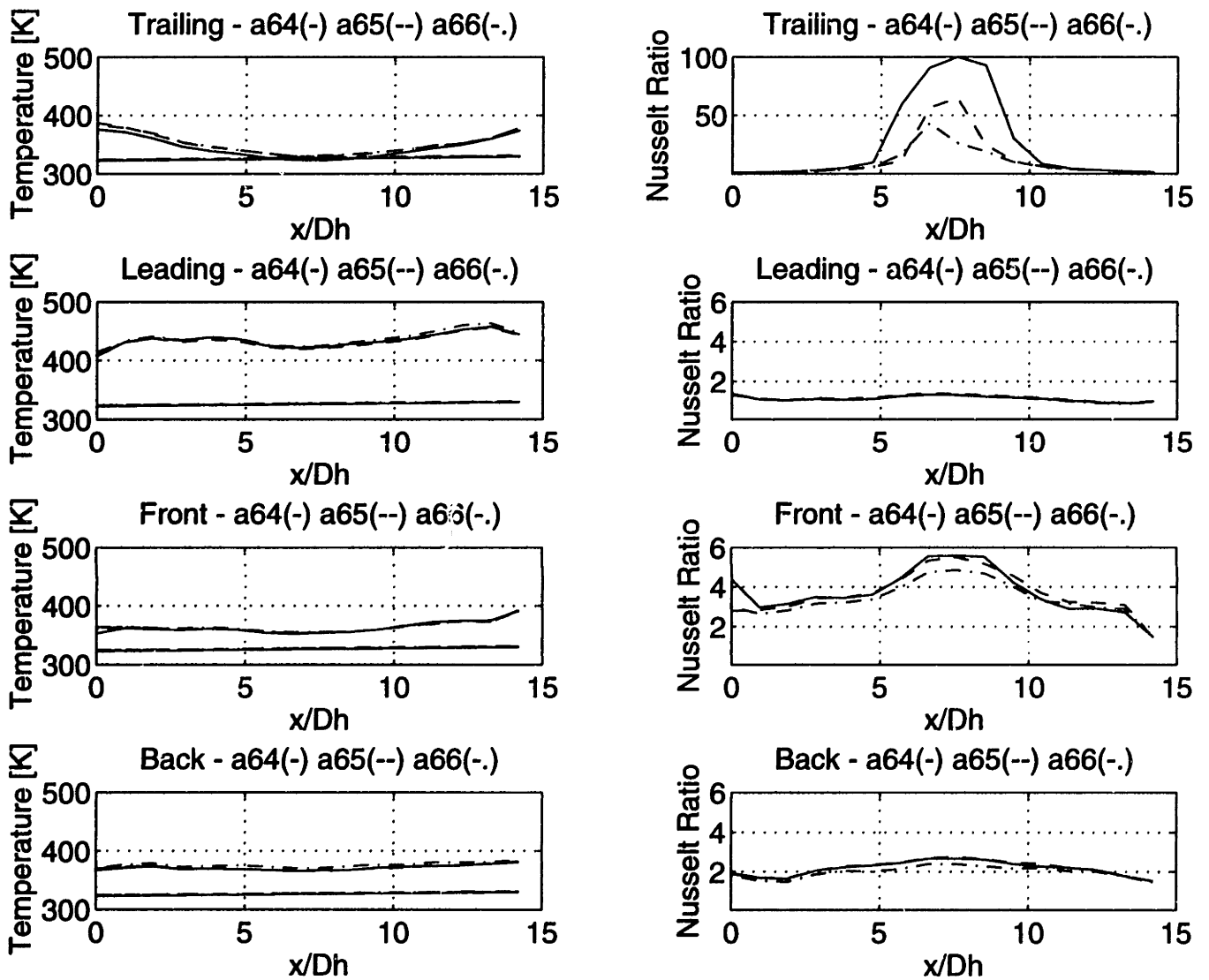
Figure 4-24: Uneven Smooth Rectangle-Variation with Rotation number

69

4.4.2   Uneven Rectangle:Effects of Density parameter

As in previous results, increasing Density parameter shows a minimum in the heat transfer at some moderate Density parameter. Figure 4-26, demonstrates this phenomena. On the leading face, the Nusselt ratio varies from 1.64 to 1.46 to 1.60 as the Density parameter varies from 0.107 to 0.231 to 0.331 at an x/D_h of 8.5. The other faces show that Nusselt ratio continues to decrease at higher Nusselt ratio. Increasing the density ratio from 0.231 to 0.331 decreases the Nusselt ratio approximately 0.5-0.6 on the trailing face and 0.1-0.2 on the front and back face. The same trend exist at a high Rotation number of 0.24 as shown in figure 4-26. The leading face shows a minimum at some moderate Density parameter, 0.241 in this case. In figure 4-26, the Nusselt ratio varies from 2.21 to 1.90 to 1.96 as the Density parameter varies from 0.103 to 0.242 to 0.311. The Nusselt ratio decreases with increasing density on the other three surfaces.

4.4.3   Uneven Rectangle: Effects of Reynolds Number

It is difficult to determine the variation of heat transfer with Reynolds number in figure 4-27. Referring to runs a52 and a63 which are at approximately the same Density parameter and Rotation number, the nusselt ratio on the leading face decreases with Reynolds number. On the other three faces, the Nusselt ratio increases with increasing Reynolds number. The temperature profiles duplicate the phenomena. According to the data, the leading face boundary layer gets thicker as Reynolds number increases while the boundary layer on the other faces gets thinner as the Reynolds number increases. High Reynolds data at moderate Density parameter is necessary to make more accurate observations.

4.5   The Effect of Geometry

Geometry can have a large effect on the heat transfer as seen in this discussion. Figure 4-28 show how the Nusselt ratio changes with geometry at high Density pa-

Line	Test	Reynolds Number	Density Parameter	Rotation Number	Buoyancy Parameter
Solid	a52	24,000	0.107	0.13	0.115
Dashed	a57	24,000	0.231	0.13	0.266
Dash-Dot	a58	21,000	0.331	0.13	0.368
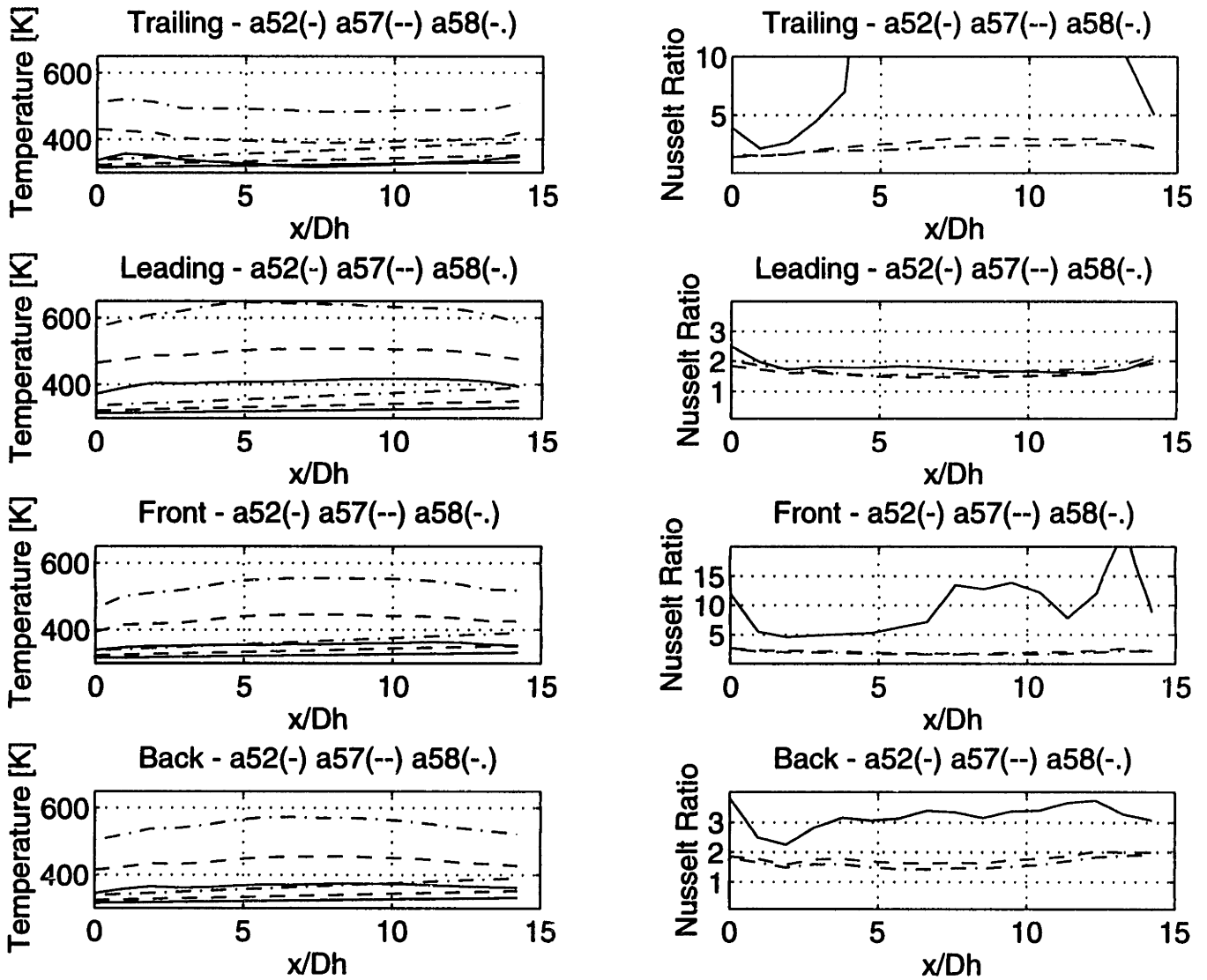
Figure 4-25: Uneven Smooth Rectangle-Variation with Density parameter

Line	Test	Reynolds Number	Density Parameter	Rotation Number	Buoyancy Parameter
Solid	a53	25,000	0.103	0.24	0.393
Dashed	a56	24,000	0.241	0.24	0.909
Dash-Dot	a59	21,000	0.311	0.22	1.007
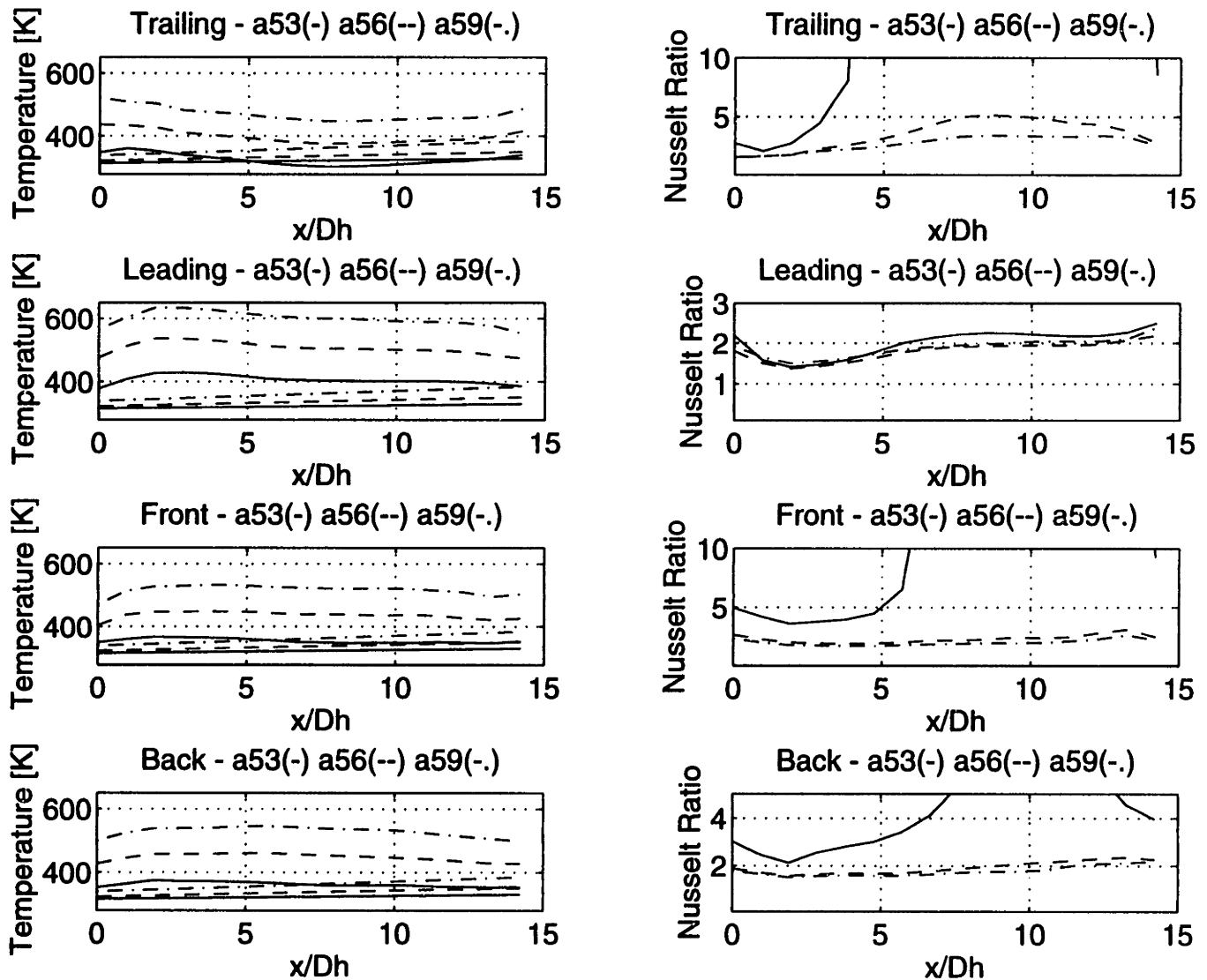
Figure 4-26: Uneven Smooth Rectangle-Variation with Density parameter

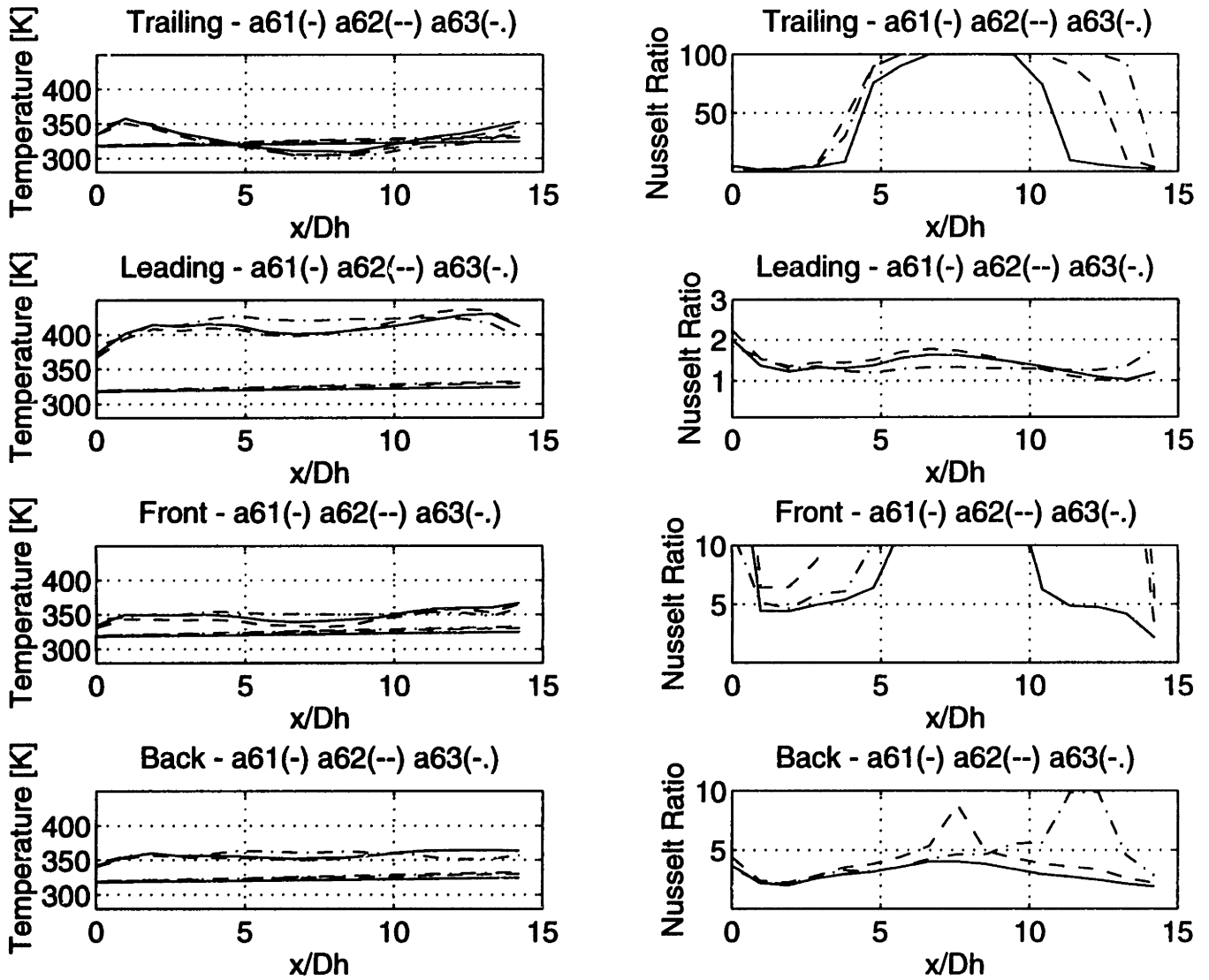| Line	Test	Reynolds Number	Density Parameter	Rotation Number	Buoyancy Parameter
Solid	a52	24,000	0.107	0.13	0.115
Dashed	a63	60,000	0.089	0.14	0.126
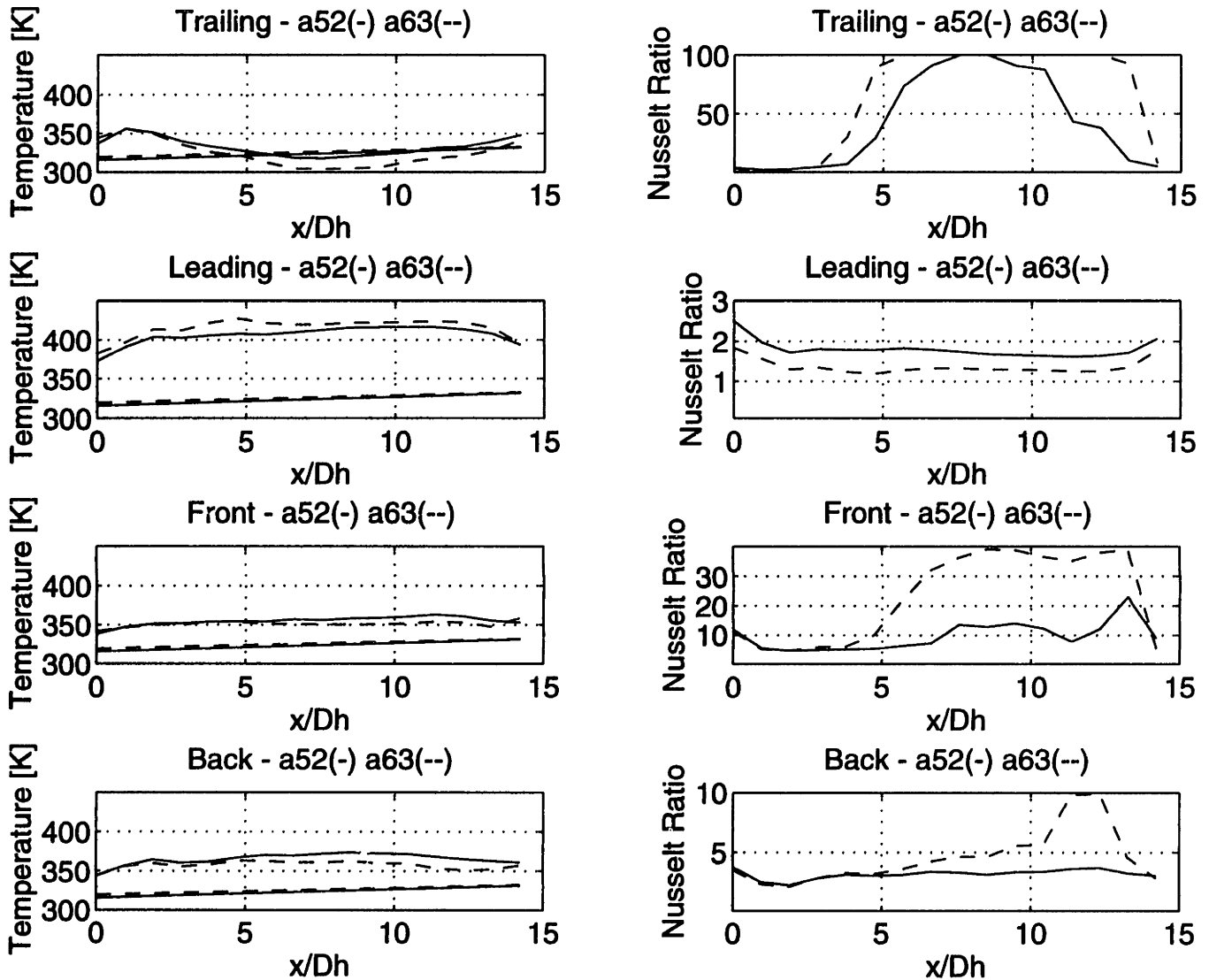
Figure 4-27: Uneven Smooth Rectangle-Variation with Reynolds Number

Line	Test	Reynolds Number	Density Parameter	Rotation Number	Buoyancy Parameter	Geometry
Solid	m45	29,000	0.306	0.24	1.061	Square: Smooth
Dashed	a16	25,000	0.289	0.25	1.064	Rectangle: Smooth
Dash-Dot	m34	24,000	0.290	0.23	0.893	Rectangle: Turbulated
Dotted	a59	21,000	0.311	0.22	1.007	Rectangle: Uneven walls
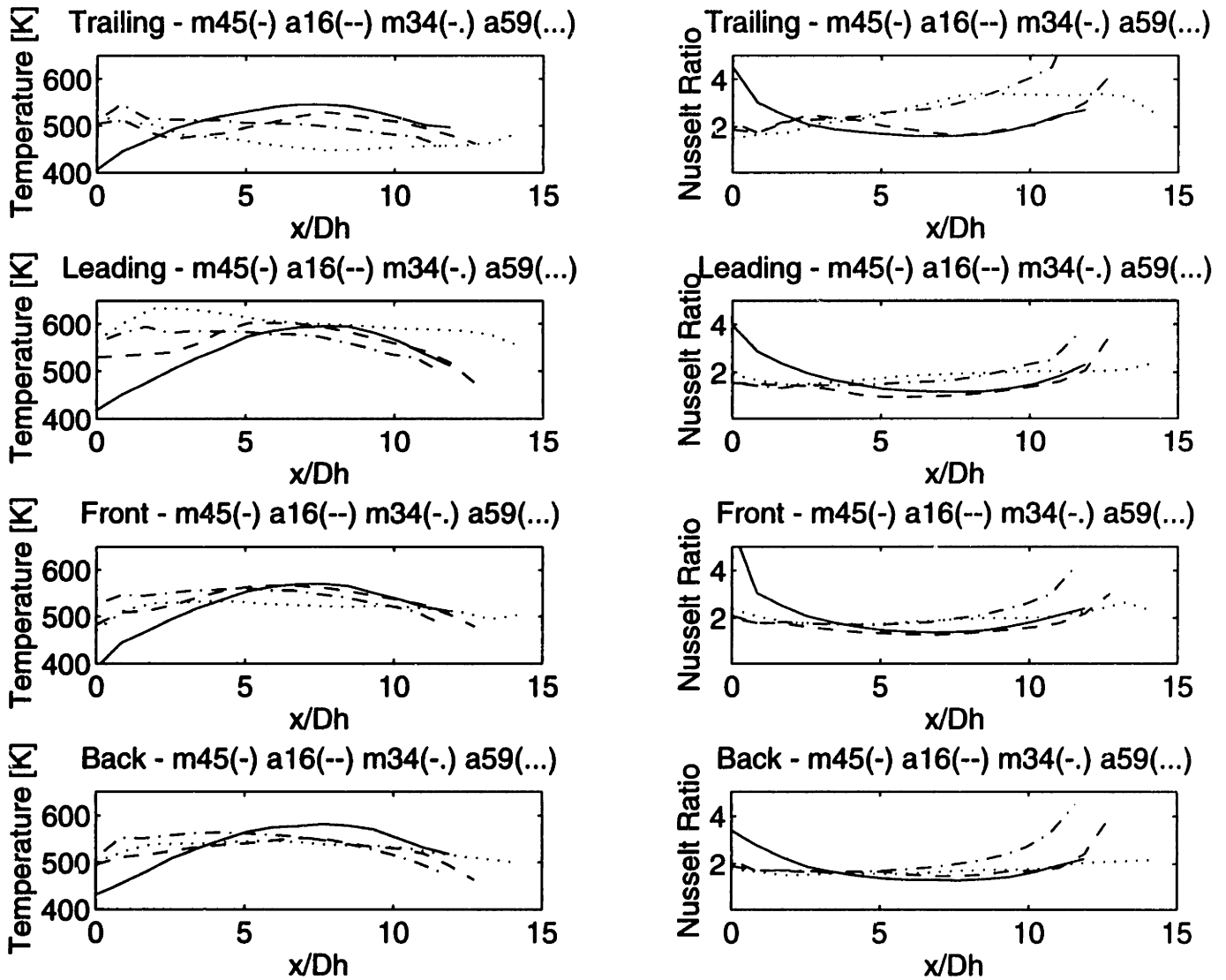
Figure 4-28: Variation of Temperature and Nusselt Ratio with Geometry

rameters. The profiles are also different. It appears that as expected the turbulators work best to get maximum heat transfer from geometry. The most heat transfer occurs between the turbulated rectangle and the uneven rectangle. The square module experience more heat transfer at the inlet due to the larger entry region. The heat transfer on the smooth rectangle, the turbulated rectangle, and the uneven rectangle varies minimally in the inlet region below an x/D_h of 5. Between and x/D_h of 5 and 10 the turbulated rectangle transfers less heat than the uneven walled, smooth rectangle. As the turbulators continue to work, the turbulated rectangle transfers more heat above an x/D_h of 9. The variation of the Nusselt ratio with geometry merits the study of a turbulated square section in a constant flux condition. Johnson and Wagner studied a turbulated square section with constant wall temperature[17]. The smooth square transfers heat slightly better than the smooth rectangle.

Chapter 5

CONCLUSIONS

5.1 The Effects of Rotation number

In almost all cases, the Nusselt ratio increases with rotation at low Reynolds number. The degree of the effect varies with geometry. Rotational effects are most noticeable above Rotation numbers of 0.10. For this reason, it is difficult to discern the effect of rotation at high Reynolds number above 100,000. All the high Reynolds data is at a low Rotation number because of high flow velocities and limitations on the drive system. At a moderate Rotation number, the effect of rotation also enhances heat transfer. The results are more conclusive when the Density parameter is high.

In pursuing further data about the effect of rotation on heat transfer, low Density parameter cases are difficult to analyze as shown on many plots in Chapter 4. A more accurate measurement of the bulk temperature helps to reduce the error. The error increases tremendously as the temperature difference between the wall and the bulk flow decreases. Further studies should be conducted at Density parameters of 0.15 or greater just to have more confidence in the heat transfer data. Another data reduction scheme can also help. The Density parameter on the trailing face is the limiting factor. If the error for measurements on the trailing face is small, the error on the other three faces is even smaller.

5.2 The Effects of Density parameter

The leading face consistently shows a minimum in the heat transfer as the Density parameter increases. The leading face is always the hottest side when rotating. Even though the overall Density parameter is low, the Density parameter for the leading faces is higher. The variation in all cases shows that the minimum is located at some moderate Density parameter around 0.2. The result does not agree with Johnson & Wagner who found the heat transfer to constantly increase with Density parameter between values of 0.07 and 0.22.

Even though the leading face shows a minimum in the heat transfer as Density parameter increases, the heat transfer continues to decrease with Density parameter on the other three faces. The low density data is difficult to quantify because of small differences between the wall and bulk temperature which drive the Nusselt ratio up. Alternative ways of reducing the data at low Density parameters are necessary to eliminate the uncertainty. On the leading face, heat transfer increases as the Density parameter is increased from approximately 0.2 to 0.3. The opposite happens on the other three faces.

5.3 The Effects of Reynolds Number

Dividing the Nusselt Number by the Colburn equation, does not entirely eliminated the Reynold number effects. Each test module shows a different variation in Nusselt ratio as a function of Reynolds number. The smooth square shows an increase in Nusselt ratio with increasing Reynolds number. Han shows a similar result for flow in a square channel above an x/D_h of 6[9]. For the uneven walled, smooth rectangle, the Nusselt ratio increases on the trailing, front, and back while it decreases on the leading face. Increasing the Reynolds number decreases the Nusselt ratio for flow through the smooth rectangle. The test for the rectangular sections are conducted at low Density parameters while those for the square section are conducted at high Density parameters. The variations in the effect of Reynolds number on the Nusselt

ratio are the result of variations in Density parameter or variations in geometry. The addition of more data at high Density parameters can help make more conclusive statements about the effect of the Reynolds number on the Nusselt ratio at constant heat flux.

5.4 The Effects of Geometry

The uneven wall and the turbulated test section show the largest Nusselt ratios for a set condition. The accumulation of hotter fluids near the leading face as a result of additional flux works to enhance the Nusselt ratio for the uneven walled, smooth rectangle. The uneven module enhances heat transfer best showing higher values of the Nusselt ratio between x/D_h of 5 and 8. The turbulated module enhances heat transfer better as the radius increases. Above a x/D_h of 8, the turbulated rectangle improves the Nusselt ratio best. The turbulators force the boundary layers to re-start after each turbulator obtaining maximum heat transfer in the thinner boundary layer.

The smooth rectangle and smooth square are very similar. There is not much advantage in choosing the rectangular geometry over the over geometry. The smooth square clearly enhances the Nusselt ratio best in the inlet region due to the increased entry length. Heat transfer is enhanced in the thinner boundary layer. The smooth rectangle forces the boundary layer to merge quickly due to its aspect ratio. A study of a turbulated square is necessary to determine if a square turbulated section is optimal in a constant heat flux condition.

Chapter 6

ERROR ANALYSIS

6.1 Temperature Calculation Error

Each temperature measurement is the result of a K-type thermocouple measurement taken at some point. Standard K-type thermocouples have an accuracy of 2.2^oK or 0.75% of the measured current, whichever is greater. The thermocouple error exists in all temperature measurements including the infrared detector. The flow temperature measurements are the direct result of thermocouple measurements. The bulk temperature error is the error in the K-type thermocouple plus the drift error over the time span of the test. In order for a test to be considered steady, the temperature has to remain within 5^oK over the course of the fifteen to twenty minute test run. In most cases the temperature difference varies at most 3^oK.

In addition to the above mentioned data, there is an error associated with not knowing the cold junction temperature for the thermocouples. The cold junction temperature is not monitored for the data presented in this thesis. The cold junction is assumed to be at room temperature, an assumption which is not necessarily valid. Given this error, all the bulk temperatures are actually higher. In order to estimate the cold junction block temperature, a control volume is drawn around the entire experiment. The flow transports energy in and out. The joule heating is the energy

Test	I^2RW	$\dot{m}$kg/s	C_pJ/kg-K	$T_o^\circ K$	$\frac{I^2R}{2\dot{m}C_p}$	$\frac{T_3}{T_o}$	$\frac{T_3-T_o}{T_w-T_b}\%$
a06	27.7	0.0027	624.58	304	0.027	1.03	36.0
a12	61.5	0.0028	647.88	303	0.06	1.06	19.0
a45	150.8	0.0029	682.06	302	0.13	1.13	24.5
a34	78.0	0.0075	640.31	304	0.03	1.03	21.0
a40	111.5	0.0155	641.50	302	0.02	1.02	14.4

Table 6.1: Cold Junction Error

put into the system. The following equation models the system.

$$T_4 = \frac{Q}{\dot{m}C_p} + T_o \tag{6.1}$$

T_4 is the exit flow temperature. T_o is the inlet flow temperature. Q, $\dot{m}$ and C_p are the joule heating, massflow and specific heat. The frictional heat in the seals and bearings is neglected. The heat removed by the cooling system for the seals is also neglected in the above model. The block is not connect directly to the shaft. It is mechanically connected to the large rotor plates described in Chapter 8 but rests directly on the shaft. The model only provides an idea of the size of the error introduced. Upon knowing the inlet and outlet flow temperature, the metal temperature is assume to settle between the flow temperatures at $T_3 = \frac{T_4+T_o}{2}$. Using the model described, the following block temperatures are estimated along with the potential error.

The infrared detector is calibrated using thermocouple measurements. The surface temperature profiles are the result of temperature measurements processed through a calibration involving a linear fit to a parabolically distributed temperature measurement taken using thermocouples. There is error involved in the parabolic fit to the surface temperature which comes directly from the error in the thermocouple measurement. There is also the error associated with fitting the five or six calibration points with a line.

Dens.	Q	Nu_{inf}	ΔT_{err}	$T_w - T_b$	Nu_{id}	Nu_{err}	Error
0.067	7100	68.39	$5^o K$	$20^o K$	5.19	6.92	33%
0.198	14100	66.23	$5^o K$	$80^o K$	2.66	2.84	7%
0.297	37900	63.33	$5^o K$	$170^o K$	3.52	3.63	3%
0.067	7100	68.39	$10^o K$	$20^o K$	5.19	10.38	100%
0.198	14500	66.23	$10^o K$	$80^o K$	2.66	3.15	19%
0.297	37500	63.33	$10^o K$	$170^o K$	3.52	3.70	5%

Table 6.2: Error as a function of Density Parameter

6.2 Heat Transfer Coefficient Error

The error in the temperature profiles is derived from the information above. The error in the temperature measurements have a larger effect on the Nusselt ratio as depicted below.

$$h = \frac{Q_t}{Area * (T_w - T_b + \Delta T_{err})} \tag{6.2}$$

According to equation 6.2, the heat transfer coefficient changes depending on the relative size of the error compared to the the temperature difference between the wall and the bulk flow. The temperature is allowed to vary at most $5^o K$ for a valid test plus the thermocouple and calibration error. For a typical case in which the temperature error is about $5\text{-}10^o K (9\text{-}18^o F)$, the error is calculated in Table 6.2.

As mentioned earlier, the error increases as the density parameter decreases. The error in Table 6.2 is calculated considering only the joule heating without taking radiation and conduction losses into consideration. It becomes obvious that the magnitude of the heat transfer computation is unreliable at low density parameters. The density parameter actually represents an average over the entire test section. Therefore, the error is greater on the trailing face and smaller on the leading face. At high rotations, the trailing face is cooled tremendously and the error goes toward infinity.

Due to large error, most observations at low Density parameter are based on the temperature profiles. Observation about heat transfer are thus drawn mostly from the temperature profiles when low density parameters are involved. The error

computation suggest that another reduction scheme is necessary to compute the heat transfer coefficient at low density parameters.

In addition to the temperature error, there are also two other sources of error which affect the heat transfer coefficient. There is error in the computation of joule heating as well as error in computing the radiation and conduction losses.

6.3   Conduction Correction Factor

Conduction plays a significant roll in the heat transfer process for the modules being tested. The curvature of the parabolic fits during the calibration procedure shows that this is the case. In order to compute the local heat transfer coefficient, a local conduction factor is necessary for each element.

At first the conduction correction factor was calculated using finite differences after converting the raw data into temperatures. The finite difference method generated conduction factors on the order of 50-100% of the joule heating in some cases. Another method was deemed necessary. The problem revolves around the calculation of the derivative.

The elemental conduction correction is calculated by fitting the temperature data with polynomials [5]. Once the temperatures for a given test condition are know, the conduction is calculated based on these profiles. For each element, a circumferential fit is performed at each radial pass. In addition, a radial fit is performed for each element. Appendix B gives an example of the equations generated by these polynomial fits and the size of the conduction correction factor. Given the coefficients of the polynomial, the derivative is computed analytically. Both radial and circumference conduction corrections are computed for each element. In most cases, the conduction factor is less than ±10% relative to the joule heating. In worst cases, the factor may jump to 25%. The radial fits works well. Polynomial fits between third and sixth order generate answers within the same range. In all cases for all tests, the radial conduction term is calculated based on a fourth order polynomial fit to the radial data for each element.

82

Dens.	Q_{elem}	q_{xdir}	ΔT_x	q_{ydir}	ΔT_y
0.067	0.0278	8600	0.351	89300	37.8
0.205	0.0618	19200	0.783	198000	83.8
0.298	0.1516	47000	1.92	487000	206.0

Table 6.3: Temperature Gradient considering Total Conduction

The circumferential fit varies with geometry and is extremely sensitive to the order of the polynomial fit. Dealing first with the leading and trailing sides of the rectangular faces, no circumferential conduction is computed. The temperature variation across the short leading and trailing faces is so small that it is not feasible to justify a polynomial fit greater than first order. Considering a possible error of 5-10^oK, the linear fit is the most sensible for a polynomial fit in the circumferential direction of the leading and trailing faces. Given a first order polynomial fit, there is no circumferential conduction correction factor on these faces, only radial. Any higher order fits generate conduction factors that are approximately 50% of the joule heating at numerous locations. No circumferential conduction factor is used for the square module because a linear fit is best on the short sides. Higher order fits generated unreasonably large conduction factors.

Unlike the leading and trailing, the front and back surfaces are a lot longer making circumferential conduction feasible. In most cases, the temperature curves are best fitted by a second or third order polynomial. The third order polynomial gives high conduction correction factors at many points which seemed unreasonable. Therefore, the second order fit is used to computed circumferential conduction on the front and back faces of the rectangular modules.

In addition to this method, the feasibility of adding a conduction correction factor is analyzed for each test case by calculating the temperature difference required if all the joule heating is dissipated through conduction.

In the radial direction, the temperature difference is large. ΔT_x represents the temperature difference required to drive all the elemental heating through a $\Delta Y \times \Delta t$ face. The circumferential direction is more sensitive. These are cases in which

a large amount of power is passed through the test module. According to Table 6.3, introducing a circumferential conduction factor requires a very high resolution measuring device. The ΔT in the circumferential direction is less than 2. For a ten percent conduction correction, the measurement system requires a 0.03 to $0.19^{o}K$ measurement accuracy according to the error model. In low density cases it is not beneficial to add a conduction correction in the circumferential direction as it may increase the error.

6.4 Joule Heating Error

The error in the joule heating decreases as more power is put into the model. The current measuring device is accurate to 1 Amp or 1%. The current is thus accurate to the same degree. The error in the resistance on the order of 2%. The voltage and current is measured and the resistance is calculated using Ohms law, $R = \frac{V}{I}$. The Joule heating error is determined by the equation 6.3.

$$Q_{err} = \frac{I^2 R - (I \pm 0.01I)^2 (R \pm \Delta R)}{I^2 R} * 100 \qquad (6.3)$$

At high power levels the error becomes small. The resistive error may cause a problem. The error analysis suggests the use of a module which requires high levels of power to reduce error in the computation of the joule heating.

6.5 Massflow Error

The error in the massflow is significant because it is used to compute the Reynolds number which is the normalizing factor for all the data. The mass flow rate is computed using equation 3.2 that it is proportional to the square root of temperature over pressure. The error in the temperature measurement is described above. The pressure gauges are only good to the accuracy of the human eye which is half an increment assuming they are properly calibrated. The pressure never varies more than 2 psi over the course of a test. Like the pressure gauges, the flow tube is only

84

Perc(%)	Pres(psig)	$\Delta Pres_{err}$	$Tb_{avg}(^oK)$	ΔT_{err}	$\dot{m}$	Error
20%	50	2	320	10	0.079	6%
50%	50	2	320	10	0.198	4%
100%	50	2	320	10	0.395	4%
20%	50	5	320	20	0.079	11%
50%	50	5	320	20	0.198	9%
100%	50	5	320	20	0.395	8%

Table 6.4: Mass Flow Error

accurate to half an increment which is 5%.

$$\dot{m} \propto Const. * (Perc \pm .05)\sqrt{\frac{Pres \pm 2}{T \pm \Delta T_{err}}} \tag{6.4}$$

In most cases, the pressure is approximately 50 psig and the flow temperature varies with the bulk temperature. The mass flow rate error is proportional to the flow meter error times the square root of the pressure divided by the temperature error. The mass flow rate error is directly translated into the Reynold number error as in equation 6.4. Table 6.4 shows the level of error at various flow rates. The error decreases with increasing bulk temperature.

$$Re_{d_h} = \frac{(\dot{m} \pm \Delta\dot{m}_{err})d_h}{\mu A} \tag{6.5}$$

Chapter 7

EXPERIMENTAL PROCEDURE

7.1 Focusing

The first step in preparing to run a series of tests is to determine the focal position of the four sides of the test module. Each side of the test module has a different focal length. Upon determining the focal length of the front side, the focal length of the other three sides are theoretically determined based on the location of the test frame mirrors. The focus run should re-confirm the theoretical values. The focal length of the front side is theoretically determined from the radii of the primary and secondary mirrors, and then experimently determined.

Ideally, the focus, calibration, and test are performed in succession without re-positioning the model. The focal lengths are determined by retracting the optical system and indexing it forward through the focal positions of all four surfaces of the test section. The infrared detector information is recorded and analyzed to determine the focal position. The data is sampled every 0.02 inches based on the speed determined from the optical encoder. Knowing the sampling rate, speed, and module dimension, the number of points on each surface are known. The optical system is set at a magnification of approximately 1.1, so a set number of points appear when the model is in focus. The signal level is also highest when the system is in focus. Since there is no flow during the calibration, the proper number of point appear on a relatively square signal. Upon analyzing the data, a range of focal locations which
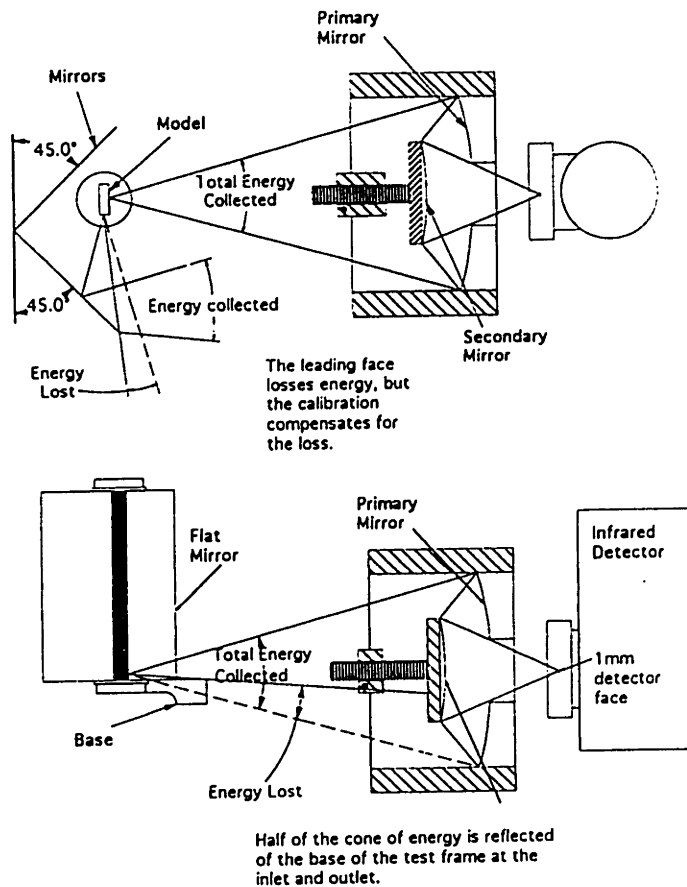
Figure 7-1: Optical System Distortions

seem identical to the human eye are chosen. The focal length is compared to the theoretical focal length. A length within the range is programmed into the code for each surface prior to the calibration and test run. Both the calibration and test are run at these pre-determined focal lengths.

In addition to providing the focal length, the procedure provides information about the depth of focus of the optical system. A relative large range of data which looks identical means a large depth of focus. If the depth of focus is large, the measured temperature is insensitive to lack of focus.

7.2 Calibration
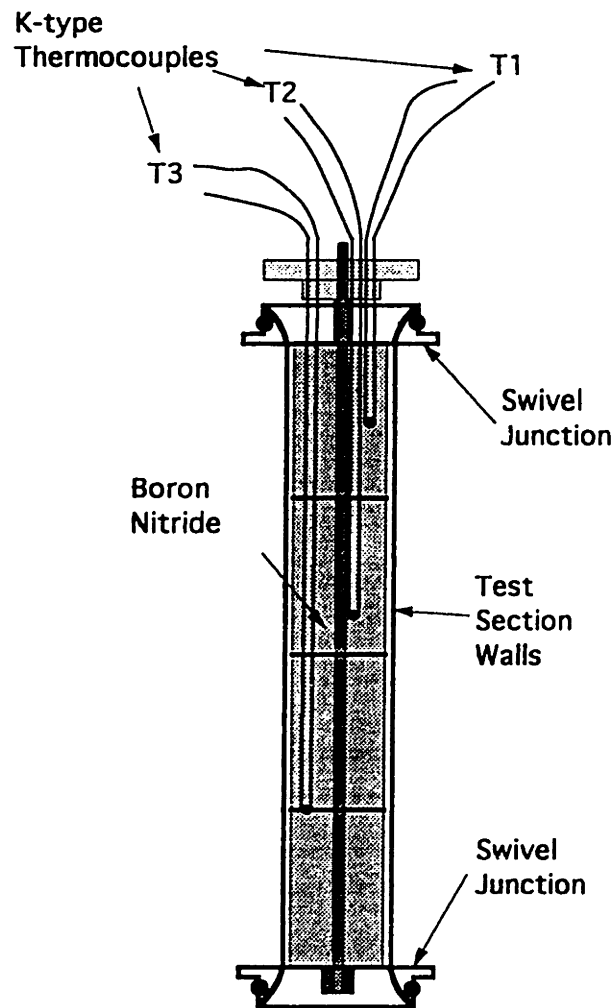
Figure 7-2: Calibration Device

The calibration produces the information necessary to convert the infrared detector signal which is in volts to surface temperature measurements in Kelvin or Fahrenheit. The calibration procedure eliminates any differences in emissivity across the surface and any geometrical distortion introduced by the mirrors. The same amount of energy is not received from all sides. Referring to Figure 7-1, the entire cone of energy does not always make it to the optical system. In the case of the leading edge, some of the energy misses the flat mirror. Near both the inlet and outlet, the base or the upper channel blocks a fraction of the energy before it reaches the optical system. The calibration procedure corrects for such effects.

The calibration is done by filling the test section with a boron nitrite plug fitted with three thermocouples and its own top upper channel plug(See Figure 7-2). The
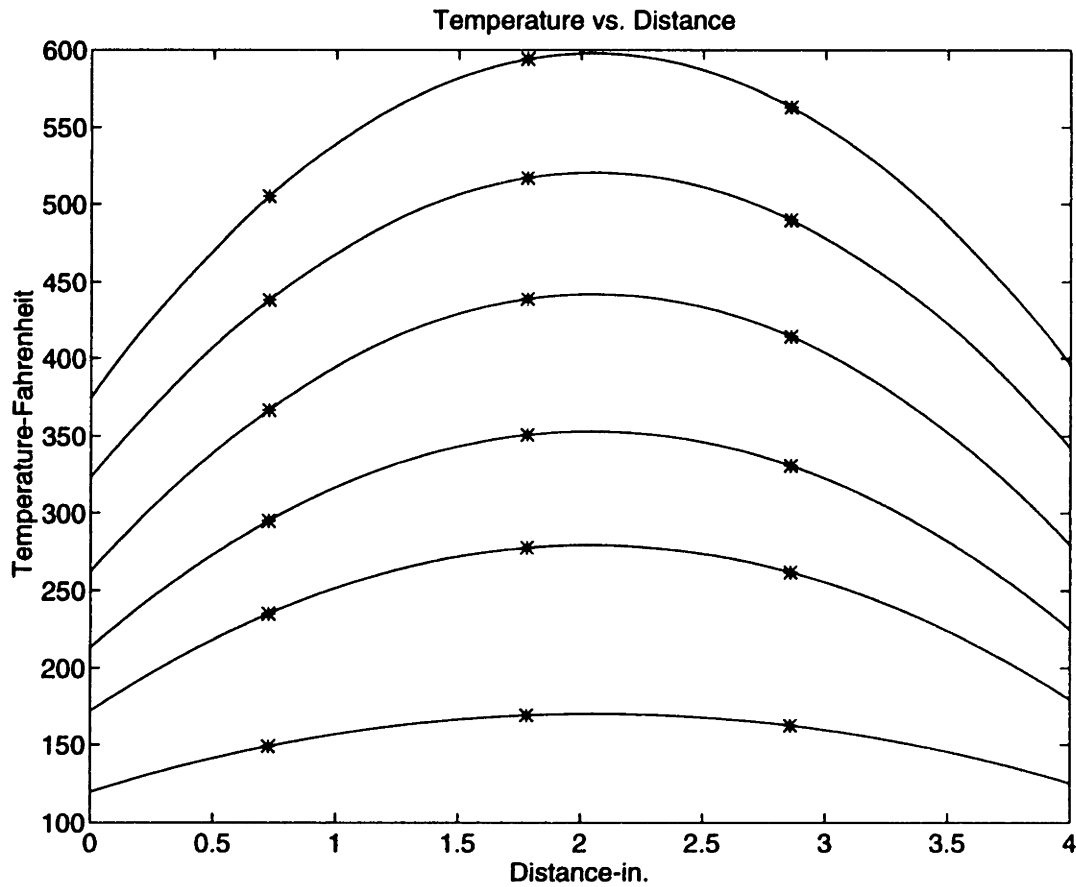
Figure 7-3: Parabolic fit for Calibration Data

positions of the thermocouples are measured relative to the test section. No flow is used during the calibration process so the plug is made to fill the entire test section.

Once the plug is in place, the calibration procedure begins. The temperature is assumed constant circumferentially at each radial location as discussed in Chapter 2: Experimental Overview. The assumption is confirmed by the infrared signal which shows a square profile when each face is in focus except on the leading face where some of the energy is not reflected as shown in figure 7-1.

The entire test section is scanned with a set amount of current flowing. The test section is scanned at five or more different current levels, making sure the surface temperatures pass through the test regime that is usually around $(300\text{-}600^{o}K)$. The three radial thermocouple measurements are recorded for each calibration test case.

Since heat is lost through the ends due to conduction, a parabolic distribution along the test section is assumed and fit to each set of calibration data. Figure 7-3 shows the parabolic fits for the uneven walled, smooth rectangle. Once both of these procedures have been performed, each element on the test section has five voltage-temperature pairs. These five data points are then fitted with a line. There is one curve for each element on the surface. When a test is performed, the data reduction program uses the fit for the given element to determine the temperature from the voltage measured by the infrared detector. A detailed example of the linear fit is given in Appendix B. The calibration procedure has been tested for variance over time. Two calibrations were performed a week a part and the curves were within 1% of each other. They also generate average wall temperatures with $5^o K$ of each other.

7.3   Test Run

7.3.1   The Infrared Detector and the Optical System

In order for the detector to function properly a number of checks are performed. The first task is to perform a system check. The mirrors are cleaned with lint free clothes and alcohol. All lose screws and bolts are tightened and optical system is locked in place. The location of the secondary mirror determines the magnification of the surface element being viewed. Once the integrity check is finished, the infrared chamber is filled with liquid nitrogen to provide a cool reference temperature for proper detector operation. The detector dewar has a holding time of twelve hours. As the detector is cooling, the power to the infrared detector, the potentiometers, and the axes motors is activated. The infrared detector signal is triggered off the optical encoder's index pulse. The ADTEK board is set to record and collect two hundred and fifty six points spanning the width of the four sides of the test frame each revolution. Once cooled, the infrared detector signal appears on the oscilloscope upon rotating the arm. The axes motors are check occasionally to ensure proper operation. The horizontal and vertical axes are controlled by a computer program that converts

90

programmed distances into motor commands. Roughness and loud crackling during operation are signs of system damage. Once all the measurement, translating, and flow systems are activated, the data collection program 'try' is initiated

7.3.2 Setting the Flow

Upon determining the test parameters, the compressor is switched 'on' and the flow pressure and massflow are set. The bypass valve is fully opened when the compressor is activated so that flow is circulated through the closed loop outside the experimental system. Fluid is introduced into the system until the desired recovery tank pressure is achieved . This pressure is usually well above the flow pressure to provide a steady flow of freon.

Having set-up the flow outside the system, the system outlet valve is opened immediately followed by the system inlet valve. The fluid begins to circulate through the main system. The bypass is adjusted to compensate for the flow that is not passing through the main system. The massflow is set by adjusting the system outlet valve until the desired massflow is reached. The pressure is set by adjusting both the system inlet and outlet valves. The two valves require a lot of fine adjustments to achieve the exact operating conditions. Once the desired conditions are reached, the fluid supply valve is adjusted to compensate for leakage in the main system.

7.3.3 Setting the Current

Once the flow is established, the Airco welder is used to drive current through the system. If all the leads properly attached, the Airco welder puts out approximately 60 to 70 amperes minimum depending on the model resistance. For that reason, it is important to establish the flow before turning on the current supply. It only takes a few seconds to damage the test module. The current is adjusted until the desired inlet and outlet temperatures are reached. It is a game of trial and error because the internal heat exchangers take a very long time to heat up and cool down. The signal is monitored on an oscilloscope to make sure the module surface is not too hot. At

this time, it can take approximately ten to thirty minutes to reach steady state.

7.3.4 Steady State

As the system approaches steady state, the vacuum pump is activated and the drive system is adjusted to the proper rotation. Vacuum reduces the amount of heat lost to the surroundings. It also allows the drive system to rotate at high speeds. The rotation introduces some changes so the system is allowed to approach steady state once again. It takes an additional five to ten minutes. If running at low speeds, the arm rotation may begin immediately after the system reaches vacuum. High speeds generate a lot of heat in the seals and it is optimal to only rotate the arm during the test to preserve bearing life and preserve the seals. Steady state is determine by the steadiness of pressure, massflow, and temperature. The massflow and pressure reach steady state in a matter of seconds but the temperature takes a lot longer. Steady state is assumed once the inlet and outlet thermocouples remain within two to three degrees Fahrenheit over five minutes. Therefore, the temperature does not vary more than five degrees over the course of the fifteen minute test.

7.3.5 Data Collection

Once steady state is reached, data collection begins by activating the computer program presently named 'try'. The program scans all four sides of the test section over a four inch span. The program records 256 points of data 0.02 inches apart each radial increment. These points include data from all four sides. But, only one face is in focus at a time so the program scans the first face from bottom to top before moving to the next face. The focal points are added to the data collection program prior to the run based on the focus run described earlier. The program can be modified in numerous ways. The number of passes may vary to gain better radial resolution. The circumferential spacing of 0.02 inches may change to obtain more or less points per face. The radial starting point can change depending on whether the inlet, outlet, localized, or complete data is desired. Presently, the program is set up to take sixteen

radial passes at 0.25 increments starting at the very bottom of the test section. In addition, an ensemble of ten revolutions of data is averaged for each radial location to reduce noise. The program is very flexible having the ability to be adapted to the experimentalist's needs.

Once scanning begins, important parameters are recorded on the data sheet shown in figure 3-1. In recording the data, random variation are documented under comments. The parameters are recorded each time the optical system focuses on a new face. The program notifies the user each time the optical system moves by printing the coordinates out on the screen. It is necessary to index the optical system manually via a linear actuator to focus on the leading and rear faces. The computer notifies the user when this is necessary. Near the end of the scan, all the parameters are recorded to evaluate variation over the course of the test. If the flow temperatures are within 5^oF, the test is considered steady. The massflow and pressure usually do not vary significantly over the course of the test unless a large leak develops or the compressor fails.

Upon completing the test, all the scan*.dat files are copied to 'test'*.dat files. Now new operating parameters are set. Upon reaching steady state again, the procedure is repeated. After running five tests, the integrity of the system is checked.

Once all testing is over for a long period, the speed of the drive motor is reduced until the arm stops rotating. The current to the test model is slowly decreased and the power supply is switched 'off'. After allowing the test section to cool to a satisfactory temperature, the flow is collected in the compressor system by first closing the inlet valve to the system. Once the pressure drops to vacuum, the exhaust valve is closed and the compressor is switched 'off'. The vacuum is released by closing the vacuum chamber valves and opening the vent to atmosphere.

7.4 Data Reduction

Once the test is over, the data has to be stripped using a program called 'strip'. Two hundred and fifty six points are collected for each revolution. Only one face of the

four included is relevant. 'Strip' allows the experimentalist to strip the relevant data by knowing what face is in focus and saving only the points between the rise and fall of the detector signal for that face. The relevant data is located by modifying a file called test_strp.dat which contains the approximate location of the first point of each pass on each surface. Upon being stripped, the files are copied into another directory for further reduction. Barry discusses the process in further detail[3].

The data is still in the form of voltages. These voltages have to be converted into temperatures and eventually Nusselt number ratio for industrial use. The conversion is performed by the program 'Reduce'. 'Reduce' also computes the non-dimensional parameters of the test run. The program is slightly different depending on the module geometry. These changes are easily made in the code. 'Reduce' takes the voltages from the infrared detector and converts them into temperature using the calibration curve for each element. It determines the cooling fluid parameters using curve fits to experimental data and look up tables[1, 2]. It is important to use the same number of passes and points in the calibration and the test because the program accesses the calibration curves based on pass and point. The average wall and bulk temperatures are used to determine the Density parameter. All other parameter are also averaged and entered into an input file which 'Reduce' accesses to compute the test variables described in Chapter 2: Experimental Overview.

'Reduce' creates four temperature and nusselt number files. These files can be plotted using any data analysis package or manually. 'Lookd' and 'nd' are two 'Matlab' files which are used to view the temperature and Nusselt numbers on the four faces. Once satisfied, the test is complete.

Chapter 8

EXPERIMENTAL APPARATUS

The rotor of the Gas Turbine Lab Heat Transfer Facility(See figure 8-1) is housed in a vacuum chamber approximately 50 inches in diameter on the inside. The on-rotor instrumentation, that holds the thermocouples, passes along a strut through the center of the rotor into a conduit in the shaft and out to a slip ring. From the slip ring, the eight thermocouples leads (1 ground / 7 thermocouples) are connected to a thermocouple meter. The primary temperature measurement system is an infrared detector which measures the infrared energy received from the test section. The infrared detector and optical system is mounted on a platform which has two degrees of freedom, up and down relative to the ground and inward or outward relative to the test section. The optical system directs energy onto the infrared detector. The digital stages allow the infrared detector to focus and traverse the test section. The following section describes the details of the G.T.L's Heat Transfer Experiment.

8.1 The Rotor

A shaft, mounted on two deep groove ball bearings passes through the center of the chamber. Inside the vacuum, a rotor is constructed around the shaft. The rotor is shaped like an arm made of two large 1/2" plates of 17-4PH steel and four 1/2" spacers of 17-4PH steel held together with 1/2" high strength steel bolts. The steel (17-4PH) is used for its strength and temperature characteristics. A pair of heat

1. Vacuum Chamber
2. Model and Flat Mirrors
3. Imaging System (Primary and Secondary Mirror)
4. Infrared Detector
5. Heat Exchangers
6. Optical Encoder
7. Power slip Rings
8. Gun Bored shaft
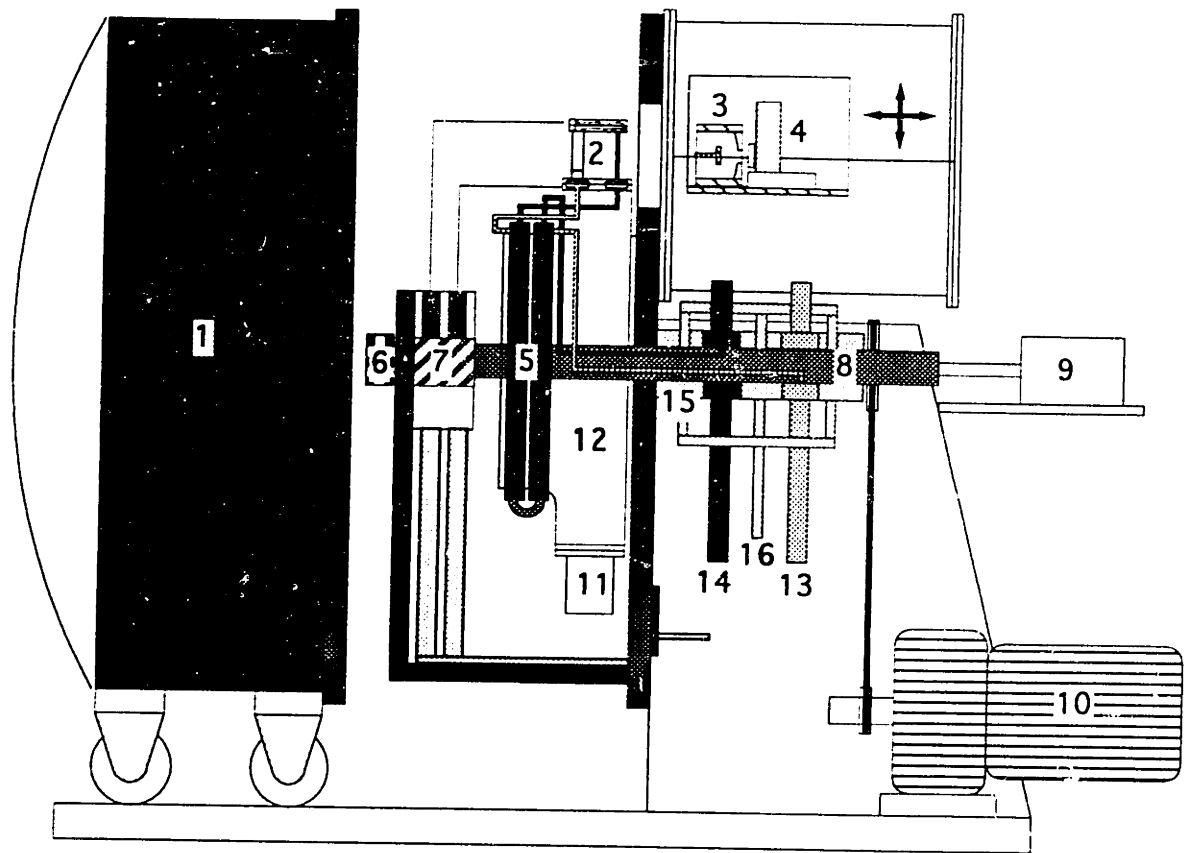
9. Instrument Slip ring
10. Variable Speed Motor
11. Counter Balance
12. Rotor
13. Freon Inlet Flow
14. Freon Outlet Flow
15. Seals
16. Seal Cooling System

Figure 8-1: Experimental Layout

exchangers is attached to each side of the rotor. One end of the rotor is used to mount the test section with a balance weight at the opposite end. The rotor contains additional holes for the purpose of balancing.

8.2 Flow System

The flow path begins at the compressor which circulates the cooling fluid. The fluid leaves the compressor and enters the main system passing through the rotating shaft past seals into the heat exchangers. The exchangers pre-heat the fluid before it reaches the test section. Then, the fluid exchanges energy with the test section and exits back into the heat exchangers. The incoming fluid cools the outgoing fluid as it travels inward toward the shaft. At the end of its journey, it flows past the seals, out of the main system, and back into the compressor for re-circulation.

8.2.1 Oil Free Compressor

The fluid is circulated by a Blackmer HD362A-TU refrigeration unit. All the data presented in Chapter 4: Result and Discussion uses freon-12 but it is soon to be replaced by R134A. R134A is the environmentally friendly substitute for freon-12. The compressor is oil free in an attempt to reduce the amount of contaminants in the system. In addition, there is a liquid trap at the inlet to protect the compressor from liquefied fluid. The compressor has a pressure ratio of 5 to 7 depending on the suction pressure and a maximum capacity of 36.0 CFM($61.2m^3/hr$) at 825 rpm.

The coolant passes from the compressor outlet through two water cooled shell and tube heat exchangers connected in series that cool the pressurized fluid prior to entering the main system. The water temperature is adjusted via a shower mixer to vary the temperature of the fluid prior to entering the main system. Leaving the heat exchanger cooler, the coolant collects in a large receiving tank where it waits to be circulated.

Due to small leaks in the flow path, fluid is periodically introduced into the system to maintain a high receiver pressure. The fluid is introduced into the system
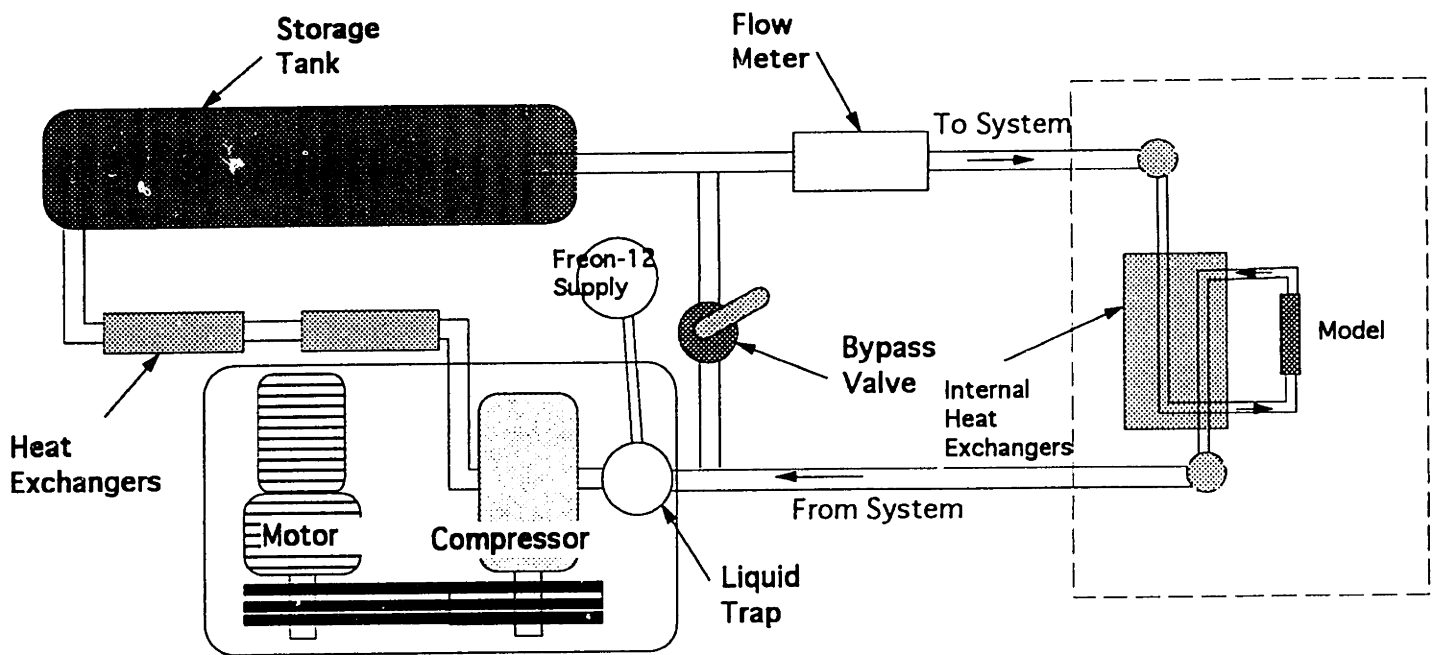
Figure 8-2: Compressor Circulation System

immediately after the liquid trap prior to the compressor inlet. Figure 8-2 shows a schematic of the compressor system.

8.2.2 Shaft Seals

Fluid flows out of the receiving tank into the rotating shaft which has graphite face seals. They are pressure balanced to allow operation at high speeds and pressures. In order to preserve their life, fluid passes through the seals cool as mentioned earlier. Upon passing the seals, the fluid enters a rotating heat exchanger.

The seal housing also provides three chambers for oil cooling of the seals. Regular vacuum pump oil is used for this purpose. See figure 8-1 for more detail.

8.2.3 Heat Exchangers

As mentioned earlier, two pairs of heat exchangers are attached to the rotor. The exchangers are connected at one end forming four exchangers connected in series. The exchangers are connected with an O-ring seal to prevent leakage and allow easy removal. As the cooling fluid flows toward the test section, it receives heat from the hot fluid flowing out of the test section. The incoming flow is pre-heated while simultaneously cooling the outgoing flow before reaching the shaft. Thus, only cool fluid flows through the shaft and seals. The fluid enters the shell and tube counter-flow heat exchanger through 61 small diameter (1.8 mm o.d. / 1.4 mm i.d.) stainless steel tubes. The outflow fills the space between these tubes and the large diameter(38.1 mm / od 28.6 mm id) stainless steel tube. The overall length to diameter ratio is 1780[11].

8.3 Coolant Flow Measurements

8.3.1 Massflow

As mentioned earlier, the massflow is measured at the inlet to the main system. The Massflow is measured using a F. & P. Co. Precision Bore Flowrator Tube which has an accuracy of 0.5%. A steel float determines the maximum capacity of the meter. The massflow is has more error because of errors in both the temperature and pressure The flow temperature and pressure are measured immediately after the flow meter. The massflow is necessary to compute both Reynolds number and flow velocity.

The compressor system generates a set massflow which is controlled by the inlet, outlet, and bypass valves to the main system. The position of these valves set massflow and pressure. The massflow can also be controlled by varying the compressor crankshaft speed. The speed can be changed by changing the pulley ratio on the compressor. A bypass is used to compensate for overflow. Numerous pressure measurements are taken outside the main system at the inlet, outlet, compressor outlet, compressor inlet, and the tank outlet. Unfortunately, setting the massflow and

pressure is more of an art than a science.

8.3.2 Temperature Measurements

There are seven thermocouple locations, limited by the number of wires which can pass through the center of the shaft. The thermocouple wires meet at a cold junction in the interior of the rotor. The seven thermocouple connections share a common ground. Thermocouple wire has to run from the measurement point to the cold junction. By knowing the temperature of the cold junction, the actually temperature is determined. Regular Copper wires run from the cold junction through the slip ring to the thermocouple meter. The cold junction eliminates the need for a thermocouple slip ring which is very expensive. Since the Omega thermocouple meter has cold junction compensation, a constant cold junction offset temperature can be programmed into the meter. The cold junction offset is presently set for room temperature. Up to ten different readings can be recorded by the meter. The thermocouple wires are KK-K-24 from Omega. It is K-type thermocouple wire, 24 gauge wire with Kapton insulation around each lead and Kapton insulation on the exterior. Kapton was chosen for its high temperature capabilities and the ability to strip it easily. GG-K-30 can also be used but the fiber-glass insulation is not so easy to strip. The fiber-glass is much more temperature resistant. See Figure 8-3 for more detail.

Not all seven thermocouple measurements are used in the experiment. Three are used for the calibration and only four are used in an actual experiment. Two measurements are taken at both the inlet and the outlet to the test section in an actual experiment. During the calibration, three surface temperature measurements are taken along the length of the test section. The thermocouples are located inside a special plug which allows the surface temperature to be measured. The two inlet thermocouples remain in place. Since, there is no flow during calibration they really serve no purpose. The sixth thermocouple wire remains attach to the exit plug which is now measuring the ambient temperature inside the vacuum. The seventh thermocouple is reserved for later use.

There is also one other important thermocouple measurement taken outside the
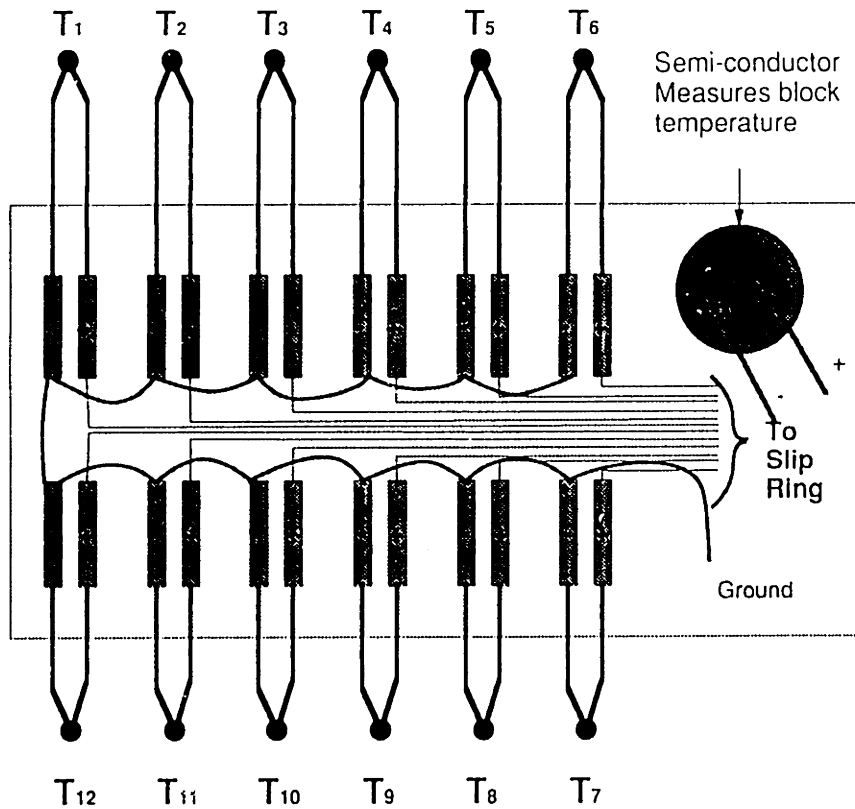
Figure 8-3: Thermocouple Wiring Diagram

system at the flow inlet. The measurement is necessary to calculate some flow parameters and to check the efficiency of the heat exchangers. Once again, it provides a way to check the efficiency of the heat exchangers.

8.3.3 Pressure Measurements

The pressure is measured by gauges located at the inlet and the outlet of the main system. The pressures are used to calculate massflow. These pressure gauges are accurate to 1/2 psi, upon initial calibration. The pressure drop across the system can be determine by the difference in these gauges.

8.4 Current Supply System

The current is supplied by one of two devices: an Airco welding power supply or a Hewlett Packard D.C. power supply. The Hewlett Packard is used to supply 60 or less Amperes while the Airco is used for 60 or more Amperes. Inside the vacuum
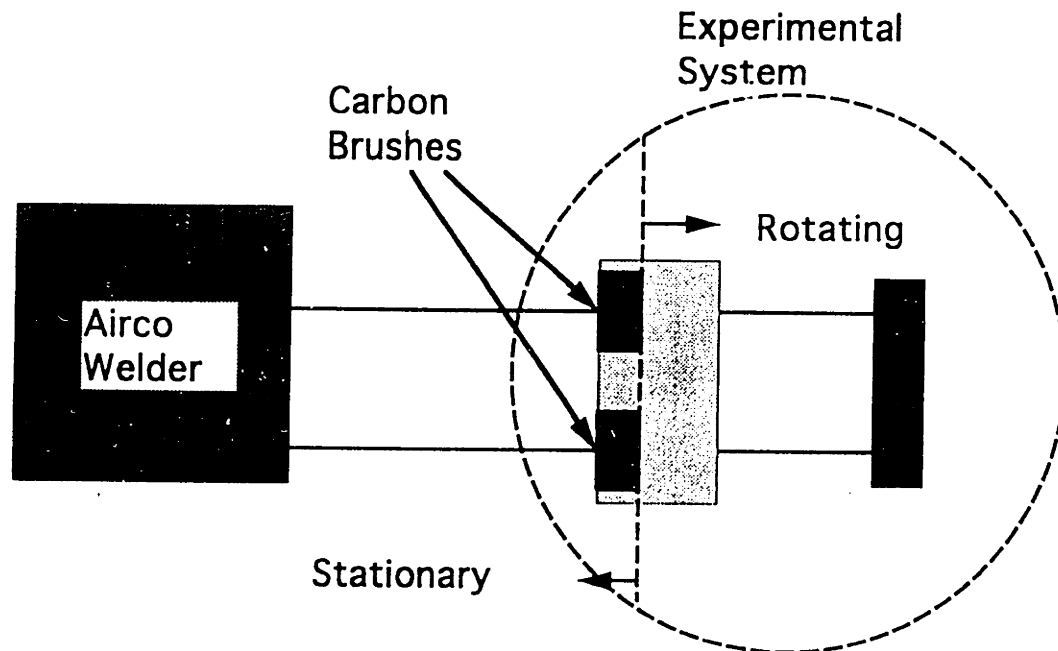
Figure 8-4: Current Supply System

chamber, 1"x1/16" copper strips lead to a power slip ring. These copper strips are insulated from the vacuum chamber by G10 (fiber-glass) strips placed between the copper and the chamber. The slip ring uses two 1"x1.5" carbon brushes press fitted against the rotating arm by constant force springs to transmit power. See figure 8-4 for a schematic.

The current supply system is easily switched outside the vacuum chamber. The range of operation varies between 20 and 150 amperes. The Hewlett Packard power supply is used mostly during the calibration process. The Airco is used mostly during actual test. The current is measured using a high precision TIF 1000 DC ammeter. The meter easily clamps around any wire less than 1 inch and the current is displayed on a digital reading with an accuracy of 2%. The current is also measured at the

power supply on a meter which is less accurate. The current is used to calculated the amount of joule heating introduced into the system.

8.5   Drive System

The shaft is driven by a 7.5 horsepower motor. The motor is attached to an armature that controls the friction on the output shaft thus varying the speed. The armature is controlled via a U.S. motor controller, with a speed range from 0 to 3600 revolutions per second(RPM).

Due to torque limits, a pulley reduction is necessary. Therefore there is a two-thirds reduction in speed between the shaft and the motor. The rig is only capable of reaching speeds up to 2400 RPM. One V-belt is used to connect the drive motor to the shaft.

The shaft speed is measured using an BEI L25G-500-ABZ-7404-ED15-5 optical encoder. The encoder allows speed, direction, and location. to be measured The computer data acquisition is triggered by the index pulse of the optical encoder. Using optical encoder data, the location of the data points is accurately determined. In addition, the sampling frequency is determined based on the speed measured by the optical encoder.

8.6   Surface Temperature Measurements

The surface temperature measurement is one of the characteristics that make the G.T.L.'s heat transfer experiment unique. An infrared detector system replaces the tedious cumbersome thermocouple maze of past experiments. Using an optical system, the energy emitted by a $1mm^2$ area is measured. The system allows hundred of temperature measurements to be taken on one surface.

8.6.1 Infrared Detector

The most important piece of apparatus is the Electro-Optical Systems, Inc. HgCdTe (MCT Series) infrared detector which actually measures the temperature of the test section by sending out a voltage directly portion to the amount of energy it receives from an object. The infrared detector contains an internal pre-amplifier which has a high/low gain switch. It absorbs a given amount of energy and converts that energy into a signal which is transferred to the computer. The detector receives power and sends out a signal approximately proportional to the temperature to the fourth power.

As the heated test section rotates, a signal is emitted from the detector. The detector is triggered by the location of the rotor as mentioned earlier. The detector is mounted on a platform that has two degrees of freedom. The motion is controlled by linear motion slides driven by motor-lead screw arrangements. The horizontal axis focuses the four faces of the test section. Each face has a different focal point. The vertical axis traverses the test section from inlet to the outlet. The rotation of the rotor provides circumferential data points for the stationary infrared detector.

8.6.2 The Optical System

The infrared detector receives radiation through the optical system. There are three subsystems to the optical system. All four sides of the test section are viewed using two flat mirrors positioned at 45° angles. The cone of energy emitted from points on the surface is focused on the infrared detector element using a primary and a secondary mirror.

The Flat Mirrors

The flat mirrors are positioned behind the test section inside the test frame. These mirrors are position at 45° to allow the leading , trailing, and back surfaces of the test section to be viewed by the detector. The leading and trailing faces are viewed by the optical system through one reflection while the back requires two reflections. By setting the mirrors at 45° angles, each side has only one focal point. As the rotor
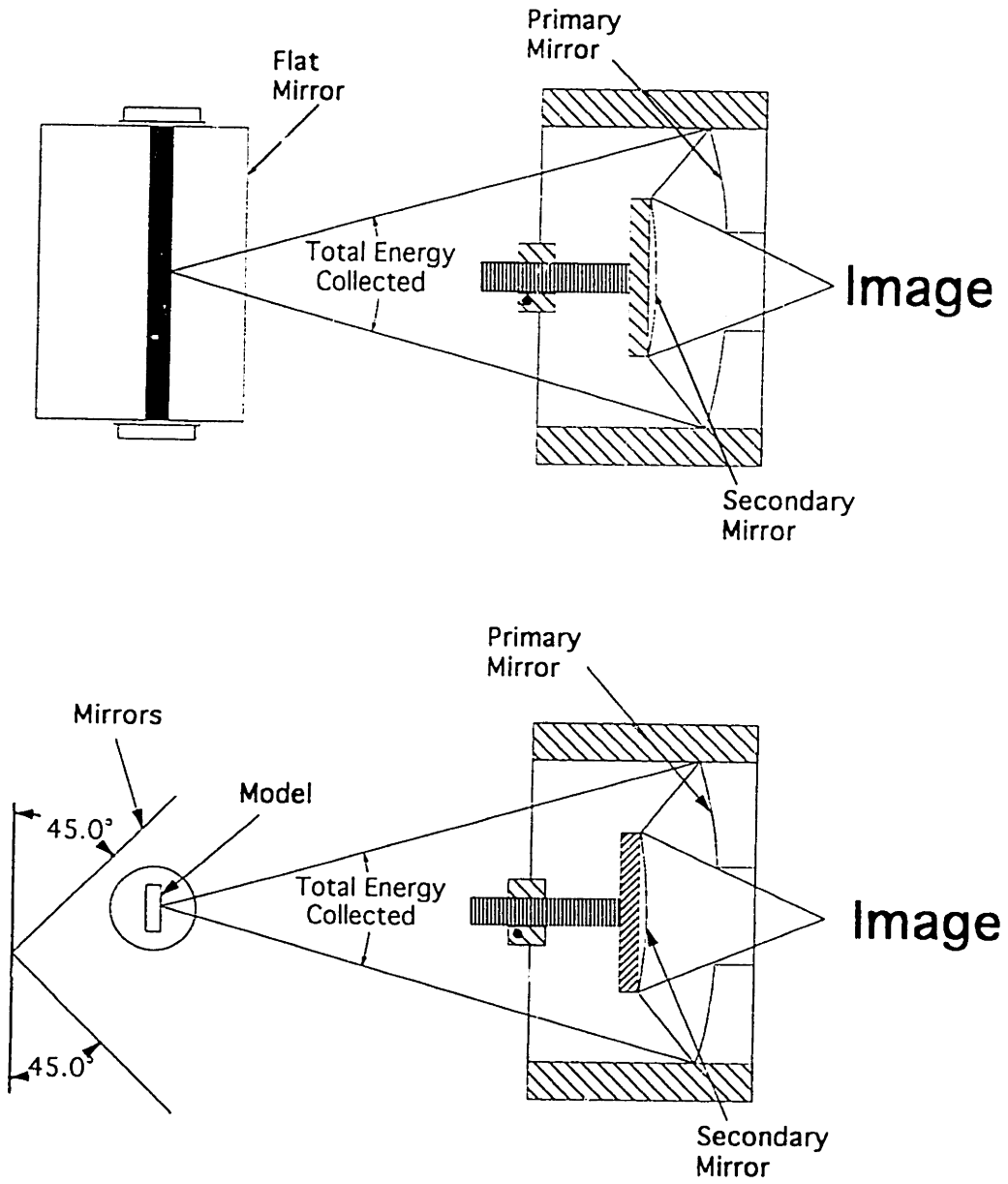
Figure 8-5: The Optical System

rotates counterclockwise, the leading side is viewed followed by the back, then the front, and finally the trailing. The mirrors are fitted inside two mirror mounts within the test frame.

The Primary and Secondary Mirror

The Primary mirror collects a cone of radiation from each element on the test module. It then re-directs the energy onto the secondary mirror which focuses the energy directly onto the infrared detector. The spherical convex secondary mirror has a radius of curvature of 138 mm while the spherical concave primary mirror has a radius of curvature of 150 mm. These mirrors are coated with Aluminum Silicate(AlSiO) to produce a reflectance of 97% in the infrared regime. The location of the secondary relative to the primary determines the magnification of the system. The spot seen on the model is approximately the same size as the detector element. The primary and secondary mirror are mounted inside a housing that permits the secondary mirror to be translated via a finely threaded screw, changing the magnification factor if necessary. Once the mirror housing and the infrared detector are fixed, the secondary mirror is translated to provide the appropriate magnification. Once the magnification is set, the threaded screw is locked in place and the horizontal axis is used to bring the test section into focus.

Translation System

The translation system serves two purposes: bringing the test section into focus and radially traversing the test section. The linear motions are controlled via stepper motors which drive lead screws to produce linear motion. The motors are controlled using Slo-Syn controllers that translate computer commands into digital signals. The location of these axes is determined using linear potentiometers.

8.7 Test Section

The test section is a critical component of the experiment. It has to hold together under centripetal stresses. It has to pass current through the test module. It must be flexible enough to hold modules of numerous different geometries. It must pass a flow of cooling fluid through the test module without any leakage. It has to provide room for the measurement of temperatures, pressure, and other parameters. It has to allow all four faces of a test module to be viewed by the detector.

8.7.1 Test Frame

The first part of the test section is the base. The main function of the base is to hold all the components of the test frame and separate the inlet and outlet streams. It also provides a channel for the inlet plenum instrumentation. The base provides a 1" hole for the test section, a 1/2" hole for the exit stream, and mounting holes for the mirror mounts and clamping bolts.

The next part of the test frame is the exit passage. The exit passage has to allow fluid to exit the test section. It has to be strong enough to withstand the centripetal forces but current cannot pass through the exit channel. The exit channel is simply a circular tube with flanges on both ends. It is broken by a fiberglass plug to stop current from flowing through it. The exit passage is 4 inches long with a 1/2" hole through the center. An O-ring seal is located at both the beginning and end of the exit passage.

The upper channel of the test section has to allow the flow to make a smooth transition from the test section to the outlet plenum. It is made up of two halves that form a 1/2" diameter channel when clamped together with an O-ring seal to prevent leakage. The top half of the upper channel contains a plug for the instrumentation directly above the test module. The plug is bolted into a 1/2" hole with an O-ring seal. The plug has two thermocouple taps and three pressure taps. The thermocouples measure the exit temperature of the flow stream as mentioned earlier. The pressure taps measure the pressure distribution of the exit flow. The bottom half of the upper
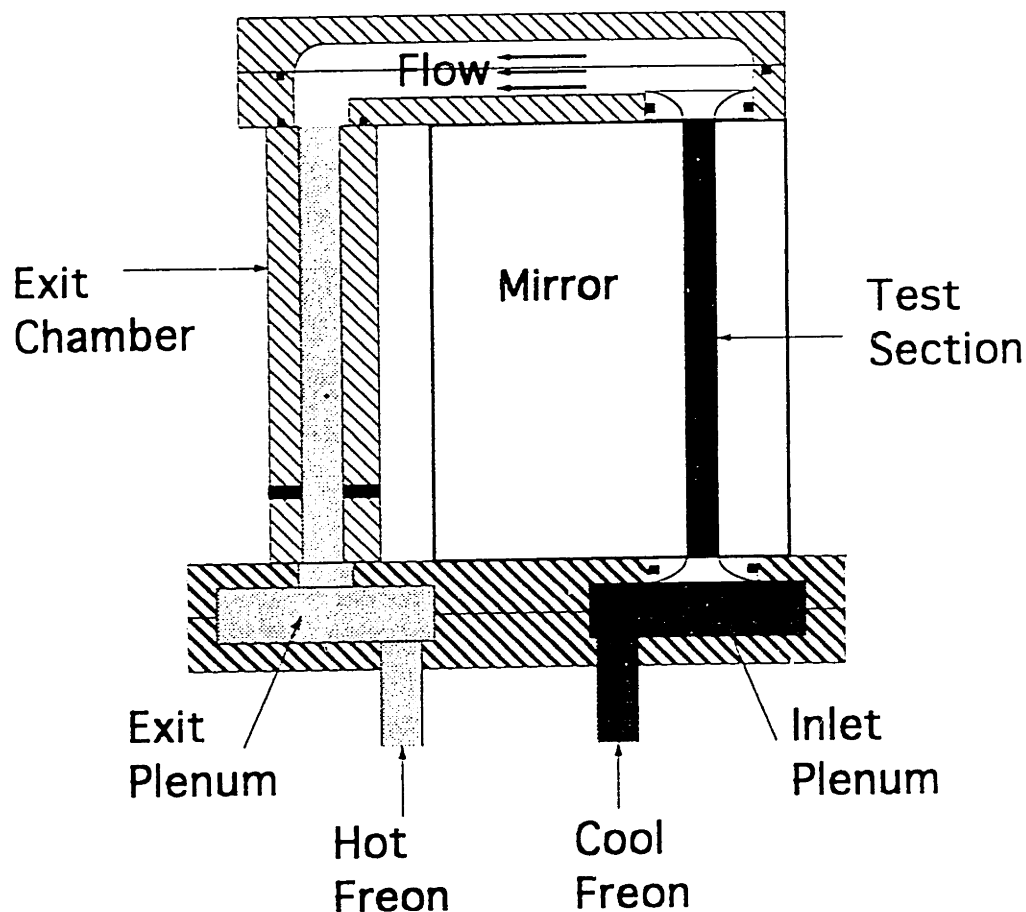
Figure 8-6: Test Frame

channel contains a 1" inch hole for the test section. The bottom half of the upper channel also has holes to clamp the test frame together and hold the mirror mounts in place at 45 ° angles. See figure 8-6 for a layout of the test frame.

8.7.2   Cooling Passage Model

The test section is designed to meet the criteria listed in the introduction of the thesis. The dimensions of the test section are determined based on the strength and flow requirements necessary for these parameters. All the test sections have a hydraulic diameter approximately 7.5 mm (.295 "). Each test section is four inches long and has walls approximately 0.01 to 0.02 inches thick. The ends are design to allow a smooth transition from the inlet plenum to the test section for a uniform inlet
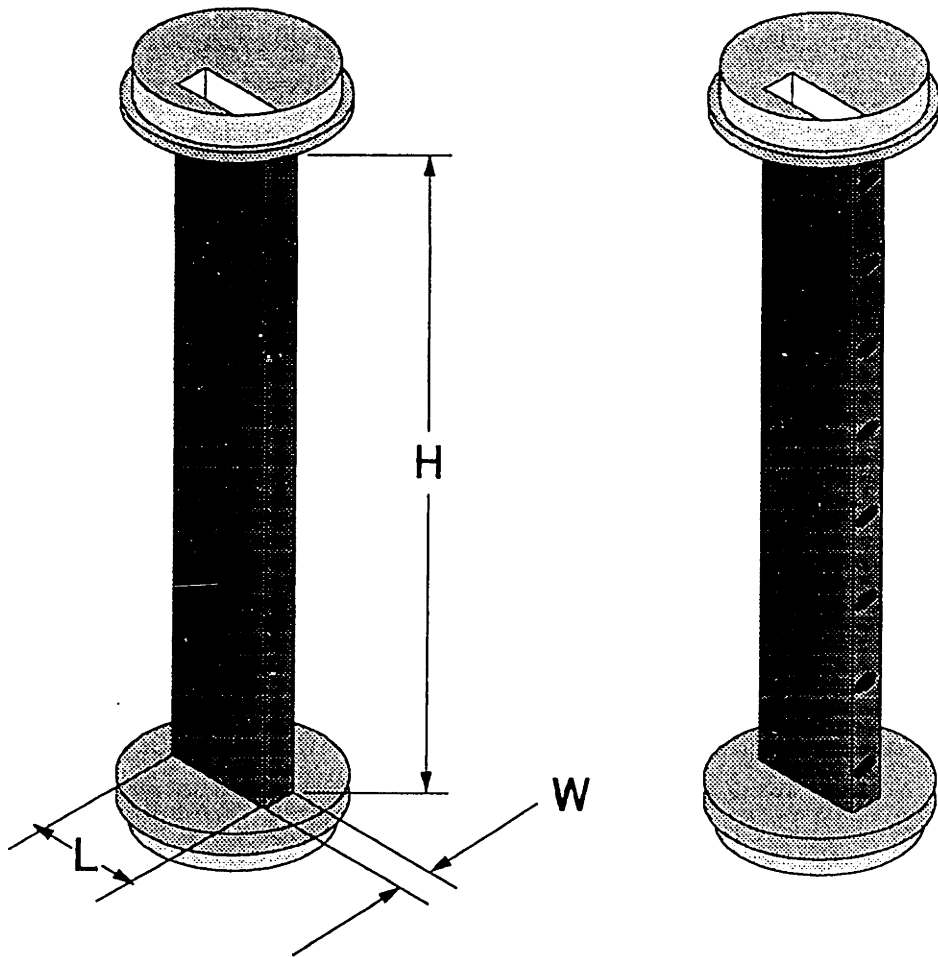
Figure 8-7: Test Modules

velocity profile. The ends make a smooth transition from circular to rectangular. There is a smooth square, a smooth rectangular, a turbulated rectangular, and an uneven walled, smooth rectangular test module. For the turbulated rectangle, the turbulators are at 45° to the flow direction. For the uneven walled, smooth rectangle, one face is approximately twice the thickness of the other. Using these test sections, the effect of geometry on heat transfer in rotating turbine blade cooling passages can be studied. In addition, the 1" hole in the base and upper section provide the ability to turn the test section at different stagger angles. Different geometries can be used in the same test frame as long as the ends have a 1" swivel junction on them. Characteristic such as thickness, uniformity, aspect ratio, and material may vary without changing the test frame.

The present models are made of Nichrome 80/20. It has properties that are very advantageous for the experiment. The thermal conductivity is nearly constant with temperature so the resistance does not change very much with temperature. The material is used in radiation heaters. See figure 8-7 for an example of the smooth rectangular and turbulated rectangular test section.

The test sections fit tightly between the base and upper channel of the test frame. O-ring seals prevent fluid leakage. A copper clamp maintains metal contact between the base and the bottom of the test section. A copper spring maintains contact between the lower half of the upper channel and the top of the test module. Contact is very important to minimize changes in resistance during rotation. If proper contact is not maintained, the current through the test section varies over the duration of the test. The top clamp has to be a flexible because the test section expands as it heats up. If the test section is over constrained, it buckles. A flexible mechanical connector allows the test section to float in the lower half of the upper channel.

Appendix A

LIMITATIONS

A.1 Reynold Number

The Reynolds Number is a measure of the relative influences of inertial forces to viscous forces. The Reynolds number is given by the following equation.

$$Re = \frac{uD_h}{\nu} \tag{A.1}$$

u is mean velocity in the radial direction, D_h is hydraulic diameter, and ν is kinematic viscosity. In the present set-up, the cooling fluid used is freon-12. The density,ρ, is determined using a look table extracted from *Thermophysical Properties of Refrigerants* by ASHRAE[1]. The dynamic viscosity,μ, is computed using equation 3.1

For equation 3.1, the temperature, Tb_{avg}, is in degrees Kelvin. The mean radial velocity, u, is determined from continuity.

$$u = \frac{\dot{m}}{\rho A} \tag{A.2}$$

$\dot{m}$ is the mass flow rate and A is the cross sectional area. Upon plugging equation A.2 into equation A.1 and using the volume flow rate instead of the velocity, the maximum Reynolds number range is determined based on the maximum flow rate of the mass flow meter, the hydraulic diameter of the test section, and the physical

P(psig)	$\rho(kg/m^3)$	$\mu(m^2/s)$	$Tc(^oK)$	Re
50	21.0	1.4×10^{-5}	328	1.52×10^5
50	20.1	1.4×10^{-5}	339	1.45×10^5
50	18.7	1.4×10^{-5}	361	1.33×10^5
100	40.2	1.4×10^{-5}	328	2.02×10^5
100	38.2	1.4×10^{-5}	339	1.93×10^5
100	35.0	1.4×10^{-5}	361	1.77×10^5
150	62.5	1.4×10^{-5}	328	2.43×10^5
150	58.7	1.4×10^{-5}	339	2.32×10^5
150	52.6	1.4×10^{-5}	361	2.12×10^5

Table A.1: Reynolds Number Computations

properties of the fluid.

$$Re_d = \frac{\rho \dot{Q}}{\mu D_h} \tag{A.3}$$

$\dot{Q}$ is the volumetric flow rate. Table A.1 shows the Reynolds numbers that are obtain at selective pressures and temperatures. The pressure and temperature are limited by the maximum stresses which the thin walls of the test section can withstand. The hydraulic diameter of the test section is approximately 7.5mm(0.295in). The maximum Reynolds number can be increased by obtaining a different mass flow meter or decreasing the hydraulic diameter of the test section.

A.2 Rotation Number

The Rotation number is a measure of the rotational versus coolant velocity. It is the inverse of the Rossby Number which John Kreatsoulas uses in an experiment performed using the same apparaวus[11].

$$Rot = \frac{\Omega D_h}{u} \tag{A.4}$$

Ω is the rotational frequency. As mentioned in the introduction, the drive system is capable of speeds up to 2400 RPM. The maximum speed used for the data presented in this thesis is approximately 1900 RPM. Table A-2 shows the maximum rotation

Reynolds	$\Omega(RPM)$	Rot
2.5×10^4	2400	0.82
6.0×10^5	2400	0.34
1.2×10^5	2400	0.17
2.0×10^5	2400	0.10
2.5×10^5	2400	0.08

Table A.2: Rotation Number Computations

number attained at various Reynolds numbers for a bulk temperature of $339^o K$ and a pressure of 50psi. The maximum rotation numbers obtained at a given Reynolds number are increased by decreasing the flow velocity as a result of changing the flow properties, density and viscosity.

A.3 The Density Parameter

$$Dens = \frac{\Delta \rho}{\rho} = \frac{Tw_{avg} - Tb_{avg}}{Tw_{avg}} \qquad (A.5)$$

The density parameter is controlled by the current and flow rate. The density parameter is determined by averaging the wall temperatures and computing an overall bulk temperature based on the inlet and outlet temperatures. Setting the density parameter is a result of experience and previous results. In a constant heat flux experiment where both the wall temperature and the bulk temperature vary along the test section, the density parameter is difficult to set in advance.

A.4 Buoyancy Parameter

$$Bu = \frac{\Delta \rho}{\rho} \frac{\Omega^2 D_h^2}{u^2} \frac{R_m}{D_h} \qquad (A.6)$$

The Buoyancy parameter is a correlation that attempts to combine the effects of rotation number and density parameter for a given geometry. Thus the limitation on the maximum Buoyancy parameter the experiment can attain is a function of rotation number and density parameter. For the data presented in this thesis, the Buoyancy

Geometry	$D_h(mm)$	L/D_h	R/D_h
Smooth Square	7.5	13.5	61.0
Smooth Rect.	7.5	13.5	61.0
Turbulated Rect.	7.7	13.2	59.4
Uneven walled Rect.	6.7	15.2	68.2

Table A.3: Geometry

parameter ranges from 0.004 to 6.188.

A.5 Geometrical Parameters

The range for L/D_h and R/D_h are 12-14 and 61-67, respectively depending on the test sections hydraulic diameter. Table A.3 below shows the parameters for each test section based on a mean radius of 457.2mm(18in) and a test section length of 101.6mm(4in).

Appendix B

COMPUTATION OF TEMPERATURE AND NUSSELT RATIO

The temperatures are obtain from calibration curve created by the data reduction code. The calibration procedure is explain in Chapter 3. After completing the calibration, there are four files containing voltages for each surface. The calibration plug is used to obtain surface temperature measurements. The reduction code matches each temperature with a voltage based on element location. The element is located based on its pass number and its point location. There are either 15 or 16 passes taken radially. There are 13 points on all faces of the square module. There are 29-30 points on the front and back faces and 8-9 points on the leading and trailing faces of the rectangular modules. The calibration procedure creates a temperature voltage curve for each element on the surface. Figure B-1 shows the curve for the ninth radial pass and the fifteenth circumferential point on the front surface. The points in the table are fitted with a line to form the calibration curve for this element.

Voltage vs. Temperature
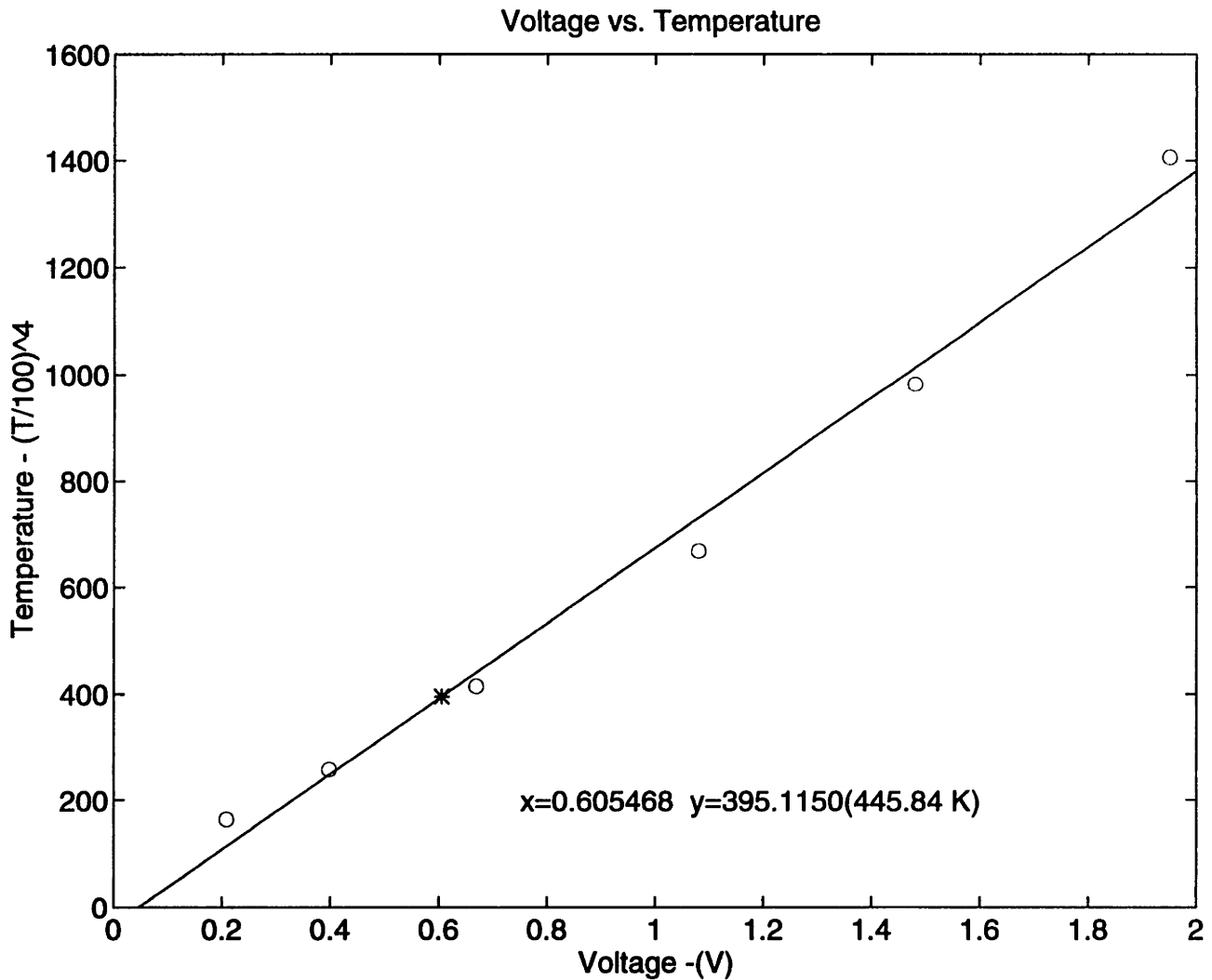
Figure B-1: Calibration Curve

Voltage	$(\frac{T}{100})^4$
0.208008	164.219345
0.397462	258.025513
0.668945	414.177533
1.080078	667.720032
1.479981	981.889465
1.950684	1405.890625

The star represents the test voltage for one random case. It is 0.605468 which has a value of 395.1150 which is $445.84^{o}K$ when converted. The procedure above is performed for each element on the surface. Upon scanning the four test files, four new temperature files are created. The temperature files are then used to compute Nusselt

numbers. Knowing the temperature of the surface, the Nusselt ratio is calculated using equation 3.7. The joule heating per element for this random case is 0.0497 W as calculated using the equation below.

$$Q_{elem} = \frac{I^2 R * V_{elem}}{V} \tag{B.1}$$

I, R, V, and V_{elem} represent the current, resistance, volume, and element volume. The conduction correction factor is calculated using polynomial fits to the temperature profiles. The equations below show the polynomial equations for the radial and circumferential fits of the particular element.

$$T_{radial} = 401.22 + 2120.84 * y - 45065.57 * y^2 + 557536.94 * y^3 - 3395308.25 * y^4 \tag{B.2}$$

$$T_{circumferential} = 449.49 - 4.90 * x - 0.231943 * x^2 \tag{B.3}$$

Using these equations, the derivatives in the radial and circumferential direction are computed analytically. The location of the point in x-y coordinates is (0.008385, 0.05715)m. The conduction in the radial direction is 0.000768W or 1.55% of Q_{elec}. The finite difference method yields a radial conduction of 0.00563W or 11.3%. The conduction in the circumferential direction is -0.000125W or -0.25% of Q_{elec}. The finite difference method yields are circumferential conduction of -0.00346W or -6.96%. In this case, the conduction correction is 0.000642W or 1.3%. The radiation term is 0.004422W or 8.9% at an emissivity of 0.7. For the test case in question, the local bulk temperature is 343.06°K. Now all the terms necessary to compute the heat transfer coefficient are known. Using equation 3.7, the heat transfer coefficient is 129$W/m^2 - K$. The hydraulic diameter is 7.5mm. The thermal conductivity of freon-12 at the local bulk temperature is 0.013W/m-°K using equation 3.4. In equation 3.4, the temperature is in degrees Rankine. The local value of the Nusselt number using the Colburn equation is 67.06. The ratio $\frac{hD_h}{kNu_{inf}}$ is 1.11 for this element. The same procedure is performed on each element.

Appendix C

NOMENCLATURE

A	Cross Sectional Area, m^2
Bu, Buoy	Buoyancy Parameter
C_p	Specific heat, J/Kg-K
D_h, d_h	Hydraulic Diameter, m
Δx	Circumferential Increment, m
Δy	Radial Increment, m
Δt	Model Thickness, m
Eck	Eckert number
ϵ	Emissivity of Nichrome
γ	Ratio of specific heats
Gr	Grashof number
h	Heat Transfer Coefficient, $W/m^2 - ^o K$
I	Current, Amps
k	Thermal Conductivity of Nichrome, W/m-K
k_f	Thermal Conductivity of Freon-12, W/m-K
L	model length, m
$\dot{m}$	Mass Flow Rate, kg/s

μ	Dynamic viscosity, kg/m-s
M	Mach number
ν	Kinematic viscosity, m^2/s
Nu	Nusselt number
Nu_∞	Nusselt number from Colburn correlation
Ω	Rotational Speed, radians/s
P	Perimeter
Pres	Pressure, N/m^2 or psi
Pr	Prandtl Number
$\dot{Q}$	Volumetric Flow rate, m^3/s
q	Flux, energy per unit area, W/m^2
Q_{elec}	Joule Heating(I^2R), W
Q_{cond}	Conduction Correction, W
Q_{rad}	Radiation Correction, W
ρ	Density, kg/m^3
$\frac{\Delta\rho}{\rho}$, Dens	Density parameter
x	Circumferential Location
r, y	Radial location
R	Resistance, Ohms
Ra	Rayleigh number
Re	Reynolds Number
R_m	mean radius, m
Rot	Rotation Number
σ	Boltzmann Constant, 5.6697 $\times 10^{-8} W/m^2 -^o K$
T_{wall}	Local wall Temperature, K
T_{bulk}	Local bulk Temperature, K
t	time, s, or thickness, m
u, V,v_m	Mean Radial Velocity, m/s
V	Volume
V_{elem}	Volume of an element

Appendix D

DATA

D.1 Smooth Square

Test	Reynolds Number	Density Parameter	Rotation Number	Buoyancy Parameter
m43	29,000	0.229	0.55	4.300
m44	29,000	0.274	0.35	2.102
m45	29,000	0.306	0.24	1.061
m46	29,000	0.349	0.12	0.325
m47	32,000	0.239	0.21	0.671
m49	61,000	0.323	0.10	0.192
m50	56,000	0.290	0.26	1.232
m51	59,000	0.302	0.15	0.424
m53	124,000	0.278	0.10	0.173
m54	120,000	0.302	0.06	0.066
m55	33,000	0.266	0.11	0.197
m64	86,000	0.301	0.07	0.0.081

D.2 Smooth Rectangle

Test	Reynolds Number	Density Parameter	Rotation Number	Buoyancy Parameter
a03	26,000	0.061	0.16	0.088
a04	25,000	0.046	0.16	0.074
a05	25,000	0.063	0.32	0.397
a07	26,000	0.063	0.46	0.810
a09	21,000	0.278	0.16	0.459
a10	25,000	0.205	0.15	0.299
a11	25,000	0.198	0.29	0.979
a12	26,000	0.205	0.40	2.039
a13	25,000	0.302	0.13	0.306
a16	25,000	0.289	0.25	1.064
a18	25,000	0.297	0.39	2.696
a19	141,000	0.103	0.03	0.004
a21	144,000	0.106	0.05	0.016
a24	73,000	0.095	0.05	0.016
a25	70,000	0.102	0.06	0.020
a26	69,000	0.096	0.10	0.059
a34	69,000	0.104	0.26	0.442
a36	71,000	0.114	0.20	0.291
a40	141,000	0.104	0.13	0.106
a41	144,000	0.107	0.10	0.066

D.3 Turbulated Rectangle

Test	Reynolds Number	Density Parameter	Rotation Number	Buoyancy Parameter
m33	25,000	0.312	0.13	0.317
m34	24,000	0.290	0.23	0.893
m35	25,000	0.271	0.32	1.673
m72	25,000	0.076	0.18	0.140
m77	25,000	0.110	0.36	0.832
m78	24,000	0.088	0.51	1.373
m79	24,000	0.083	0.70	2.421
m80	25,000	0.089	0.36	0.679
m82	25,000	0.191	0.18	0.353
m83	24,000	0.186	0.34	1.277
m84	25,000	0.181	0.50	2.722
m87	24,000	0.196	0.73	6.188

D.4 Uneven Walled, Smooth Rectangle

Test	Reynolds Number	Density Parameter	Rotation Number	Buoyancy Parameter
a52	24,000	0.107	0.13	0.115
a53	25,000	0.103	0.24	0.393
a55	23,000	0.225	0.38	2.169
a56	24,000	0.241	0.24	0.909
a57	24,000	0.231	0.13	0.266
a58	21,000	0.331	0.13	0.368
a59	21,000	0.311	0.22	1.007
a60	21,000	0.287	0.35	2.412
a61	61,000	0.100	0.05	0.018
a62	60,000	0.083	0.09	0.050
a63	60,000	0.089	0.14	0.126
a64	114,000	0.124	0.03	0.006
a65	113,000	0.122	0.05	0.019
a66	113,000	0.127	0.07	0.048

Bibliography

[1] ASHRAE. *Thermodynamic Properties of Refrigerants*. American Society of Heating, Refrigeranting and Air-Cinditioning Engineers, New York, N.Y., 1969.

[2] ASHRAE. *Thermophysical Properties of Refrigerants*. American Society of Heating, Refrigeranting and Air-Cinditioning Engineers, New York, N.Y., 1973.

[3] Pamela Barry. Rotational effects on heat transfer in turbine blade cooling. Master's project, Massachusetts Institute of Technology, Department of Aeronautical/Astronautical Engineering, 1994.

[4] G.K. Batchelor. *An Introduction to Fluid Dynamics*. Cambridge University Press, N.Y., New York, 19August 1968.

[5] Phillip R. Bevington. *Data Reduction and Error Analysis for the Physical Sciences*. McGraw-Hill Book Company, New York, New York, second edition, 1969.

[6] C.Prakash and R.Zerkle. Prediction of turbulent flow and heat transfer in a radially rotating duct. *Journal of Turbomachinery*, 114:835–846, October 1992.

[7] Phillip M. Gerhardt and Richard J. Gross. *Fundamentals of Fluid Mechanics*. Addison-Wesley, Reading, Massachusetts, 1985.

[8] J. Guidez. Study of the convective heat transfer in a rotating coolant channel. *Journal of Turbomachinery*, 111:43–50, 1989.

[9] J.C.Han and Y.M. Zhang. Effect of uneven wall temperature on local heat transfer in a rotating square channel with smooth walls and radially outward flow. *Journal of Heat Transfer*, 114:850–858, November 1992.

[10] Jack L. Kerrebrock. *Aircraft Engines and Gas Turbines*. The MIT Press, Cambridge, Massachusetts, second edition, 1992.

[11] John Constantine Kreatsoulas. An experimental study of impingement cooling in rotating turbine blades. Master's project, Massachusetts Institute of Technology, Department of Aeronautical/Astronautical Engineering, 1983.

[12] Frank Kreith. *Principles of Heat Transfer*. International Textbook Company, Scranton, Pennsylvania, second edition, 15 December 1965.

[13] J,hn H. Lienhard. *A Heat Transfer Textbook*. Prentice-Hall,Inc., Englewood Cliffs,New Jersey, second edition, 1987.

[14] Anthony F. Mills. *Heat Transfer*. IRWIN, Boston, Ma, 1992.

[15] W.D. Morris and R. Salemi. An attempt to uncouple the effect of coriolis and buoyancy forces experimentally on heat transfer in smooth circular tubes that rotate in the orthogonal mode. *Journal of Turbomachinery*, 114:858–864, October 1992.

[16] J.H. Wagner, B.V. Johnson, and F.C.Kopper. Heat transfer in rotating serpentine passages with smooth walls. *Journal of Turbomachinery*, 113:321–329, October 1991.

[17] J.H. Wagner, B.V. Johnson, R.A. Graziani, and F.C. Yeh. Heat transfer in rotating serpentine passages with trips normal to the flow. *Journal of Turbomachinery*, 114:847–857, October 1992.